

Summer 2016

Linking In-Situ Data with Remote Sensing to Analyze Tropical Glacier Stability and Retreat in the Cordillera Blanca, Peru

Chandler H. Santos

Western Kentucky University, chandler.santos458@topper.wku.edu

Follow this and additional works at: <http://digitalcommons.wku.edu/theses>



Part of the [Environmental Monitoring Commons](#), [Geology Commons](#), and the [Glaciology Commons](#)

Recommended Citation

Santos, Chandler H., "Linking In-Situ Data with Remote Sensing to Analyze Tropical Glacier Stability and Retreat in the Cordillera Blanca, Peru" (2016). *Masters Theses & Specialist Projects*. Paper 1629.
<http://digitalcommons.wku.edu/theses/1629>

This Thesis is brought to you for free and open access by TopSCHOLAR®. It has been accepted for inclusion in Masters Theses & Specialist Projects by an authorized administrator of TopSCHOLAR®. For more information, please contact topscholar@wku.edu.

LINKING IN-SITU DATA WITH REMOTE SENSING TO ANALYZE TROPICAL
GLACIER STABILITY AND RETREAT IN THE CORDILLERA BLANCA, PERU

A Thesis
Presented to
The Department of Geography and Geology
Western Kentucky University
Bowling Green, Kentucky

In Partial Fulfillment
of the Requirements for the Degree
Master of Science

By
Chandler Santos

August 2016

LINKING IN-SITU DATA WITH REMOTE SENSING TO ANALYZE TROPICAL
GLACIER STABILITY AND RETREAT IN THE CORDILLERA BLANCA, PERU

Date Recommended 5-6-2016



John All, Director of Thesis

Jun Yan


Jun Yan



Aaron Celestiano



Carl Schmitt

 7/28/16

Dean, Graduate Studies and Research Date

ACKNOWLEDGEMENTS

These past two years have been long and grueling at some points, but were also two of the most fulfilling years of my life. It would not have been possible without my thesis advisor, Dr. John All, who worked with me to find a topic that I was passionate about. Nor would it have been possible without my committee members, Drs. Jun Yan, Aaron Celestian, and Carl Schmitt, who all offered their expertise and advice throughout the process. Special thanks also goes to the American Climber Science Program for the research opportunity I was given, and to WKU's Department of Geography and Geology for being my academic home over the last five years. I can never thank you all enough for the chance to learn, travel, and grow as an academic and a person.

If there is any reason why I am where I am today, it's due to my family, and I want to dedicate this entire work to you. To my mom, for being my best friend and confidant, always supporting my decisions; my dad, for pushing me to go above and beyond to pursue any and every dream I have; Vincent, for loving me even though I've been absent for the past seven years; Sarah, for giving me somebody to look up to, and always providing comedic relief; and to Zac and BumBum because I know you're both here as well.

Dylan, thank you so much for always being here for me, keeping me focused, making me laugh, and encouraging me when I need it. You'll never understand how much that means to me. These two years would have been miserable without you. To the Callisons, thank you for giving me a home away from home and loving me like one of your own. To Katie Moore, thank you for being my best friend for a decade, even when school and life got in the way. To Logan Billhartz, thank you for girls' nights, vent sessions, and your constant friendship and understanding. To Annie Wheeler, thank you

for the joy and silliness you brought to our apartment and our friendship the last three years. And to my mentors along the way, who will always hold a special place with me: Joe Percefull, Chris Carlton, Carrie McElfresh, Pokey Bowen, Tim Gott, and Beth Hawke.

Thank you, to all of you. Of all the places I have been, I'm no place without you.

CONTENTS

List of Figures	viii
List of Tables	ix
Abstract	xi
Chapter 1. Introduction	1
Chapter 2. Background	4
2.1 Climate Change.....	4
2.1.1 Anthropogenic Forcings and Outcomes.....	4
2.2 Glaciers	5
2.2.1 Tropical Glaciers.....	7
2.2.2 Melt-Off Hazards	9
2.3 Black Carbon	10
2.3.1 Black Carbon Sourcing	12
2.3.2 Effects on Albedo	14
2.4 Remote Sensing	14
2.4.1 Remote Sensing of Glaciers.....	16
Chapter 3. Study Area.....	19
Chapter 4. Data and Methodology	21
4.1 Data	21
4.1.1 Snow Samples.....	21
4.1.2 Remote Sensing	23
4.1.3 Albedo Values.....	24
4.1.4 Sourcing and Local Data.....	27

4.2 Analysis.....	28
4.2.1 Proximity Calculation	29
4.2.2 Regression and Correlation Analysis.....	29
4.2.3 Interpolation Technique	30
4.2.4 Glacier Extent	30
Chapter 5. Results and Discussion.....	32
5.1 Mineral Analysis.....	32
5.2 Correlation of Snow Sample Attributes	34
5.3 Proximity Analysis.....	38
5.3.1 Mines.....	38
5.3.2 Huaraz	39
5.3.3 Aspect Analysis	41
5.4 Glacier Extent	44
Chapter 6. Conclusions	46
References.....	50
Appendix A: Maps	62
Appendix B: Tables	92

LIST OF FIGURES

Figure 2.1. Process of transformation from snow to ice	7
Figure 2.2. Glaciers of Peru	8
Figure 2.3. Black carbon deposition	11
Figure 2.4. Black carbon emissions in 2000	13
Figure 2.5. Differences in spectral resolution	16
Figure 2.6. Reflectance values of ice surfaces	17
Figure 3.1. The Cordillera Blanca Mountain Range	19
Figure 4.1. Temperature profile of filters	23
Figure 5.1 Huascarán National Park glacier loss	44

LIST OF TABLES

Table 4.1. MOD10A1 albedo values	25
Table 4.2. Calculated albedo levels	27
Table 4.3. Strength of association guidelines	30
Table 5.1. Mineralogy correlation analysis, 2011.....	33
Table 5.2. Mineralogy correlation analysis, 2012.....	33
Table 5.3. Mineralogy correlation analysis, 2013.....	33
Table 5.4. Variable correlation analysis, 2011	35
Table 5.5. Variable correlation analysis, 2012	35
Table 5.6. Variable correlation analysis, 2013	35
Table 5.7. Snow sample and mineralogy correlation analysis, 2011	37
Table 5.8. Snow sample and mineralogy correlation analysis, 2012.....	37
Table 5.9. Snow sample and mineralogy correlation analysis, 2013.....	37
Table 5.10. Mine proximity and mineral correlation analysis	38
Table 5.11. Mine proximity and attribute correlation analysis	39
Table 5.12. Huaraz proximity and attribute correlation analysis.....	39
Table 5.13. Huaraz proximity and mineral correlation analysis	41
Table 5.14. Mine proximity based on sample aspect, Pierina	42
Table 5.15. Mine proximity based on sample aspect, Antamina	42
Table 5.16. Mine proximity based on sample aspect, Huanzala.....	42
Table 5.17. Huaraz proximity based on sample aspect.....	43
Table 5.18. Glacial loss by cluster	45
Table 5.19. Retreat by aspect.....	45

LINKING IN-SITU DATA WITH REMOTE SENSING TO ANALYZE TROPICAL
GLACIER STABILITY AND RETREAT IN THE CORDILLERA BLANCA, PERU

Chandler Santos

August 2016

108 Pages

Directed by: John All, Jun Yan, Aaron Celestian, and Carl Schmitt

Department of Geography and Geology

Western Kentucky University

Glaciers are a major source of freshwater around the world, but they are melting at an increased rate due to atmospheric warming resulting from anthropogenic climate change. In addition to temperature increases, light-absorbing particulates on glaciers also are contributing to glacial melt. This research examines how black carbon, released into the air through partial combustion of biofuels, is affecting the surface albedo of glaciers. I also delineate possible sources of black carbon in the Cordillera Blanca region of Peru. Ground data were collected each year from 2011 to 2013 during the local dry season. Effective black carbon (eBC) values were determined using the Light Absorption Heating Method and satellite-derived albedo values were retrieved from NASA's MODIS MOD10A1 data. Effective black carbon (eBC) values and albedo levels were moderately correlated, showing that albedo decreases with an increase of black carbon, and that this impact can be measured using satellite instruments. Values of eBC did not correlate with spatial proximity to mines, but did correlate with proximity to Huaraz, which likely is the major source of light-absorbing particulates in the region. Further research would benefit from a more extensive source dataset and surface albedo measurements over different seasons.

Chapter 1. Introduction

Living in the contemporary world, we are constantly surrounded by harmful pollutants that have put our health at risk, contaminated our waterways, and helped to drive temperatures to record highs over the past few decades. Though climate change has always been a natural process on our planet, humans are now releasing high levels of carbon dioxide, methane, and other harmful gases into the atmosphere through fossil fuel burning, and these releases are intensifying climate change impacts. These gases have high heat-absorbing properties that trap radiation in the atmosphere and warm it to unusual levels. A warmer atmosphere has the capability to hold more water for longer periods of time, leading to more frequent droughts and floods (IPCC, 2013).

Our cryosphere is also at risk from these changes, and both ice caps and glaciers are melting at an alarming rate, reducing overall global albedo, raising sea levels, and lowering water availability to downstream users (Lemke et al., 2007). This research examines how anthropogenic climate change and atmospheric pollutants, specifically black carbon, are affecting glacier stability and retreat in the Cordillera Blanca range of the Andes. This area is an important source of water for over a million people in the Ancash region of Peru. As both local livelihoods and long-term economic stability depend on the water that is sourced in local glaciers, it is crucial to find answers about what specifically may be causing local glacier recession.

Glaciers are very sensitive to changes in precipitation, radiation, and temperatures; which are all factors that determine their growth and recession. Their seasonal melt-off provides water to local communities, their high reflectivity helps cool the Earth's atmosphere, and they can be used to monitor changes in climate. Glaciers take

hundreds to thousands of years to form, and many glaciers are remnants from the last ice age (Paterson, 1994). Approximately 80% of the people living in tropical and subtropical montane environments rely strictly on snowfall and glaciers for their water supply (Vuille et al., 2008). This is especially important in the Andes Mountains, particularly Peru. The Andes are home to over 90% of the world's tropical glaciers, and 70% of these are located in Peru (Rabatel et al., 2013).

While greenhouse gas warming and precipitation changes are the major reason for glacial retreat, black carbon and other particulates also have an impact, especially in developing countries (Bice et al., 2009). Black carbon results from incomplete combustion of biofuels and is dangerous due to its high solar absorptive properties. It has a surface warming effect of up to 1° C, meaning the temperature of surfaces covered with black carbon can rise by 1° C (Ramanathan and Carmichael, 2008). Black carbon has one million times the heat-trapping capacity of carbon dioxide ounce per ounce (Schmidt, 2011), and the capability to reduce glacial albedo levels dramatically (Warren and Wiscombe, 1985).

This research measures levels of black carbon in the Cordillera Blanca mountains of Peru and evaluates how local emissions might be affecting glacier retreat and albedo levels. Since black carbon has high solar absorption properties, deposition of these particles will reduce surface albedo, thus causing the glaciers to absorb more heat and ultimately increase the rate of ablation. When ablation rates are higher than accumulation rates, the glacier begins to retreat (Paterson, 1994). Correlating black carbon concentrations with albedo levels and with glacier size can elucidate what influence the particulates have on local retreat. In addition to examining black carbon's impact on

glacial retreat, potential sourcing of black carbon was investigated during this research. Sources including the large population center of Huaraz, and multiple mining sites were examined as possible sources of black carbon and other dust.

Chapter 2. Background

Everyday our actions leave behind a footprint on the Earth. One major impact is on the retreat of glaciers, especially tropical glaciers. Temperature increases have been measured globally as far back as the 1930s, suggesting that retreat has been in process for some time due to atmospheric warming. In addition to temperature, local and global sources of pollutants are suspected to play a role in increased glacier melt-off around the world. Black carbon is of special interest as its high radiative absorption can change the radiative balance of snow and ice. Though black carbon has not been researched extensively, recent studies show how black carbon and dust are influencing melt rates (Andreae and Ramanathan, 2013; Barnett et al., 2005; Shrestha et al., 2010).

2.1 Climate Change

Variations in climate around the world are not a new phenomenon. Climate change can happen due to volcanic eruptions, varying outputs of solar radiation, global ice or snow coverage changes, or natural earth cycles (Le Treut et al., 2007). Even as recently as the 1700s, the Little Ice Age brought cooler temperatures to North America and Europe (Painter et al., 2013). The current change in climate has been attributed to anthropogenic factors rather than a natural shift in climate, and scientists working with the Intergovernmental Panel on Climate Change agree that the rapid rate of warming since the mid-20th century is caused by anthropogenic forcing (IPCC, 2007).

2.1.1 Anthropogenic Forcings and Outcomes

Greenhouse gas concentrations have been increasing since the Industrial Revolution such that anthropogenic climate drivers are contributing to warming the atmosphere. Concentrations of carbon dioxide, methane, and nitrous oxide in 2011

surpassed the 1750s' concentrations by 40%, 150%, and 20%, respectively (IPCC, 2013). As industry advanced, so did emissions. In 1990, a study concluded that 43% of the increase in radiative forcing over the prior 10 years could be attributed to these gases (Lashof and Ahuja, 1990). In 2010, the highest levels of greenhouse gases in human history were recorded at 49 gigatonnes of carbon dioxide equivalent per year, with 76% of the impact being contributed by carbon dioxide (IPCC, 2014). An increase in surface, atmosphere, and upper-level ocean temperatures has resulted. NASA's Goddard Institute for Space Studies has found that the average global temperature has risen by 0.8°C since 1880, two-thirds of which have occurred since 1975, and, in 2014, the National Oceanic and Atmospheric Administration (NOAA) found that ocean heat content in the majority of the world's ocean basins was above the historical average (Kennedy, 2015). The most dramatic change occurred in June, 2009, when the world's oceans reached their highest average temperature in recorded history (Biello, 2009). More frequent heat waves in the 21st century have also been attributed to higher emissions (Marengo et al., 2009)

Most climate change modeling has been done at a global scale. Regional climate change drivers and their feedback loops need to be studied further, especially in sensitive environments such as mountainous or glaciated regions.

2.2 Glaciers

A glacier is a mass of ice at least 0.1 km² in size that originates over land and often moves due to gravity and its own mass (Paterson, 1994). During the last ice age, glaciers covered over 60% of earth's surface, but now only 10% of the land area is covered by glaciers (Lemke et al., 2007). Glaciers are continuing to shrink worldwide in length, area, volume, and mass, with an average rate of loss of 275 gigatonnes of ice per

year (IPCC, 2007). Glaciers and snow melt provide water for over one-sixth of the world's population (Barnett et al., 2005) and help to stabilize the Earth's temperature through radiative reflectance. Although tropical glaciers are not large enough to impact significantly planetary albedo, studying current glacial processes could help to safeguard regional water supplies and provide critical information regarding future glacial melting at the higher latitudes.

Glaciers form through years of snow accumulation. When the loss of snow is less than the accumulation of snow, over time the weight of each snowfall layer causes the previous layer to recrystallize, first into firn and then into ice (Paterson, 1994) (Figure 2.1). The area where this happens is appropriately called the accumulation zone. The opposite occurs in the ablation zone, where the loss of snow exceeds snowfall amounts. Accumulation occurs through precipitation and refreezing of liquids, while ablation results from surface melting, calving, and sublimation; both ablation and accumulation can be impacted by avalanches and wind patterns (Vaughan et al., 2013). The boundary between the two zones where ablation and accumulation are equal is known as the equilibrium line (Paterson, 1994).

A glacial moraine is an accumulation of debris, typically dirt and rock, which is pushed by the snout and, occasionally, the lateral edges of a glacier (Boulton, 1986). Moraines allow measurement of the maximum extent a glacier has reached. In certain cases, moraine dams develop over time and create glacier lakes as the ice melts and retreats, portending hazardous glacial lake outburst flooding (GLOF) (Richardson and Reynolds, 2000). Other components of a typical glacier include meltwater streams, headwalls, and occasionally medial moraines.

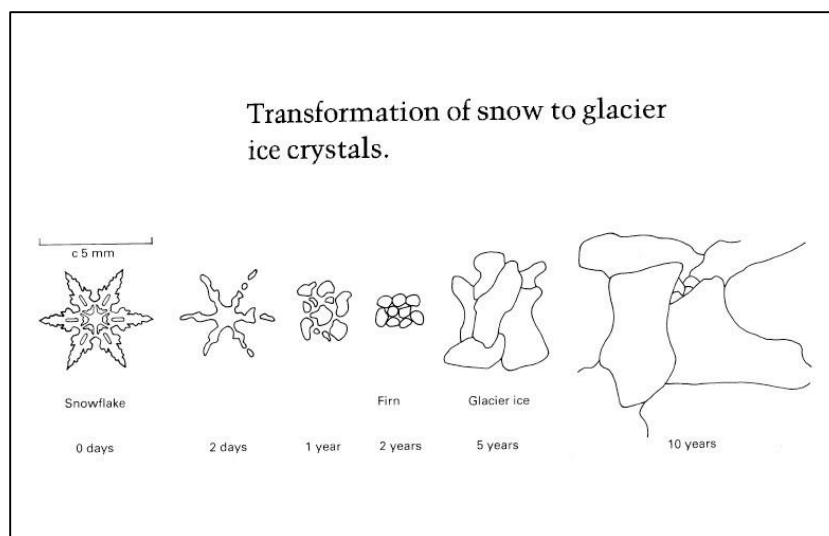


Figure 2.1. Process of transformation from snow to ice. On average, snow will take 5 years to reach the stage of glacier ice.

Source: Hambrey and Alean (1992).

2.2.1 Tropical Glaciers

Tropical glaciers are found between the Tropic of Cancer and the Tropic of Capricorn - though 99% are located in the Andes Mountains. These Andean glaciers have an area of 1920 km² (Rabatel et al., 2013) and Peru contains 70% of those glaciers (Figure 2.2). All glacier landscapes are extremely sensitive to changes in temperature, precipitation, albedo levels, and even to human factors such as road development or mining (Knight and Harrison, 2014). Tropical glaciers, though, respond to these conditions more quickly and dramatically due to their smaller size and the greater solar radiation loads at the low latitudes (Bahr et al., 1998). This vulnerability to slight environmental changes is helpful for monitoring and research purposes, but is detrimental for the long-term survival of tropical glaciers. This is critical because these glaciers provide freshwater to 80% of people in tropical and subtropical mountain regions (Vuille et al., 2008).



Figure 2.2. Glaciers of Peru. 70% of the world’s tropical glaciers are located in Peru. Source: Somerville (2011).

Glaciers in the Peruvian Andes have not had a period of advancement since the early 20th century (Rabatel et al., 2013). Between 1962 and the early 2000s, the northern part of the Cordillera Blanca showed a 20% to 30% decrease in surface area (Raup et al., 2007), while the southern part showed a 35% decrease (Mark and Seltzer, 2005). This degree of retreat has not been seen since the Little Ice Age (Rabatel et al., 2013). Factors behind such glacier retreat include climate variables and light absorbing particulates that alter the energy and mass balance of the glaciers. (Salzmann et al., 2013).

Various studies have examined the rate of temperature change in the tropical Andes. Generally, there has been a 0.68°C increase in temperature over the last 70 years, about 0.1°C per decade (Vuille et al., 2008). Mark and Seltzer (2005) concluded that

there was a 0.26°C increase per decade from 1951 to 1999. Between 1939 and 1998, Vuille et al. (2000) found a decadal increase of 0.10-0.11° C. As of the early 2000s, the warming rate of the Andes had almost tripled in the previous 25 years, jumping from 0.10°C to 0.32°C per decade (Vuille et al., 2000). Not only has there been a temperature increase, but the daily temperature range is decreasing (Vuille et al., 2008). Cold nights are getting warmer, and the number of these warm nights are increasing (Vuille et al., 2008). Rain-snow lines retreat up slope with warmer temperatures, which, in turn, exposes glaciers to more rain in the ablation zone (Vuille et al., 2000). Ablation occurs year-round in the lowest portion of tropical glaciers, so extra rain in the ablation zone potentially could become a constant event in the future if these trends continue.

2.2.2 Melt-off Hazards

Glacial environments subject to rapid melting potentially can experience glacial lake outburst floods, river floods, and rock slope failures (Knight and Harrison, 2014). With a sudden increase in melt water, local rivers are inundated with excess water that overflows into surrounding flood plains. Not only is this bad for farmlands, but it can harm those communities close to the riverbank. Softening of permafrost causes human-made structures to collapse, especially roads. In 1941, the city of Huaraz, located near the Cordillera Blanca, was devastated by a glacial lake outburst flood. A chunk of ice crashed into a glacial lake, forcing waves over the moraine dam and creating a wall of mud, water, and debris with cement-like consistency that wiped out one-third of Huaraz and killed 5,000 people (Carey, 2010). Though measures have since been taken by the government to drain reservoirs and strengthen the moraine dams, the threat of a catastrophic flood is always there.

It is important to note that an increase in temperature is not the only factor that can influence glacial retreat. A report on the cryosphere released by the IPCC stated that the extent of glaciers is not in balance with current climate conditions, so glacier loss will continue, whatever happens to global temperatures (Vaughan et al., 2013). Additionally, studies have found that a decrease in precipitation and cloud cover, along with rising temperatures, contributed to glacier retreat in the Cordillera Blanca between 1930 and 1950 (Kaser and Georges, 1997). Beyond this, in the Cordillera Vilcanota region of the southern Peruvian Andes, another study also concluded that both decreased precipitation and increased temperatures cannot completely explain the observed ice loss, and that albedo changes are probably responsible (Salzmann et al., 2013). Another study found the same processes occurring in the Cordillera Blanca (Schauwecker et al., 2014). Instead of looking solely at climate as the cause of glacier retreat, more local causes should be investigated, including black carbon particulates.

2.3 Black Carbon

Black carbon, sometimes referred to as soot, results from partial, incomplete combustion of biomass or fossil fuels that releases light-absorbing particles into the atmosphere (Ramanathan and Carmichael, 2008). These particles play a large part in degrading air quality and generally are released from diesel engines, forest fires, and other biomass burning (Bahadur et al., 2011; Zimmer, 2013). Particles mix with clouds and water droplets and can linger over an area as brown haze or be brought down to earth via precipitation (Ramanathan and Carmichael, 2008; Monroe, 2008; Zimmer, 2013). Air polluted with black carbon creates health concerns for local residents, especially those with respiratory problems (Kim et al., 2004). Black carbon has a short residence time in

the air, but has the ability to travel long distances in that short amount of time (Lelieveld et al., 2002). Black carbon particulates can make their way onto glaciers through precipitation or dry deposition and can influence melt rates by darkening the snow and reducing the albedo (Figure 2.3) (Shrestha et al., 2010).

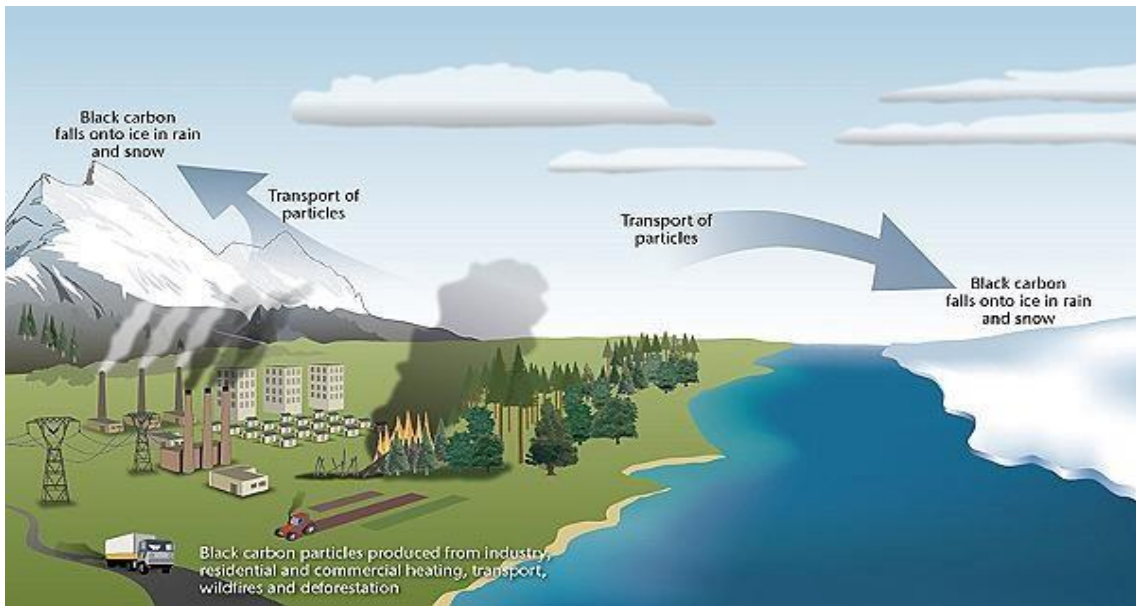


Figure 2.3 Black carbon deposition. Particles are carried via air and precipitation onto ice and snow. Source: Leake (2011).

Research on how black carbon might be affecting the planet's climate is fairly new, with evidence being gathered only since the mid-1990s (Schmidt, 2011). However, scientists have identified airborne black carbon as the second leading cause of global warming, behind carbon dioxide (Ramanathan and Carmichael, 2008). Recent studies show that, while carbon dioxide is accountable for 40% of global warming, black carbon is potentially responsible for nearly 18% of the warming (Rosenthal, 2009).

From 2000 onwards, 7,500 kilotonnes of black carbon were emitted globally per year (Bond and Doherty, 2013). By 2009 that value had risen by an additional 500 kilotonnes (Bice et al., 2009). One of the dangers of black carbon, as noted by Schmidt (2011), is that it has about one million times the heat-trapping capabilities of carbon

dioxide per ounce. With a surface warming effect from 0.5 to 1°C, even if the levels of black carbon are not extremely high or have not increased quickly, it will still have an influence on warming due to direct absorption solar radiation. Black carbon mixed with other aerosols such as sulphates can enhance that forcing factor by two and, in hotspots, the solar heating may increase by up to 50% (Ramanathan and Carmichael, 2008).

2.3.1 Black Carbon Sourcing

Unlike carbon dioxide, black carbon does not have a long residence time in the air, usually being removed quickly by precipitation within two weeks (Doherty and Warren, 2009; Ramanathan and Carmichael, 2008). The problem is that, because of its very small size, it travels easily and quickly through the air, and thus it can be deposited in locations far from its source. While there have been many sourcing studies for aerosols, most of the research does not include sourcing black carbon (Artaxo et al., 1998; Tyagi and Singh, 2013). An important case study on black carbon sources in the Arctic was completed in 2007 (Hegg et al., 2009), with the results showing that black carbon found in Arctic snow was connected to sources in Russia, North America, and also marine environments near sea-ice sites of the North Pole. Black carbon produced by diesel fuels and other combustion sources in the U.S. and India have been found in the Arctic and Maldives, respectively (Rosenthal, 2009). Such long-distance transport of particulates means not only that source areas are affected by black carbon but neighboring regions are as well.

Most sources of black carbon are located in tropical regions with high solar irradiance values, with emissions sourced from open burning, diesel engines, industrial coal, and residential solid fuel (Figure 2.4) (Bond and Doherty, 2013; Ramanathan and

Carmichael, 2008). Depending on the region, main emission sources vary. Coal and biomass contribute 60% to 80% of emissions in Asia and Africa; diesel engines make up 70% of emissions for European, North American, and Latin American countries; and China, the former USSR and some Eastern European countries have dominant emissions from residential coal (Figure 2.4) (Bond and Doherty, 2013). Overall, 77% of black carbon emissions are from developing countries (Bice et al., 2009). A major contribution to this problem is the use of cookstoves. The soot released while burning biomass such as wood to cook has a large impact on black carbon emissions, and is normally found in countries where the technology and economy are not advanced enough for more efficient means of producing energy (Rosenthal, 2009).

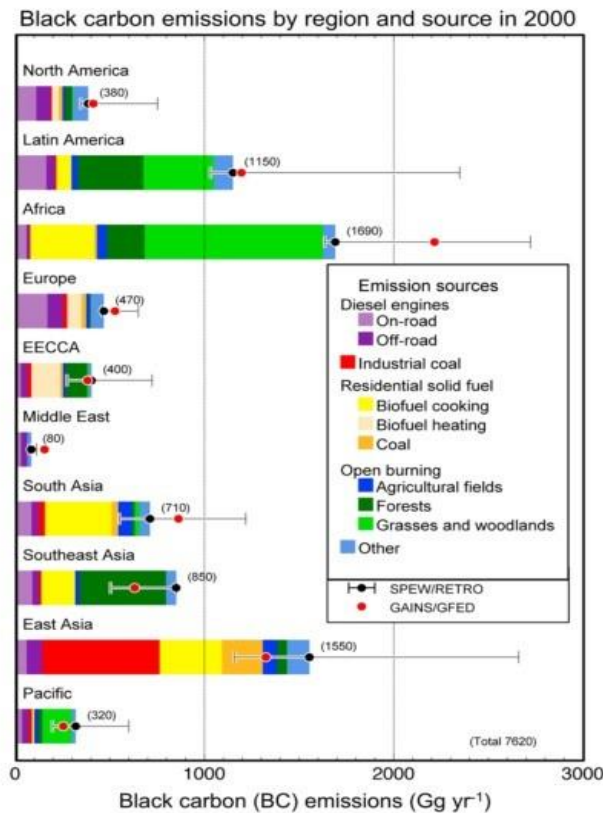


Figure 2.4 Black carbon emissions in 2000. For each region, amount and source of black carbon are detailed Source: Bond and Doherty (2013).

2.3.2 Effects on Albedo

Black carbon and other particulate deposition can greatly affect the albedo and melting rate of ice (Reznichenko and Davies, 2010). Black carbon can even overwhelm factors such as temperature and precipitation that would otherwise cause a glacier to advance (Painter et al., 2013). Ice is highly reflective, but the albedo can be dramatically impacted by particles in or on the ice (Schmitt et al., 2014a). Different particles have different radiative properties, and many have lower light-absorbing capabilities than black carbon. According to Clarke and Noone (1985), black carbon can reduce glacial albedo up to 4%. Warren and Wiscombe (1985) found a 6% reduction in albedo values due to black carbon. Higher levels of black carbon result in decreased albedo, which leads to faster melting of the glaciers through heat retention. Although increased melt water might seem advantageous in the short term, loss of glacier area will diminish stream flow and water availability in the long term (Bradley et al., 2006). As discussed above, glacial melt water in the Cordillera Blanca is a critical contributor to drinking water, farmland irrigation, and hydropower, so it is important to sustain the water source.

2.4 Remote Sensing

Remote sensing uses specialized instruments from an overhead vantage point to measure electromagnetic (EM) radiation reflected or emitted by an object or area to interpret characteristics of said object or area (Jensen, 2007). Before the creation of satellite reconnaissance, distant remote sensing was limited to aerial photography. With the launch of Landsat 1 in 1972, remote sensing science gained a powerful new tool (Rocchio, 2016). Remotely sensed imagery can now be collected via ground-based

devices, aircraft, and satellites. Satellite imagery is most common, with instruments such as Landsat, MODIS, and AVHRR providing daily images of our planet.

A geographic information system (GIS) is a computer-based tool used to represent, question, investigate, and interpret data to understand spatial relationships and trends (Chang, 2010). When combined with data acquired through remote sensing, GIS is a powerful platform to monitor glacial changes quickly and effectively. Whether through a database table of information or through visual representation, GIS has the necessary power to help accurately measure and map glacier size, displacement, movement, and the factors that may be impacting their retreat.

Remote-sensing sensors can be either passive or active. Passive sensors use natural external energy emissions for object observations. This source is normally the sun, whose energy can be reflected by objects but also absorbed and re-emitted as thermal infrared energy. Unlike passive sensors, active sensors emit their own radiation. This radiation is then reflected or refracted by objects and measured by the sensor. Radar is a common type of active sensor that uses radio or microwave frequencies as the source of EM radiation. When measuring glacier properties via remotely sensed imagery, passive sensors typically are used because ice and water are so absorptive in the typical active remote sensing wavelengths (Roshani et al., 2007).

Different types of sensors can be used for data collection. Panchromatic sensors create greyscale images by recording light reflected at a broad segment of the electromagnetic spectrum. More commonly, multispectral sensors record light from several parts of the electromagnetic spectrum and display them as separate band images (Jensen, 2007). When the bands are merged together, the result is an image that most

would refer to as a true-color image. LiDAR sensors use light pulses to measure distances between objects and present them in 3-D (McIntosh, 2012). This type of imagery is especially useful for measuring heights of objects from the ground (Figure 2.5).



Figure 2.5. Differences in spectral resolution. The first image is from a panchromatic sensor. The middle image is from a multispectral sensor. The last image is from a LiDAR sensor. Source: McIntosh (2012).

2.4.1 Remote Sensing of Glaciers

Remote sensing is useful for examining the cryosphere, especially in alpine environments that are often inaccessible (Gao and Liu, 2001; Quincey et al., 2005). In glaciology, remote sensing has been used to study mass balance, areal extent, and albedo levels (Gao and Liu, 2001; Rabatel et al., 2005). The most common parts of the electromagnetic spectrum discussed in the literature are the visible bands and near infrared bands (Bindschadler et al., 2001; Knap et al., 1999). Figure 2.6 shows reflectance curves of different glacial surface types (Rees, 2009). These curves help determine which bands to use when examining different phenomenon.

Glaciers are mostly found in mountainous regions and, depending on the time of day that the imagery was recorded, shadows from the mountains and cloud cover can obscure the imagery and glacial extent. Also, in some cases, it can be hard to differentiate between bare soil and shadowed glaciers through remote sensing imagery. There have

been techniques developed to solve this problem, such as the Normalized-Difference Snow Index (NDSI) (Dozier, 1989; Racoviteanu et al., 2008). The NDSI uses two bands to eliminate the problems associated with topography and cloud cover previously mentioned to determine boundaries of glaciers. Glaciers captured in shadows from surrounding hills or cloud cover are less likely to be mistaken for land or rock.

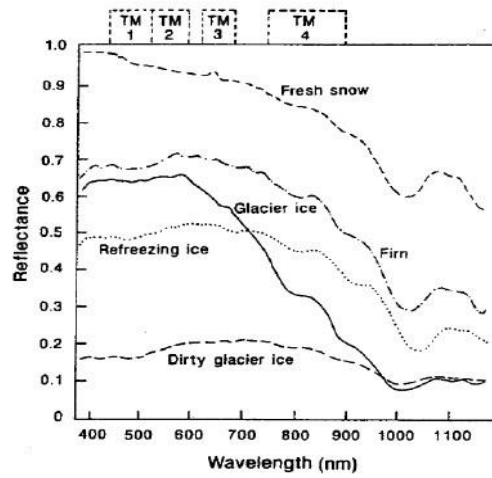


Figure 2.6. Reflectance values of ice surfaces. Corresponding Landsat TM bands also shown. Source: Rees (2009).

In order to resolve a glacier (minimum 0.1 km^2), you need appropriate remote sensing tools. An instrument may have high spatial resolutions of 1-30 m, which is acceptable for observing glaciers. Lower resolutions, such as a typical 1 km^2 resolution, mean a loss in detail, which can make smaller glaciers indistinguishable. For this reason, spatial resolution may be a limiting factor when studying glaciers, depending on their size (Gao and Liu, 2001).

Glacial mass balance is a product of averaging accumulation and ablation rates, measuring the change in mass over a given time (Rees, 2009). Climate change has accelerated the post-Ice-Age retreat of glaciers since the industrial revolution (Lemke et

al., 2007). Recently, tropical glacier mass balance methods have been devised using remotely sensed imagery (Rabatel et al., 2013). The approach of using remotely sensed equilibrium line altitude measurements to calculate mass balance was originally developed by Rabatel et al. (2005) for mid-latitude glaciers, but it works for tropical glaciers as well. Another model for mass balance using remote sensing (GMB-RS) was developed by Rott et al. (2007). Advance Synthetic Aperature Radar and MODIS data, daily accumulation, and ablation rates are calculated for different surface elevations. The GMB-RS model combines temperature parameters and melt amounts with the remotely sensed accumulation and ablation rates to calculate the overall net balance. Comparing current mass balance with past mass balances can shed light on overall glacier loss, even when loss is not noticeable through areal extent changes.

There are multiple methods to gather albedo measurements through remote sensing. MODIS provides a 16-day albedo product at a 500-m resolution accessible through the USGS and Department of the Interior (USGS, 2014). Knap et al. (1999) used Landsat TM band 2 and 4 to measure albedo levels before the MODIS albedo product was available. The Global Land Ice Measurements from Space (GLIMS) Program analyzes ASTER imagery to draw glacier outlines using a Normalized Difference Snow Index that is then made available for the public (Raup et al., 2007). Mass balance, glacier extent, and albedo levels all can be observed and compared to each other thanks to remote sensing, shedding light on glacial loss worldwide and areas of special interest.

Chapter 3. Study Area

This research focused on the Cordillera Blanca range of the Andes Mountains, located in the Ancash Region of Peru. All samples were collected from inside Huascarán National Park. The Cordillera Blanca range stretches 180 km from north to south and 21 km from east to west on average (Racoviteanu et al., 2008). As of 1970, there were 722 glaciers that covered 723 km² in the Cordillera Blanca (Kaser et al., 1990). There are 12 mountain groups, with the highest peak reaching 6,768 meters (Figure 3.1) (Georges, 2004).

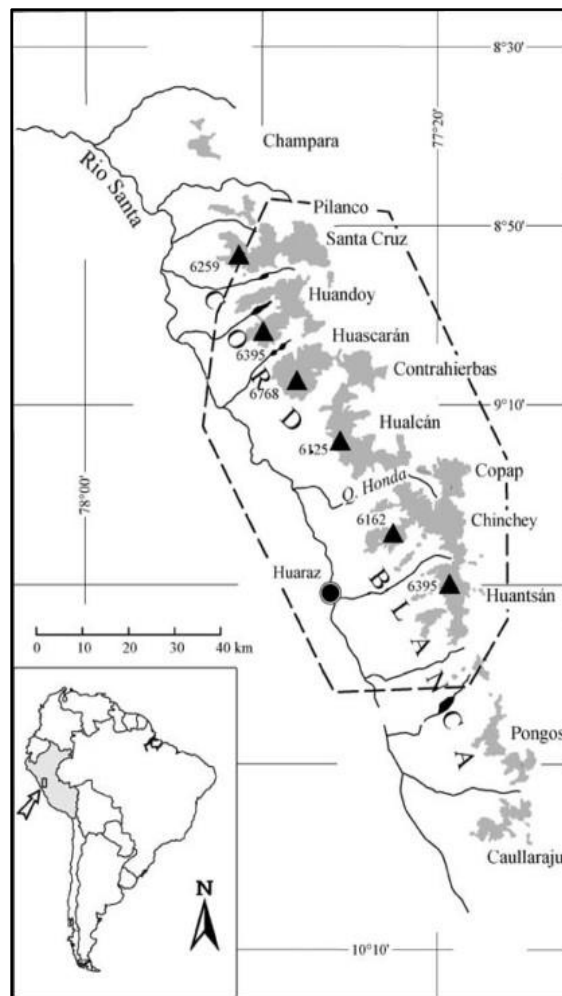


Figure 3.1. The Cordillera Blanca Mountain Range. The 1970 ice extent is shaded in grey. Also displayed are the 12 mountain groups of the region and the six highest peaks. Source: Georges (2004).

Climatically, the Cordillera Blanca has a wet season from October to May, during which snow accumulates, and a dry season from June to September, with less snow accumulation (Mark et al., 2010). Due to the location of the Amazon Basin and its contribution of moisture, the eastern side of the mountain range can be up to three times wetter than the western side (Racoviteanu et al., 2008). Huaraz is the largest city in the region, with a population estimated at just over 100,000 according to U.N. data. Most residents are engaged in agriculture and raising livestock (Mark et al., 2010). The Rio Santa is a major river transporting water to Huaraz and the other population centers at the foot of the mountains. The Cordillera Blanca provides up to 40% of the Rio Santa's water throughout the year, with that number jumping to more than 66% during the dry season. Shorter wet seasons have caused shifts in the river's flow timing, which, in turn, affects local farmers (Mark et al., 2010). Local land use includes extensive grazing, which has severely endangered *Polylepis* forests in the region and increased erosion in the valleys (Zimmerman et al., 2009).

Chapter 4. Data and Methodology

This research investigated how black carbon levels are influenced by altitude, mineralogy, and proximity to pollution sources. Albedo levels from MODIS data were compared to quantities of black carbon found in collected snow samples to correlate any influence on solar absorption. The mineral profile was also compared to albedo levels to determine which particulates contribute the most to heat absorption. The effective black carbon values of the snow samples were compared with surrounding sources such as population centers and mines to determine which sources contribute to black carbon pollution. Inverse Distance Weighting was used in a GIS platform to interpolate black carbon levels across the glaciers, as sampling at every point was unfeasible.

4.1 Data

4.1.1 Snow Samples

In-situ snow sampling was the primary data source for this research. Each snow sample was collected at an altitude of at least 4,800 meters, and the data contain information on the location, depth, date of the sample, an effective black carbon value, and associated mineralogy. Sample locations for each year are mapped in Appendix A.

Schmitt et al. (2014a) developed a method for collecting and analyzing snow samples for black carbon levels that can be used on glaciers across the world. The American Climber Science Program has collected over 200 of these snow samples from 2011 to 2013. Samples were collected from glaciers at least 4,800 m in altitude, 100 m above the snow line and at regular intervals of 500 m of elevation to the mountain summit. To study long-term trends, ice samples were also collected from crevasse walls at varying depths. Location was recorded using a Global Positioning System device at

every sampling point. Sampling locations across the range are standard year to year, though some vary based on weather conditions and overall safety for climbers.

At the time of sampling, approximately 1 kg of snow from the surface (down to 2.5 cm) and 1 kg from the sub-surface (past 2.5 cm) were hand-scooped into appropriately labeled 1-liter Ziploc bags. Once returned to basecamp, the samples were melted down to liquid. The snowmelt of each sample was pulled into a 60 mL syringe and then pushed through a filter. The filter used was a 0.7 micron “Pallflex tissuquartz” 25mm quartz fiber filter. This was repeated 10 times, until 600 mL of snowmelt had been filtered. The filters were kept in plastic coin holders and sun-dried, then kept frozen until analysis.

Filters from snow samples underwent the LAHM process (Schmitt et al., 2014b) to analyze the particles on the filter and quantify their light absorption properties. During the LAHM technique, the temperature of a filter with a known amount of black carbon is exposed to directed visible light in the 300-800 nm range for 30 seconds using the Cole-Parmer Fiber-Lite Fiber Optical Illuminator. An infrared thermometer measures the temperature of the filter before the visible light exposure, during the 30 seconds of exposure, and another 50 seconds after exposure. A temperature profile curve of known levels of black carbon is used to determine effective black carbon mass from the heat absorption data (Figure 4.1). The temperature profile value is the temperature increase the filter had under the Light Absorption Heating Method. The data were recorded for further analysis and compared with the mineral makeup of the samples, as discussed later.

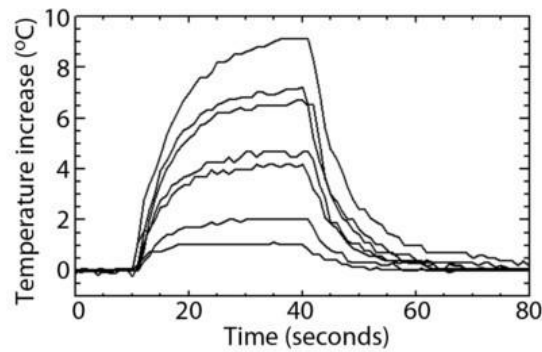


Figure 4.1. Temperature profile of filters. Each filter has a known mass of black carbon. Source: Schmitt et al. (2014b).

Mineral analysis was completed on each sample using a MiniFlex II Desktop X-Ray Diffractometer. Standard Measurement software was used to record measurements for samples. A list of peak positions and intensities were examined and indexed using Topas software. With the aim of extracting structural properties from the data, the Le Bail method was used to fit the pattern of the peaks. Results from the Le Bail method were used to profile and extract intensities of each of the phases. The intensities show the weight of that individual mineral. Le Bail's (2005) paper reviewed the applications and successes of his method.

4.1.2 Remote Sensing

In order to create a time-series analysis for the entire Cordillera Blanca, remote sensing was heavily utilized. Imagery was acquired through MODIS satellite instruments from the USGS EarthExplorer website to examine glacial albedo levels. Glacial extent data were retrieved through the Global Land Ice Measurements from Space (GLIMS) initiative.

Reflectance of snow is one of the factors affecting the mass balance of a glacier (Dumont et al., 2012). As albedo decreases, the glacier absorbs more radiation and melts more quickly. It is, therefore, important to examine the albedo when studying glacial retreat. The Moderate-Resolution Imaging Spectroradiometer (MODIS) instrument delivers a product specifically designed to produce albedo measurements around the globe. The MODIS/Terra Snow Cover Daily L3 Global 500m Grid (MOD10A1) is a daily product that maps snow cover, snow albedo, fractional snow cover, and quality assessment data in a HDF-EOS format (Hall et al., 2006). This mapping is based on the NDSI methods discussed above and was found to be 93% accurate in multiple previous studies (e.g., Hall and Riggs, 2007). MOD10A1 data were downloaded for the months of May through August for the years 2011-2013. Only images with less than 20% cloud coverage were retrieved to ensure adequate coverage of the area. Band 2 of MOD10A1 was used, as it specifically provides ground albedo values.

4.1.3 Albedo Values

The daily albedo band for MOD10A1 used pixel values that directly correlated to albedo values from 0% to 100%. Table 4.1 shows other values that were used in the case where no reflectance was recorded. To retrieve the albedo value for each sample, the Extract Values to Points tool under the Spatial Analyst™ extension in ArcMap® was utilized. This extracts the pixel values of a raster based on point features and saves the values in an output feature class. The MOD10A1 raster used for each year was for albedo values in the middle of July. The point features used were the snow sample locations for that year. When the values were extracted, the output table was then joined to the original snow sample shapefile.

Value	Description
0-100 = snow albedo	In percent
101 = no decision	No decision
111 = night	Darkness, terminator, or polar night
125 = land	Snow-free land
137 = inland water	Lake or inland water
139 = ocean	Open water
150 = cloud	Cloud obscured
250 = missing	Data missing
251 = self shadowing	Self shadowing
252 = landmask mismatch	Landmask mismatch
253 = BRDF failure	Bidirectional Reflectance Distribution Function failure
254 = non-production mask	Non-production mask

Table 4.1. MOD10A1 albedo values. Source: Hall et al. (2006).

Unfortunately, there were locations where albedo values were not between 0-100%, but instead marked snow-free land or a cloud. In these rare cases, a second MOD10A1 raster was brought in, still attempting to use data from the middle of July. Manual extraction of albedo values was attempted for all samples, but 33 of the 232 remained without an albedo reading. Of those samples, 25 were from 2013, while 12 of these were valued as land, showing resolution limitations of satellite imagery on glacier edges. These samples were not used in correlation analyses involving albedo.

Albedo estimates based on black carbon concentrations and snow parameters can also be calculated using the Snow, Ice, and Aerosol Radiation (SNICAR) model (Flanner et al., 2007). SNICAR uses snowpack thickness, snow grain radius, black carbon concentrations, and other parameters to model expected albedo values. For this example, the average snowpack thickness value used was 25 meters. Snow grain effective radius values of 50, 150, and 250 microns were tested in the model. The snow grain radius is especially important because it influences near-infrared reflectance (Dozier, 1989). Calculations of effective black carbon in the Cordillera Blanca have been measured between 0.5 and 75 ng/g. Values of 0.5, 25, and 75, therefore, were used for uncoated black carbon concentration along with snow grain radius to calculate albedo (Table 4.2). For each snow grain radius, albedo measurements do not vary more than 0.02, despite the amount of black carbon. Significant changes in albedo occur between the different radii, mainly that of 50 microns and 150 microns. The albedo values calculated in this model have a much smaller range than those found in MODIS data, so the changes in albedo found in the study area may not be influenced by black carbon. Such insignificant variations would be difficult for remote sensors to pick up as well, so even large concentrations of black carbon would not greatly influence albedo values of MODIS data. SNICAR's model shows that, in theory, black carbon does not affect albedo values significantly. Since this is a theoretical model, it is also possible there may be parameters not accounted for that affect the calculated albedo value, thus producing higher albedo values with less variation.

Snow Grain Effective Radius (µm)	Black Carbon (ppb)	Albedo
50	0.5	0.85
50	25	0.85
50	75	0.84
150	0.5	0.81
150	25	0.80
150	75	0.79
250	0.5	0.78
250	25	0.77
250	75	0.76

Table 4.2. Calculated albedo values. Based on snowpack thickness and black carbon concentration

Although the black carbon research in the Cordillera Blanca only started five years ago, it is important to look at how glaciers retreated over that time period. The Global Land Ice Measurements from Space (GLIMS) project aims to monitor glaciers around the world using multispectral satellite instruments, mainly using the ASTER instrument onboard the Terra platform, and can be used to compare with collected ground data (Raup et al., 2007). Analysis of glacier outlines is performed by regional centers such as universities and geological institutes and made available through the National Snow and Ice Data Center. Using the interactive GLIMS Glacier Viewer, a shapefile of glaciers in the Cordillera Blanca was downloaded. The file included glacier outlines for the years 2005, 2007, and 2015.

4.1.4 Sourcing and Local Data

To determine possible sources of black carbon and dust, including population centers and nearby mines, a variety of GIS data layers were used. A layer of the Huascarán National Park and its associated buffer zone obtained from the University of

Huaraz was used as the study area and analysis mask. The geographical center of Huaraz was selected to represent the town, as it is the main population center in the area. A layer of mining location data was provided by the Peruvian INGEMMET, the Institute of Geology, Mining, and Metallurgy. The overall layout of the area was displayed using a 90-meter resolution Digital Elevation Model (DEM) from the Shuttle Radar Topography Mission (SRTM) through the CGIAR-Consortium for Spatial Information. As previously mentioned, MODIS MOD10A1 imagery albedo data came from the USGS EarthExplorer. The glacier locations and outlines layer were downloaded from the GLIMS database.

4.2 Analysis

The three main software programs used for analysis were IBM® SPSS® Statistics 23, Microsoft® Excel®, and ESRI® ArcGIS™ Desktop 10.2. The SPSS® software was used for all regression analysis. ArcMap® was used for processing, refining, and presenting data. All imagery and files were projected into WGS 1984 UTM Zone 18 South using ArcMap®. Excel® was used to store regression analysis values and perform preliminary refinement of data.

Before any analysis could be completed, all of the data needed to be joined together and available in one location. The original shapefiles for the snow samples included depth of the samples, the mountain name, the year the sample was collected, and location variables such as altitude, latitude, and longitude. The mineralogy data for all the samples were compiled in a separate table, including not only mineral weight but the eBC values as well. This table was joined with the snow sample shapefiles in ArcCatalog® for each individual year. All usable data were available in a shapefile for each year.

4.2.1 Proximity Calculation

Determining dust emission locations that could impact mineral weight or eBC values was not a straightforward process, but calculating proximity of snow samples to mines and population centers can show likely sources (Underhill et al., 2015). Snow sample locations were measured for proximity to three main mines by using the Generate Near Table tool in ArcMap®. The output table listed the distance from each sample to each mine and the angle between the sample and the mine. This process was also used for proximity of the snow samples to the main population center, Huaraz. All output tables were joined to the snow sample shapefile for correlation with the other variables.

4.2.2 Regression and Correlation Analysis

With the goal of explaining how mineral weight or eBC may affect albedo values and vice versa, linear regression was performed between major variables using SPSS® software. Altitude, aspect, eBC, total mineral weight, and albedo values were all correlated against each other. Each of those was then also correlated with the weights of each individual mineral found in each sample. The resulting R-values described whether the two variables had a weak, moderate, or strong linear relationship, or no relationship at all. Since the geoscience community does not have a set correlation coefficient guideline, strength of association was determined using guidelines suggested by Cohen (1988) found in Table 4.3. Total mineral weight, eBC values, and albedo values were all used in bivariate coefficient correlation against proximity values in SPSS® software. Each mineral component was correlated with each other to determine if the amount of one mineral related to the amount of another. Mineral weights were also correlated with snow sample variables to see if they had impacts on eBC or albedo.

Coefficient Value	Strength of Association
0.1 < r < 0.3	Small correlation
0.3 < r < 0.5	Medium/moderate correlation
r > 0.5	Large/strong correlation

Table 4.3. Strength of association guidelines
Source: Cohen (1988.)

4.2.3 Interpolation Technique

While there are snow samples from many areas of the Cordillera Blanca, it is still too large and dangerous of an area for *in-situ* data to be collected across the entire range. Instead, the interpolation technique of Inverse Distance Weighting (IDW) was used. Similar interpolation techniques for pollution detection have been used in studies before, particularly for air pollution (Tyagi and Singh, 2013), but this is the first application of it for black carbon pollution. Inverse Distance Weighting is a weighted distance averaging technique that works under the assumption that objects closer to each other will be more similar than those that are farther apart (O’Sullivan and Unwin, 2003). The IDW tool in the ArcMap® Spatial Analyst™ toolbox was used to create a continuous raster of eBC values for each year and range. The rasters were then used for visual analysis of how these variables might be affected by proximity to nearest mines and the city of Huaraz.

4.2.4 Glacier Extent

The GLIMS data downloaded for the Cordillera Blanca were brought into ArcMap® and separated into shapefiles based on year. The Dissolve tool was used on each shapefile to eliminate individual glacier outlines and create one polygon feature for all glaciers in the study area for 2005, 2007, and 2015. To show the area of change, the

Erase tool was used with 2005 as the input feature and 2015 as the erase feature. The result was a polygon of glaciers in 2005 that are no longer present in 2015. The Polygon to Line tool was used to create a shapefile of just the glacial edges. Elevation values were extracted from the DEM using this glacial outline shapefile and the Extract by Mask tool. The average glacial edge elevation was calculated for 2005 and 2015 from the resulting values.

Chapter 5. Results and Discussion

5.1 Mineral Analysis

For each year between 2011 and 2013, at least five minerals were consistently detected on the filters. A complete breakdown of the minerals and their weights per year can be found in Appendix B. Quartz, muscovite, annite, albite, and kaolinite were found all three years, but illite was also found on the 2013 filters. Quartz comprised the majority of the total mineral weight on over 57% of the total 232 filters, and over 80% of the filters in 2011 alone. Since quartz is one of the most abundant minerals found in the earth, it is likely that the quartz particles found in the snow samples come from nearby agriculture sites and any local mining sites, deposited via wind and precipitation (Rosok, 2007).

Although quartz was the main mineral present in the filter analyses, there were a few oddities in the data. Annite was found in almost every sample for 2012 and 2013, but only found in small quantities in two samples from 2011. Annite is part of the mica mineral family, but is mined very rarely in South America. The only known locality is in Brazil (Ralph, 2015). The increase in annite particulates after 2011 suggests that a nearby mine might have started operations that released the mineral into the air, or that large-scale wind patterns played a bigger role in 2012 and 2013. The sudden presence of illite in 2013 is also peculiar, but may be related to previous minerals found. Illite is a clay-like mineral that can form from disintegrating muscovite, which suggests that high muscovite weight in previous years led to formation of illite minerals by 2013 (Poppe et al., 2001).

Correlation coefficients were calculated in SPSS® between all minerals within each year. The results can be found in Tables 5.1-5.3. Few moderate and strong correlations were found in any of the years. A strong positive correlation was found

between quartz and albite in both 2011 and 2013, though there was only a weak correlation between the minerals in 2012. Muscovite and annite showed a strong positive correlation in 2011 and a moderate positive relationship in 2013. In 2012, there was a very strong positive correlation between kaolinite and muscovite, but it was not as strong in the other years. A moderate positive correlation between quartz and annite was found in 2012 only. Albite had a strong positive correlation with muscovite in 2013, and a moderate positive correlation with kaolinite and illite.

2011	Quartz	Muscovite	Albite	Kaolinite	Annite
Quartz	1	-0.021	0.585	0.016	-0.033
Muscovite	-0.021	1	0.106	0.205	0.603
Albite	0.585	0.106	1	0.288	0.221
Kaolinite	0.016	0.205	0.288	1	0.176
Annite	-0.033	0.603	0.221	0.176	1

Table 5.1. Mineralogy correlation analysis, 2011. Pearson correlation coefficients, using absolute weight of minerals found in samples for each year.

2012	Quartz	Muscovite	Albite	Kaolinite	Annite
Quartz	1	0.071	0.191	0.154	0.428
Muscovite	0.071	1	0.077	0.777	-0.061
Albite	0.191	0.077	1	0.266	0.091
Kaolinite	0.154	0.777	0.266	1	-0.146
Annite	0.428	-0.061	0.091	-0.146	1

Table 5.2. Mineralogy correlation analysis, 2012. Pearson correlation coefficients, using absolute weight of minerals found in samples for each year.

2013	Quartz	Muscovite	Albite	Kaolinite	Annite	Illite
Quartz	1	0.243	0.536	0.103	0.185	0.233
Muscovite	0.243	1	0.604	0.344	0.320	0.211
Albite	0.536	0.604	1	0.462	0.343	0.474
Kaolinite	0.103	0.344	0.462	1	0.526	0.280
Annite	0.185	0.320	0.343	0.526	1	0.207
Illite	0.233	0.211	0.474	0.280	0.207	1

Table 5.3. Mineralogy correlation analysis, 2013. Pearson correlation coefficients, using absolute weight of minerals found in samples for each year.

Despite multiple strong correlations, the R-squared values rarely explained a majority of the variance in the data. The highest correlation coefficient in the data was found between muscovite and kaolinite in 2012 at 0.777, meaning the model explained 60% of the variation. The relationship between annite and muscovite in 2011 yielded the second-highest R-value of 0.603, which only explains 36% of the variance. This means that the presence or absence of a mineral, at most, will explain 36% of the variance in other minerals. There were also no values that showed statistical significance at the 0.01 or 0.05 level.

5.2 Correlation of Snow Sample Attributes

The attributes for all samples that were run through correlation analysis included altitude, effective black carbon, albedo, and total mineral weight for each year (Tables 5.4 – 5.6). The range of values for the latter three attributes is illustrated in boxplots, found in Appendix B. Very few relationships were moderate or strong, but they were important nonetheless. In 2011, the coefficient between eBC and albedo was -0.339, showing a moderate negative correlation. Since eBC is increasing as albedo decreases, this illustrates that the amount of black carbon found on snow likely does affect the absorption and reflection of light. Although this relationship was weak in 2012 and 2013, they were also negative. A negative correlation in all three years is significant because it implicates that black carbon amounts can decrease albedo, no matter the strength. Effective black carbon also had a moderate negative relationship with altitude in 2011, although this only explains less than 14% of the variance. As altitude increases eBC decreases, suggesting that black carbon particles are less abundant at higher elevations.

2011	Altitude	Albedo	eBC	Total Mineral Weight
Altitude	1	0.111	-0.369*	-0.146
Albedo	0.111	1	-0.339*	-0.020
eBC	-0.369*	-0.339*	1	0.055
Total Mineral Weight	-0.146	-0.020	0.055	1

Table 5.4. Variable correlation analysis, 2011. Pearson correlation coefficients, using variables of snow samples. *Correlation is significant at the 0.05 level. **Correlation is significant at the 0.05 level.

2012	Altitude	Albedo	eBC	Total Mineral Weight
Altitude	1	-0.062	-0.141	0.008
Albedo	-0.062	1	-0.062	0.047
eBC	-0.141	-0.062	1	0.020
Total Mineral Weight	0.008	0.047	0.020	1

Table 5.5. Variable correlation analysis, 2012. Pearson correlation coefficients, using variables of snow samples. *Correlation is significant at the 0.05 level. **Correlation is significant at the 0.05 level.

2013	Altitude	Albedo	eBC	Total Mineral Weight
Altitude	1	0.254*	-0.250*	-0.184
Albedo	0.254*	1	-0.172	-0.033
eBC	-0.250*	-0.172	1	0.343**
Total Mineral Weight	-0.184	-0.033	0.343**	1

Table 5.6. Variable correlation analysis, 2013. Pearson correlation coefficients, using variables of snow samples. *Correlation is significant at the 0.05 level. **Correlation is significant at the 0.05 level.

The analysis for 2012 did not result in any moderate or strong associations. The 2013 analysis shows a moderate positive correlation between total mineral weight and effective black carbon, indicating that eBC values increase as mineral weight of the sample increases. Unfortunately, there were no relationships consistent from year to year, implying that the other correlations found may not hold any significance or that other factors such as weather, especially snowfall, immediately before sampling may play a role. Dominate seasonal wind direction for the year, El Nino and Pacific climate patterns, location burning, and temperature inversions could all play a role.

Snow sample attributes were also correlated with the mineralogy of the samples, found in Tables 5.7 – 5.9. The total mineral weight had almost all moderate or strong positive correlations with each mineral, but this is expected since individual mineral weights sum to the total mineral weight. Other relationships found were not consistent throughout all three years. Albite had a strong positive relationship with eBC values in 2011, but only a moderate positive relationship in 2013 and a weak positive relationship in 2012. The only other strong correlation was between kaolinite and eBC in 2013, but this correlation was barely moderate in 2011 and very weak in 2012. Since all minerals analyzed are light-colored, this may explain why there was no correlation between individual minerals and albedo, nor consistent correlation with individual minerals and eBC values.

2011	Altitude	Albedo	eBC	Total Mineral Weight
Quartz	-0.038	0.033	0.093	0.721**
Muscovite	-0.142	-0.065	-0.091	0.671**
Albite	-0.201	0.107	0.518**	0.558**
Kaolinite	-0.221	-0.086	0.317*	0.234
Annite	-0.032	0.063	-0.020	0.415**

Table 5.7. Snow sample and mineralogy correlation analysis, 2011. Pearson correlation coefficients, using variables of snow samples and mineral weights. *Correlation is significant at the 0.05 level. **Correlation is significant at the 0.05 level.

2012	Altitude	Albedo	eBC	Total Mineral Weight
Quartz	-0.066	-0.071	0.187	0.437**
Muscovite	0.042	0.088	-0.041	0.786**
Albite	-0.090	0.274	0.199*	0.332**
Kaolinite	0.039	0.071	-0.078	0.947**
Annite	-0.100	-0.304	0.389**	0.060

Table 5.8. Snow sample and mineralogy correlation analysis, 2012. Pearson correlation coefficients, using variables of snow samples and mineral weights. *Correlation is significant at the 0.05 level. **Correlation is significant at the 0.05 level.

2013	Altitude	Albedo	eBC	Total Mineral Weight
Quartz	-0.141	0.003	0.024	0.784**
Muscovite	-0.122	-0.035	0.109	0.548**
Albite	-0.253*	-0.043	0.406**	0.810**
Kaolinite	-0.084	0.015	0.595**	0.561**
Annite	0.057	0.045	0.372**	0.535**
Illite	-0.164	-0.140	0.228*	0.589**

Table 5.9. Snow sample and mineralogy correlation analysis, 2013. Pearson correlation coefficients, using variables of snow samples and mineral weights. *Correlation is significant at the 0.05 level. **Correlation is significant at the 0.05 level.

5.3 Proximity Analysis

5.3.1 Mines

Regression analysis was performed to determine the relationship between a snow sample's distance to each of three mines versus albedo, total mineralogy, eBC values, and individual mineral values. These correlation coefficients can be found in Tables 5.10 and 5.11. Three main mining locations were used for this analysis (Appendix A): The Pierina mine owned by Barrick Gold Corporation mines mainly gold; the Antamina site mines copper, lead, silver, zinc, and molybdenum; and the Huanzala Mineral Company mines zinc, lead, copper, and silver.

Analysis of individual mineral weights shows a very weak correlation with a sample's proximity to any of the mines. Alternatively, analysis demonstrates that proximity to any mine influenced eBC values, but had no bearing on albedo or mineral weight. The correlation between proximity to any mine and eBC values was moderately negative, showing that eBC values increased when the sample was located closer to a mine. While the correlation coefficients were all within a small range, Pierina had a higher coefficients than the other mines. This suggests that the Barrick Pierina mine may have a slightly larger influence on eBC values than the Antamina or Huanzala mines.

Mines	Quartz	Muscovite	Albite	Kaolinite	Annite	Illite
Pierina	0.176	0.047	0.009	0.082	-0.117	0.002
Antamina	0.083	0.083	0.069	0.087	-0.203	0.003
Huanzala	0.083	0.079	0.057	0.085	-0.197	0.006

Table 5.10. Mine proximity and mineral correlation analysis. Pearson correlation coefficients, relating proximity of mines to mineralogy of snow samples for each year.

Mines	Albedo	eBC	Total Mineral Weight
Pierina	-0.034	-0.447	0.136
Antamina	-0.142	-0.408	0.112
Huanzala	-0.118	-0.419	0.109

Table 5.11. Mine proximity and attribute correlation analysis. Pearson correlation coefficients, relating proximity of mines to snow sample attributes for each year.

5.3.2 Huaraz

Since Huaraz is the most populated town in the Cordillera Blanca region, it was important to determine if proximity to the city impacted albedo, eBC, and total mineral weight. This analysis was performed exactly the same as the analysis with mine proximities. The results for the Huaraz proximity analysis can be found summarized in Table 5.12. For visual representation of eBC values in relation to Huaraz, as well as the nearest mines, maps can be found in Appendix A.

Huaraz	Albedo	eBC	Total Mineral Weight
2011	0.519**	-0.617	0.030
2012	0.487**	-0.358	0.171
2013	0.139	-0.469	0.167

Table 5.12. Huaraz proximity and attribute correlation analysis. Pearson correlation coefficients, relating proximity of Huaraz to snow sample attributes for each year.

The correlation coefficients for effective black carbon (eBC) were negative for all years and at least moderately correlated, but only 2011 had a strong correlation of over -0.60. The coefficient value for 2013 showed a moderate correlation of -0.469, though the value was only a few tenths from a strong correlation. The value for 2012 was smaller than the other years, but it was still at moderate correlation strength. R-squared values

show that the model explains 38% of the variation between effective black carbon and proximity to Huaraz for 2011. About 22% of the variance is explained by the model for 2013, but less than 13% of the variance is explained by the model for 2012.

The relationship between albedo and proximity to Huaraz is positive for all three years, unlike the negative relationships seen with the previous variables. This positive relationship indicates that as the distance from Huaraz increases, so do the albedo values. Glaciers are found farther up in the Cordillera Blanca mountains, at a distance from the town, so the likelihood that albedo-reducing particulates could travel that far from town is logical. The 2011 albedo has a strong association with a correlation coefficient of 0.519, and 2012 has a moderate association with a coefficient of 0.487. Both are statistically significant. These values show that the model explains about 27% of the variation in 2011 and about 24% of the variation in 2012. An anomaly occurs in 2013 though, as that relationship between albedo and proximity to Huaraz is very weak. The relationship between total mineral weight and proximity to Huaraz is also very weak, with no significance in any year.

To illustrate further the impact that the proximity of Huaraz has on variables such as effective black carbon, a continuous raster of eBC values was created using Inverse Distance Weighting. The search radius was 10 kilometers, but at least four samples had to be included in the search. The results show the higher values towards the west-central edge of the park, closest to where Huaraz is located. The eastern edge, as well as the northern portion of the park, shows lower values of eBC than farther south. Effective black carbon mapping was also performed for each sample region above 4,700 meters. Since the analysis area was smaller for these regions, only areas with at least five sample

locations were included to ensure a more realistic representation of interpolated values. These maps can be found in Appendix A.

The proximity of Huaraz to snow samples was also correlated with the individual mineralogy found in each sample (Table 5.13). Weak correlation was found between proximity and all minerals except for quartz in 2013. A positive moderate correlation of 0.355 means that the abundance of quartz found in snow samples increase as distance from Huaraz also increases, although this only explains about 13% of the variance.

Huaraz	Quartz	Muscovite	Albite	Kaolinite	Annite	Illite
2011	0.054	0.031	-0.254	-0.187	-0.096	-
2012	0.186	0.118	0.082	0.139	-0.177	-
2013	0.355	0.041	0.099	-0.250	-0.153	118

Table 5.13. Huaraz proximity and mineral correlation analysis. Pearson correlation coefficients, relating proximity of Huaraz to mineralogy of snow samples for each year.

5.3.3 Aspect Analysis

Proximity analysis was also broken down based on the aspect of the sample and the direction to the each mine. As seen in Tables 5.14-5.16, aspect clusters were created for each mining location. The directions can either be facing each other (North to mine – South aspect of sample, etc.), 90-degrees from each other (South to mine –East aspect of sample, etc.), or matching (West to mine – West aspect of sample, etc.).

The correlation between proximity and mineral weights based on clusters was mostly insignificant for all mines. A moderate positive relationship was found between the albite weight and proximity to Pierina for samples that faced the mine. A strong correlation was found in this same situation for the Huanzala mine. The analysis for Huanzala also shows that muscovite had a moderate positive correlation with proximity

to the main for samples that face Huanzala. For these instances, the mineral weight increases the further the sample is from the mine, but only when the sample has an aspect that faces the mine.

Pierina	eBC	Quartz	Muscovite	Albite	Kaolinite	Annite	Illite
Facing	-0.275	0.064	0.177	0.376	0.266	0.072	-0.188
Ninety Degree	-0.502	0.178	0.044	-0.016	-0.155	-0.156	-0.197
Matching	-0.426	0.322	0.061	-0.029	0.121	-0.188	0.163

Table 5.14. Mine proximity based on sample aspect, Pierina. Pearson correlation coefficients, relating proximity of mine to mineralogy and eBC of snow samples. Categories listed for direction to mine and aspect of sample.

Antamina	eBC	Quartz	Muscovite	Albite	Kaolinite	Annite	Illite
Facing	-0.148	0.051	0.139	0.103	-0.017	-0.176	-0.206
Ninety Degree	-0.579	0.130	0.120	0.111	0.083	-0.146	0.058
Matching	-0.389	-0.043	0.094	0.257	0.054	-0.280	-0.134

Table 5.15. Mine proximity based on sample aspect, Antamina. Pearson correlation coefficients, relating proximity of mine to mineralogy and eBC of snow samples. Categories listed for direction to mine and aspect of sample.

Huanzala	eBC	Quartz	Muscovite	Albite	Kaolinite	Annite	Illite
Facing	-0.580	-0.107	0.352	0.545	-0.173	0.068	-0.133
Ninety Degree	-0.290	0.078	0.095	-0.072	-0.084	-0.294	-0.159
Matching	-0.489	0.338	0.101	0.160	0.108	-0.058	0.092

Table 5.16. Mine proximity based on sample aspect, Huanzala. Pearson correlation coefficients, relating proximity of mine to mineralogy and eBC of snow samples. Categories listed for direction to mine and aspect of sample.

All correlations between effective black carbon and proximity to mine had a negative coefficient, so eBC values always increased as the distance to the mine decreased no matter the aspect cluster. These correlations were strong for the Pierina and Antamina mines when the sample had an aspect 90 degrees to the mine. This was not the

case for Huanzala though. All three mines showed moderate correlations for eBC when the sample's aspect matched the direction to the mine. For samples whose aspects faced the mine, a strong eBC correlation occurred with only the Huanzala mine. As was done with mines, the proximities of the samples to Huaraz were correlated with sample attributes based on aspects of the samples and direction to Huaraz (Table 5.17). The directions can either be facing each other (North to mine – South aspect of sample, etc.), 90-degrees from each other (South to mine –East aspect of sample, etc.), or matching (West to mine – West aspect of sample, etc.).

When the sample is facing the direction of Huaraz, the correlation between effective black carbon and proximity to Huaraz is moderate and negative. This means that as the distance to Huaraz increases, eBC values decrease if the sample faces the town. This also applies to the illite correlation. Muscovite and albite both show moderate positive correlation with proximity to Huaraz when facing the town. As the distance to the town decreases, so does the amount of albite and muscovite found in the sample. For samples with aspects that are either at 90-degrees to the direction of Huaraz or matches the direction, eBC values decrease as distance from the city increases. This correlation is stronger with sample aspects that match the direction to Huaraz.

Huaraz	eBC	Quartz	Muscovite	Albite	Kaolinite	Annite	Illite
Facing	-0.451	0.105	0.318	0.392	0.164	-0.035	-0.299
Ninety Degree	-0.386	0.140	0.069	-0.089	-0.085	-0.198	-0.090
Matching	-0.504	0.268	0.080	0.072	0.101	-0.176	0.071

Table 5.17. Huaraz proximity based on sample aspect. Pearson correlation coefficients, relating proximity of Huaraz to mineralogy and eBC of snow samples for each year. Categories listed for direction to Huaraz and aspect of sample.

5.4 Glacier Extent

Data for this study have not been collected long enough to relate directly to glacier retreat over an extensive period of time, but glacier retreat can still be calculated for the last decade and monitored throughout the continued course of this research. GLIMS data give the area of glaciers worldwide since the early 2000s using satellite instruments. Calculating the difference in glacier area from 2005 and 2015, the total area loss in the past decade is 60.24 km², approximately 6 km² per year.

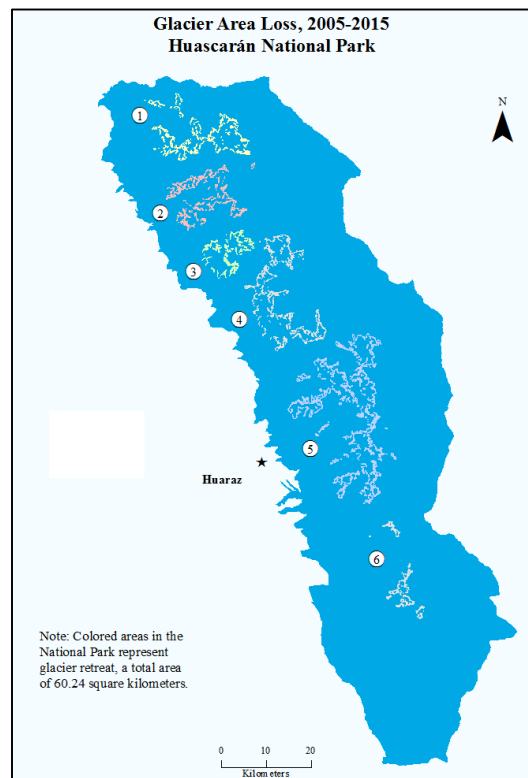


Figure 5.1. Huascarán National Park glacier loss. Total area of loss by glacier cluster. Source: Created by the author.

When the glacial edges from 2005 are mapped in respect to the DEM, the average elevation is just over 5,116 meters in 2005. When the same analysis was done for 2015, the average elevation was almost 5,289 meters. Within 10 years, that is an average of 173 meter elevation retreat of glaciers in the park.

Number	Glacier Loss (km²)	Percent Loss	Average eBC
1	7.343	9.038	5.921
2	9.162	13.187	7.007
3	6.611	11.663	11.106
4	9.887	8.609	-
5	23.591	13.112	17.244
6	3.641	23.230	-

Table 5.18. Glacier loss by cluster. Areas calculated from 2005 and 2015 GLIMS data

Although the previous analysis shows that eBC values are higher near Huaraz, glacier loss is not isolated to one specific area. As seen in Figure 5.1, glacier edges have retreated in all parts of Huascarán National Park. Table 5.18 shows glacier area lost based on mountain groups of the Cordillera Blanca. The locations of these groups are shown in Figure 5.1. When compared to aspect, over 33% of the areas that retreated had an eastern aspect, with a southern aspect close behind at over 25% (Table 5.19).

Retreat Aspect	Percent
North	23.882
East	33.352
South	25.611
West	17.155

Table 5.19 Retreat by aspect. Percentage of retreated glaciers based on aspect.

Chapter 6. Conclusions

Very little of the data allow for consistent conclusions applicable to all three years, but this may change as more data are collected every year. In the meantime, it's important to focus on what the data can already tell us. The two essential attributes examined in this study are effective black carbon and albedo. The only year that these two attributes had a moderate relationship was in 2011. The correlation was negative with significance at the 0.01 level. The relationship between eBC and albedo was negative for 2012 and 2013 as well, even though the correlation was weak. The fact that the relationship was negative means that increased eBC is lowering albedo values rather than raising them. If eBC becomes more abundant in coming years, we may see this relationship become more pronounced.

Other attributes did not significantly correlate with either albedo or eBC from any of the three years, so any changes in albedo or eBC are likely not occurring due to altitude or total mineral weight. The only year in which this does not hold true is 2011, when altitude had a moderate negative correlation with eBC values, though one year is not significant enough for a solid conclusion. Mineral analysis showed that albedo was only very weakly correlated with mineral weight, so the minerals found in snow do not decrease albedo. eBC correlations with minerals show that increases in albite, kaolinite, and annite can increase eBC values in snow samples.

Proximity analysis showed that distance to any of the mines did not have any significant correlation with individual mineral weights. Changes in these values cannot be attributed to their proximity to mining sites. Correlation showed that proximity to Huaraz did not affect individual mineral weights either, so minerals are sourced elsewhere

besides Huaraz and local mines. Possible sources that were not examined include smaller mining sites nearby, or deposition through wind and rain carried from farther sources.

Proximity to a mine does have an influence on eBC values, no matter which of the three mines were examined. There was a moderate negative correlation with eBC values for all mines, though the strongest was for the Pierina mine, just northwest of Huaraz. The total mineral weight was not correlated with proximity to the mines though, so mineral deposition is not coming from either of these mines nor affecting eBC values. Other dust particulates besides mineral dust are influencing eBC values. Albedo values were only weakly correlated with proximity to any of the mines.

Rather than proximity to mines, a sample's proximity to Huaraz has a bigger impact on eBC and albedo values. A negative correlation of at least moderate correlation occurred for eBC values in all three years. The amount of eBC found in a snow sample will increase the closer it is located to Huaraz, suggesting that this is the largest source of black carbon particulates for the Cordillera Blanca region. Proximity to Huaraz is also likely affecting albedo values, as 2011 and 2012 showed strong and moderate positive correlations, respectively. Glaciers have higher reflectance and lower eBC values the further they are from Huaraz.

Further aspect analysis shows that a sample's directional relationship to the mines does not influence mineral weight found in snow samples. This suggests that even wind blowing from different directions does not carry mineral dust to sample locations. Directionality did affect eBC values, though. A consistent moderate relationship for all three mines shows that when the sample's aspect faces the direction to the mine, eBC values will decrease further from the mine. A 90-degree directionality shows a strong

correlation with eBC, but only for the Antamina and Pierina mines. Huanzala is south of all samples, so wind from the south may not be depositing dust particulates on the glaciers. Aspect analysis for Huaraz showed similarly that directionality did not influence individual mineral weight, but all correlations with eBC were at least moderately correlated. No matter which direction the sample faces, eBC values decrease the further located from Huaraz.

Although mines are influencing eBC values, Huaraz seems to be the main culprit for glacial retreat. Huaraz is located to the south of over 84% of all samples. Glacier retreat shows that 26% of the areas that have retreat have a southern aspect, a higher percentage than any of the other aspects. As seen in Figure 5.1, location 5 is the closest glacial area to Huaraz. Over 23 km² of glacial area at that location was lost between 2005 and 2015, 13% of its total area. Samples taken in this glacial area also had the highest average eBC value over three years (Table 5.18). Albedo and eBC values were influenced by proximity to Huaraz as well. The next largest influence will most likely be Pierina, as its proximity to samples shows a higher correlation with eBC than the other mines. It is also the closest to Huaraz, and may be affecting the glacial melt in location 5. Huanzala to the south may also have an influence, as its correlations with eBC were still moderate. It is also located closest to location 6, which has experienced 23% glacial loss in the past 10 years. Antamina likely has the least impact of factors that influence glacial retreat.

It is important to note that while this research expands our understanding of glacial retreat, there are also improvements to be made. The number and location of samples taken can differ from year to year depending on timing and safety of the

expedition. Data cannot always be compared by location year to year for this reason, and certain areas will be underrepresented. Using correlation techniques such as IDW to cover these areas can result in unrealistic representations, but having more sample points can remedy this problem to a degree.

More can be done for the mineralogy scope of this research. Along with examining mining locations, particles from nearby dirt roads and soil samples should be collected and compared with the filters. The reflectance spectrum values of these particles might be affecting albedo values, and also could be a large part of particulate matter found on the filters. Mineral analysis of the filters may need refinement, as certain compounds could not be measured. The current X-ray diffraction method uses copper radiation, which causes samples containing iron to burn. Any samples with significant hematite were difficult to examine because of this problem. In the future, the X-ray diffraction could be used for certain minerals like albite and quartz, while an X-ray fluorescence analyzer could be used for iron content. These improvements would help ensure more accurate and precise data in future years, while building on what has already been collected.

References

- * Andreae, M.O., Ramanathan, V., 2013. Climate change. Climate's dark forcings. *Science* 340, 280–1.
- * Artaxo, P., Fernandes, E.T., Martins, J. V., Yamasoe, M. a., Hobbs, P. V., Maenhaut, W., Longo, K.M., Castanho, A., 1998. Large-scale aerosol source apportionment in Amazonia. *Journal of Geophysical Research* 103(D24), 31837-31847.
- * Bahadur, R., Feng, Y., Russell, L.M., Ramanathan, V., 2011. Impact of California's air pollution laws on black carbon and their implications for direct radiative forcing. *Atmospheric Environment* 45(5), 1162-1167.
- * Bahr, D.B., Pfeffer, W.T., Sassolas, C., Meier, M.F., 1998. Response time of glaciers as a function of size and mass balance: 1. Theory. *Journal of Geophysical Research: Solid Earth* 103(B5), 9777-9782.
- * Barnett, T.P., Adam, J.C., Lettenmaier, D.P., 2005. Potential impacts of a warming climate on water availability in snow-dominated regions. *Nature* 438, 303–9.
- * Bice, K., Eil, A., Habib, B., Heijmans, P., Kopp, R., 2009. *Black carbon: A review and policy recommendations*. Princeton, N.J.: Princeton University, Woodrow Wilson School of Public and International Affairs. Available online at: www.bobkopp.net/papers/pubs/Princeton2009-WWS-Black-Carbon-report.pdf.
- * Biello, D., 2009. How Will Warmer Oceans Affect Sea Life? *Scientific American*, August 25. Accessed February 28, 2016, at <http://www.scientificamerican.com/article/how-will-warmer-oceans-affect-sea-life/>.
- * Bindschadler, R., Dowdeswell, J., Hall, D., Winther, J.-G., 2001. Glaciological applications with Landsat-7 imagery: Early assessments. *Remote Sensing of*

Environment 78(1),163-179.

- * Bond, T., Doherty, S., 2013. Bounding the role of black carbon in the climate system: A scientific assessment. *Journal of Geophysical Research: Atmospheres* 118, 5380–5552.
- * Boulton, G., 1986. Push-moraines and glacier-contact fans in marine and terrestrial environments. *Sedimentology* 33(5), 677–698.
- * Bradley, R.S., Vuille, M., Diaz, H.F., Vergara, W., 2006. Climate change. Threats to water supplies in the tropical Andes. *Science* 312, 1755–6.
- * Carey, M., 2010. *In the Shadow of Melting Glaciers*. New York, NY: Oxford University Press.
- * Chang, K., 2010. *Introduction to Geographic Information Systems*, 6th edn. Boston, MA: McGraw Hill.
- * Clarke, A., Noone, K., 1985. Soot in the Arctic snowpack: A cause for perturbations in radiative transfer. *Atmospheric Environment* 19, 2045–2053.
- * Cohen, J., 1988. *Statistical Power Analysis for the Behavioral Sciences*, 2nd edn. Hillsdale, NJ: Lawrence Erlbaum Associates.
- * Doherty, S., Warren, S., 2009. *Black Carbon in Arctic Snow and its Effect on Surface Albedo*. Paper presented at the American Geophysical Union Fall Meeting, San Francisco, CA, December 14-18. Available online at:
<https://www.pnnl.gov/.../pdf/blackcarbon.pdf>.
- * Dozier, J., 1989. Spectral signature of alpine snow cover from the Landsat Thematic Mapper. *Remote Sensing of Environment* 22, 9–22.
- * Dumont, M., Gardelle, J., Sirguey, P., Guillot, A., Six, D., Rabatel, A., Arnaud, Y.,

2012. Linking glacier annual mass balance and glacier albedo retrieved from MODIS data. *Cryosphere* 6, 1527–1539.
- * Flanner, M.G., Zender, C.S., Randerson, J.T., Rasch, P.J., 2007. Present-day climate forcing and response from black carbon in snow. *Journal of Geophysical Research: Atmospheres* 112(D11202), DOI: 10.1029/2006JD008003.
- * Gao, J., Liu, Y., 2001. Applications of remote sensing, GIS and GPS in glaciology: a review. *Progress in Physical Geography* 25(4), 520–540.
- * Georges, C., 2004. 20th-century glacier fluctuations in the tropical Cordillera Blanca. Peru. *Arctic, Antarctic, and Alpine Research* 36(1), 100-107.
- * Hall, D.K., Riggs, G.A., 2007. Accuracy assessment of the MODIS snow products. *Hydrological Processes* 21(12), 1534-1547.
- * Hall, D.K., Salomonson, V.V., Riggs, G.A., 2006. *MODIS/Terra Snow Cover Daily L3 Global 500m Grid*. Boulder, CO: National Snow and Ice Data Center (Version 5.[Tile h09v04]).
- * Hambrey, M.J., Alean, J.C., 1992. *Glaciers*, 1st edn. Boston, MA: Cambridge University Press.
- * Hegg, D.A., Warren, S.G., Grenfell, T.C., Doherty, S.J., Larson, T. V., Clarke, A.D., 2009. Source Attribution of Black Carbon in Arctic Snow. *Environmental Science & Technology* 43(11), 4016-4021.
- * IPCC (Intergovernmental Panel on Climate Change), 2007. Summary for Policymakers. In Solomon, S., Qin, D., Manning, M., Chen, Z., Marquis, M., Averyt, K.B., Tignor, M., Miller, H.L. (eds.) *Climate Change 2007: The Physical Science Basis. Contribution of Working Group I to the Fourth Assessment Report of the*

Intergovernmental Panel on Climate Change. Cambridge, U.K.: Cambridge University Press.

- * IPCC (Intergovernmental Panel on Climate Change), 2013. Summary for Policymakers. In Stocker, T.F., Qin, D., Plattner, G-K, Tignor, M., Allen, S.K., Boschung, J., Nauels, A., Xia, Y., Bex, V., Midgley, P.M. (eds.) *Climate Change 2013: The Physical Science Basis. Contribution of Working Group I to the Fifth Assessment Report of the Intergovernmental Panel on Climate Change*. Cambridge, U.K.: Cambridge University Press.
- * IPCC (Intergovernmental Panel on Climate Change), 2014. Summary for Policymakers. In Edenhofer, O., Pichs-Madruga, R., Sokona, Y., Farahani, E., Kadner, S., Seyboth, K., Adler, A., Baum, I., Brunner, S., Eickemeier, P., Kriemann, B., Savolainen, J., Schlömer, S., von Stechow, C., Zwickel, T., Minx, J.C. (eds.) *Climate Change 2014, Mitigation of Climate Change. Contribution of Working Group III to the Fifth Assessment Report of the Intergovernmental Panel on Climate Change*. Cambridge, U.K.: Cambridge University Press.
- * Jensen, J.R., 2007. *Remote Sensing of the Environment: An Earth Resource Perspective*, 2nd edn. New York, NY: Prentice Hall.
- * Kaser, G., Georges, C., 1997. Changes of the equilibrium-line altitude in the tropical Cordillera Bianca, Peru, 1930-50, and their spatial variations. **Annals of Glaciology** 24. 344-349
- * Kaser, G., Ames, A., Zamora, M., 1990. Glacier fluctuations and climate in the Cordillera Blanca. *Annals of Glaciology* 14, 136-140.

- * Kennedy, C., 2015. *2014 State of the Climate: Ocean Heat Content*. Washington, D.C.: NOAA. Accessed February 28, 2016, at <https://www.climate.gov/news-features/understanding-climate/2014-state-climate-ocean-heat-content>.
- * Kim, J.J., Smorodinsky, S., Lipsett, M., Singer, B.C., Hodgson, A.T., Ostro, B., 2004. Traffic-related air pollution near busy roads: The East Bay Children's Respiratory Health Study. *American Journal of Respiratory and Critical Care Medicine* 170, 520–526.
- * Knap, W., Reijmer, C., Oerlemans, J., 1999. Narrowband to broadband conversion of Landsat TM glacier albedos. *International Journal of Remote Sensing* 20, 2091–2110.
- * Knight, J., Harrison, S., 2014. Mountain glacial and paraglacial environments under global climate change: lessons from the past, future directions and policy implications. *Geografiska Annaler: Series A* 96, 245–264.
- * Lashof, D.A., Ahuja, D.R., 1990. Relative contributions of greenhouse gas emissions to global warming. *Nature* 344, 529–531.
- * Le Bail, A., 2005. Whole powder pattern decomposition methods and applications: A retrospection. *Powder Diffraction* 20(4), 316-326.
- * Le Treut, H., Somerville, R., Cubasch, U., Ding, Y., Mauritzen, C., Mokssit, A., Peterson, T., Prather, M., 2007. Historical Overview of Climate Change. In Solomon, S., Qin, D., Manning, M., Chen, Z., Marquis, M., Averyt, K.B., Tignor, M., Miller, H.L. (eds.) *Climate Change 2007: The Physical Science Basis. Contribution of Working Group I to the Fourth Assessment Report of the Intergovernmental Panel on Climate Change* Cambridge, U.K.: Cambridge

University Press.

- * Leake, J., 2011. *Research into black carbon*. London, U.K.: National Meteorological Office. Accessed August 12, 2014, at:
<http://www.metoffice.gov.uk/barometer/guest-articles/jonathan-leake>.
- * Lelieveld, J., Berresheim, H., Borrmann, S., Crutzen, P.J., Dentener, F.J., Fischer, H., Feichter, J., Flatau, P.J., Heland, J., Holzinger, R., Korrman, R., Lawrence, M.G., Levin, Z., Markowicz, K.M., Mihalopoulos, N., Minikin, A., Ramanathan, V., De Reus, M., Roelofs, G.J., Scheeren, H. a, Sciare, J., Schlager, H., Schultz, M., Siegmund, P., Steil, B., Stephanou, E.G., Stier, P., Traub, M., Warneke, C., Williams, J., Ziereis, H., 2002. Global air pollution crossroads over the Mediterranean. *Science* 80(298), 794–799.
- * Lemke, P., Ren, J., Alley, R.B., Allison, I., Carrasco, J., Flato, G., Fujii, Y., Kaser, G., Mote, P., Thomas, R.H., Zhang, T., 2007. Observations: Changes in Snow, Ice and Frozen Ground. In Solomon, S., Qin, D., Manning, M., Chen, Z., Marquis, M., Averyt, K.B., Tignor, M., Miller, H.L. (eds.) *Climate Change 2007: The Physical Science Basis. Contribution of Working Group I to the Fourth Assessment Report of the Intergovernmental Panel on Climate Change* Cambridge, U.K.: Cambridge University Press.
- * Marengo, J.A., Ambrizzi, T., da Rocha, R.P., Alves, L.M., Cuadra, S.V., Valverde, M.C., Torres, R.R., Santos, D.C., Ferraz, S.E.T., 2009. Future change of climate in South America in the late twenty-first century: intercomparison of scenarios from three regional climate models. *Climate Dynamics* 35, 1073–1097.
- * Mark, B.G., Seltzer, G.O., 2005. Evaluation of recent glacier recession in the Cordillera

- Blanca, Peru (AD 1962–1999): spatial distribution of mass loss and climatic forcing. *Quaternary Science Reviews* 24(20), 2265-2280.
- * Mark, B., Bury, J., McKenzie, J., 2010. Climate change and tropical Andean glacier recession: evaluating hydrologic changes and livelihood vulnerability in the Cordillera Blanca, Peru. *Annals of the Association of American Geographers* 100, 794–805.
- * McIntosh, P. 2012. Exploring the Horizon of Geospatial Imagery Analysis. *Earth Imaging Journal* (online). Accessed August 10, 2014, at: <http://ejournal.com/print/articles/exploring-the-horizon-of-geospatial-imagery-analysis>.
- * Monroe, R., 2008. *Black Carbon Pollution Emerges As Major Player In Global Warming*. San Diego, CA: University of California - San Diego News Center, March 24. Available online at: <http://ucsdnews.ucsd.edu/archive/newsrel/science/03-08BlackCarbonPollution.asp>.
- * O’Sullivan, D., Unwin, D.J., 2003. *Geographic Information Analysis*, 1st edn. Hoboken, NJ: John Wiley & Sons, Inc.,
- * Painter, T., Flanner, M., Kaser, G., Marzeion, B., VanCuren, R.A., Abdalati, W., 2013. End of the Little Ice Age in the Alps forced by industrial black carbon. *Proceedings of the National Academy of Sciences*. 110(38), 15216-15221.
- * Paterson, W.S.B., 1994. *The Physics of Glaciers*, 3rd ed. Oxford, U.K.: Elsevier.
- * Poppe, L.J., Paskevich, V.F., Hathaway, J.C., Blackwood, D.S., 2001. *A Laboratory Manual for X-Ray Powder Diffraction - Illite Group*. Alexandria, VA: U.S.G.S.

Available online at: <http://pubs.usgs.gov/of/2001/of01-041/htmldocs/clays/illite.htm>.

- * Quincey, D.J., Lucas, R.M., Richardson, S.D., Glasser, N.F., Hambrey, M.J., Reynolds, J.M., 2005. Optical remote sensing techniques in high-mountain environments: application to glacial hazards. *Progress in Physical Geography* 29, 475–505.
- * Rabatel, A., Dedieu, J.-P., Vincent, C., 2005. Using remote-sensing data to determine equilibrium-line altitude and mass-balance time series: validation on three French glaciers, 1994–2002. *Journal of Glaciology* 51, 539–546.
- * Rabatel, A., Francou, B., Soruco, A., Gomez, J., Cáceres, B., Ceballos, J.L., Basantes, R., Vuille, M., Sicart, J.-E., Huggel, C., Scheel, M., Lejeune, Y., Arnaud, Y., Collet, M., Condom, T., Consoli, G., Favier, V., Jomelli, V., Galarraga, R., Ginot, P., Maisincho, L., Mendoza, J., Ménégoz, M., Ramirez, E., Ribstein, P., Suarez, W., Villacis, M., Wagnon, P., 2013. Current state of glaciers in the tropical Andes: a multi-century perspective on glacier evolution and climate change. *The Cryosphere* 7, 81–102.
- * Racoviteanu, A., Arnaud, Y., Williams, M.W., Ordonez, J., 2008. Decadal changes in glacier parameters in the Cordillera Blanca, Peru, derived from remote sensing. *Journal of Glaciology* 54, 499–510.
- * Ralph, J., 2015. *Annite mineral information and data*. Peekskill, NY: Hudson Institute of Mineralogy. Accessed February 14, 2015, at: <http://www.mindat.org/min-241.html>.
- * Ramanathan, V., Carmichael, G., 2008. Global and regional climate changes due to black carbon. *Nature Geoscience* 1(4), 221–227.

- * Raup, B., Racoviteanu, A., Khalsa, S.J.S., Helm, C., Armstrong, R., Arnaud, Y., 2007. The GLIMS geospatial glacier database: A new tool for studying glacier change. *Global and Planetary Change* 56, 101–110.
- * Rees, W.G. (ed.), 2009. *Remote Sensing of Glaciers: Techniques for Topographic, Spatial and Thematic Mapping of Glaciers*. London, U.K.: Taylor & Francis.
- * Reznichenko, N., Davies, T., 2010. Effects of debris on ice-surface melting rates: an experimental study. *Journal of Glaciology* 56(197), 384–394.
- * Richardson, S., Reynolds, J., 2000. Degradation of ice-cored moraine dams: implications for hazard development. *International Association of Hydrological Sciences Publication* 264, 187-198.
- * Rocchio, L., 2016. *Landsat 1*. Washington, D.C.: NASA. Accessed February 28, 2014, at: <http://landsat.gsfc.nasa.gov/?p=3172>.
- * Rosenthal, E., 2009. Third-World Stove Soot Is Target in Climate Fight. *New York Times*, April 16. Accessed October 20, 2014 at: http://www.nytimes.com/2009/04/16/science/earth/16degrees.html?_r=2&ref=global-home&.
- * Roshani, N., Zouj, M.J.V., Rezaei, Y., Nikfar, M., 2007. Snow Mapping of Alamchal Glacier Using Remote Sensing Data. *The International Archives of the Photogrammetry, Remote Sensing and Spatial Information Sciences* 37(2), 805-808.
- * Rosok, K., 2007. *Quartz - Silica Group of Silicate Minerals*. Minneapolis/St. Paul, MN: Univeristy of Minnesota. Accessed February 28, 2016, at: <https://www.esci.umn.edu/courses/1001/minerals/quartz.shtml#society>.
- * Rott, H., Nagler, T., Malcher, P., Bippus, G., 2007. *Modelling mass balance of glaciers using satellite data*. In Proceeding of the Envisat Symposium, Montreux,

Switzerland, April 23–27. Available online at:

<https://earth.esa.int/workshops/envisatsymposium/proceedings/sessions/4F1/452961ro.pdf>.

- * Salzmann, N., Huggel, C., Rohrer, M., Silverio, W., Mark, B.G., Burns, P., Portocarrero, C., 2013. Glacier changes and climate trends derived from multiple sources in the data scarce Cordillera Vilcanota region, southern Peruvian Andes. *The Cryosphere* 7, 103–118.
- * Schauwecker, S., Rohrer, M., Acuña, D., Cochachin, A., Dávila, L., Frey, H., Giráldez, C., Gómez, J., Huggel, C., Jacques-Coper, M., Loarte, E., Salzmann, N., Vuille, M., 2014. Climate trends and glacier retreat in the Cordillera Blanca, Peru, revisited. *Global and Planetary Change* 119, 85–97.
- * Schmidt, C.W., 2011. Black carbon: the dark horse of climate change drivers. *Environmental Health Perspectives* 119, A172–5.
- * Schmitt, C., All, J., Cole, R., 2014a Linking remote and in-situ detection of black carbon on tropical glaciers. *Photogrammetric Engineering and Remote Sensing* 80(5), 385-390.
- * Schmitt, C.G., All, J.D., Schwarz, J.P., Arnott, W.P., Cole, R.J., Lapham, E., Celestian, A., 2014b. Measurements of light absorbing particulates on the glaciers in the Cordillera Blanca, Peru. *Measurements* 8, 5077-5103.
- * Shrestha, G., Traina, S., Swanston, C., 2010. Black carbon's properties and role in the environment: A comprehensive review. *Sustainability* 2, 294–320.
- * Somerville, H., 2011. Glacier melt in Peru becomes more than a climate issue. *Washington Post*, January 16. Accessed August 12, 2014, at:

<http://www.washingtonpost.com/wp-dyn/content/article/2011/01/16/AR2011011604900.html>

- * Tyagi, A., Singh, P., 2013. Applying Kriging Approach on Pollution Data Using GIS Software. *International Journal of Environmental Engineering and Management* 4(3), 185-190.
- * USGS (U.S. Geological Survey), 2014. *MCD43A3 | LP DAAC :: NASA Land Data Products and Services*. Alexandria, VA: USGS. Accessed on November 1, 2014, at: https://lpdaac.usgs.gov/products/modis_products_table/mcd43a3.
- * Underhill, L.J., Bose, S., Williams, D.L., Romero, K.M., Malpartida, G., Breyse, P.N., Klasen, E.M., Combe, J.M., Checkley, W., Hansel, N.N., 2015. Association of roadway proximity with indoor air pollution in a Peri-urban community in Lima, Peru. *International Journal of Environmental Research and Public Health* 12(10), 13466-13481.
- * Vaughan, D.G., Comiso, J.C., Allison, I., Carrasco, J., Kaser, G., Kwok, R., Mote, P., Murray, T., Paul, F., Ren, J., Rignot, E., Solomina, O., Steffen, K. Zhang, T., 2013. Observations: Cryosphere. In Stocker, T.F., Qin, D., Plattner, G-K, Tignor, M., Allen, S.K., Boschung, J., Nauels, A., Xia, Y., Bex, V., Midgley, P.M. (eds.) *Climate Change 2013: The Physical Science Basis. Contribution of Working Group I to the Fifth Assessment Report of the Intergovernmental Panel on Climate Change*. Cambridge, U.K: Cambridge University Press.
- * Vuille, M., Bradley, R., Keimig, F., 2000. Climate variability in the Andes of Ecuador and its relation to tropical Pacific and Atlantic sea surface temperature anomalies. *Journal of Climate* 13, 2520–2535.

- * Vuille, M., Francou, B., Wagnon, P., Juen, I., Kaser, G., Mark, B.G., Bradley, R.S., 2008. Climate change and tropical Andean glaciers: Past, present and future. *Earth-Science Reviews* 89, 79–96.
- * Warren, S., Wiscombe, W., 1985. Dirty snow after nuclear war. *Nature* 313(6002), 467-470.
- * Zimmer, C., 2013. Black Carbon and Warming: It's Worse than We Thought. *Yale Environment* 360. Available online at:
http://e360.yale.edu/feature/carl_zimmer_black_carbon_and_global_warming_worse_than_thought/2611/
- * Zimmermann, H., Renison, D., Leyer, I., Hensen, I., 2009. Do we need livestock grazing to promote *Polylepis australis* tree recruitment in the Central Argentinean Mountains? *Ecological Research* 24, 1075–1081.

APPENDIX A: Maps

Figure A1

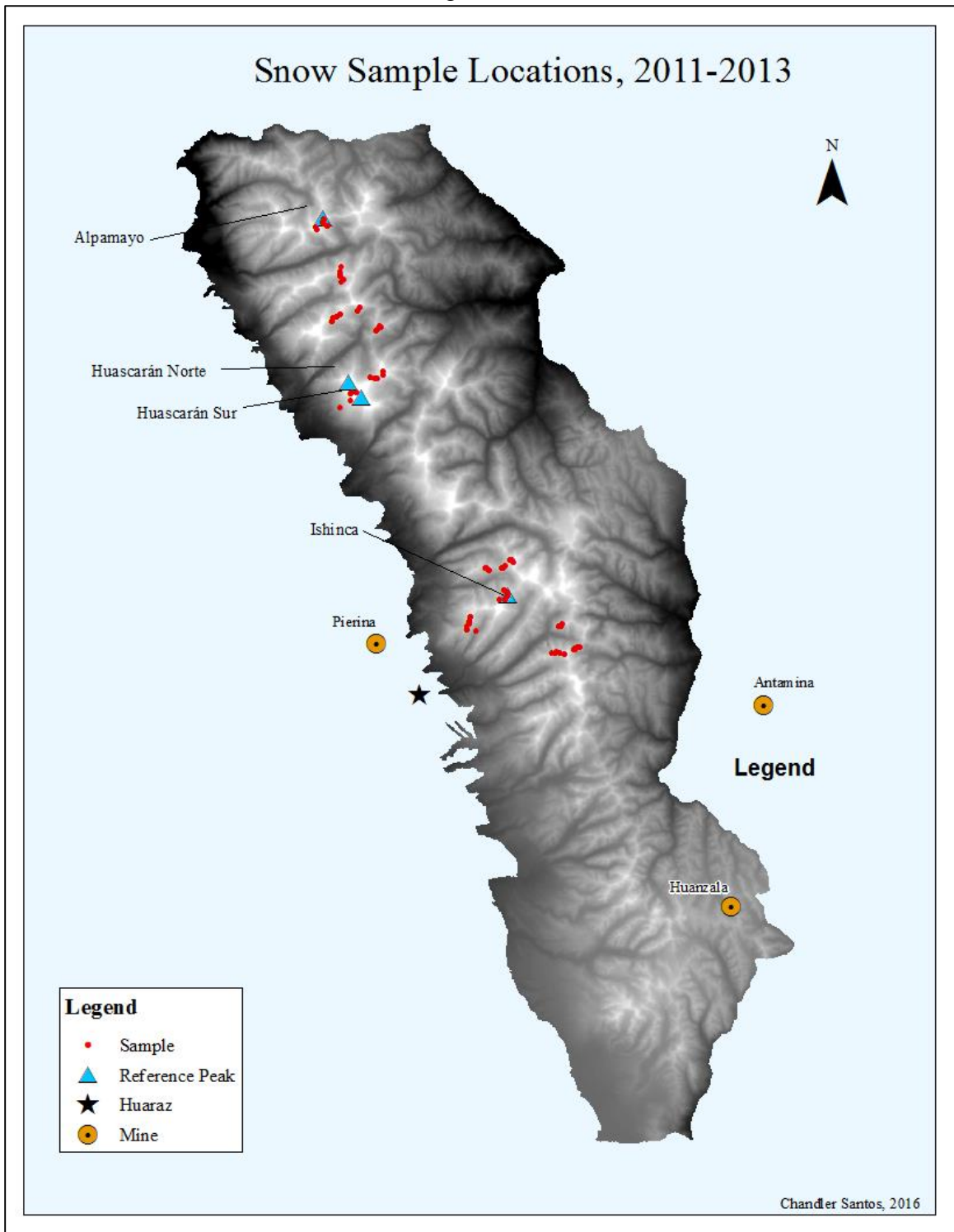


Figure A2

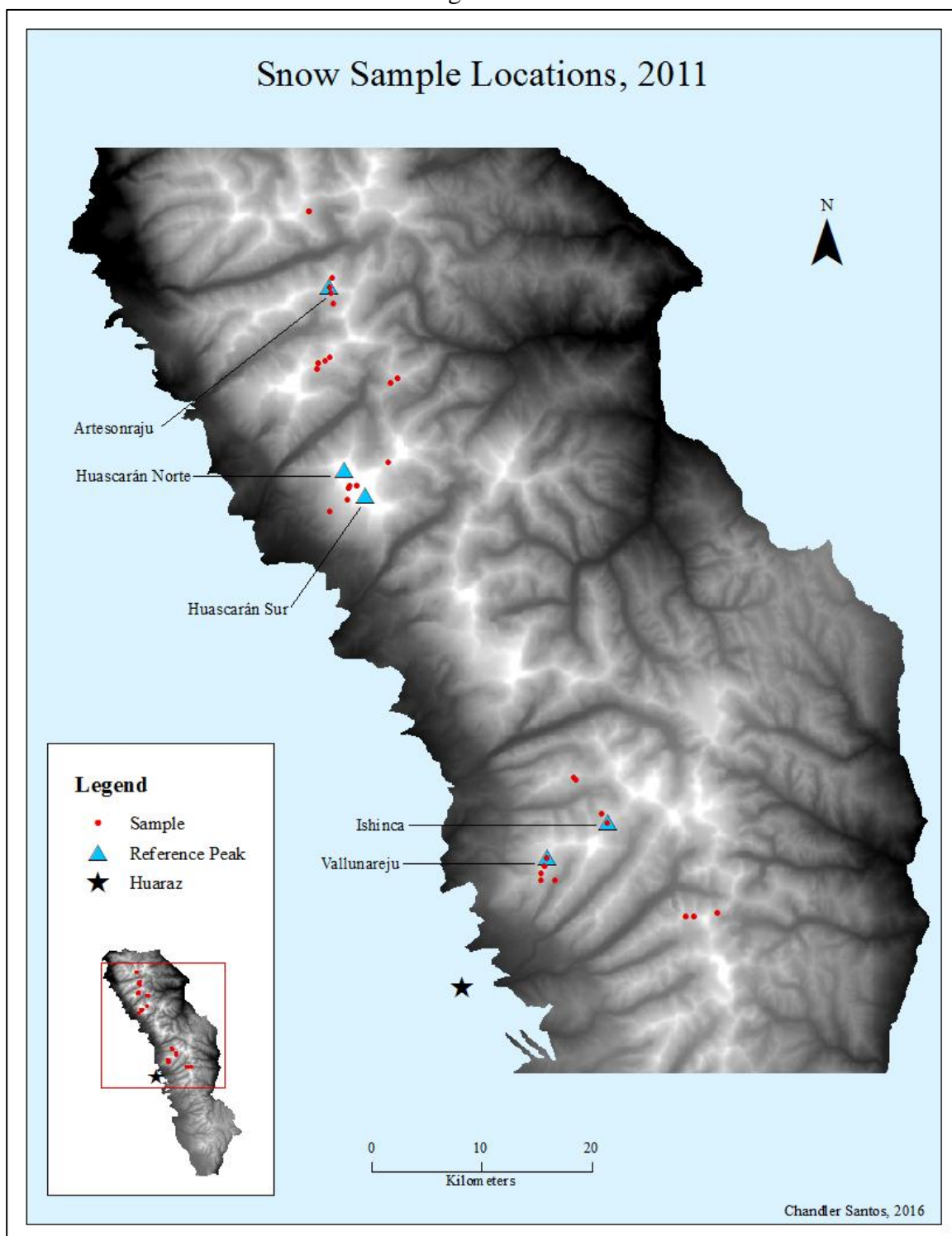


Figure A3

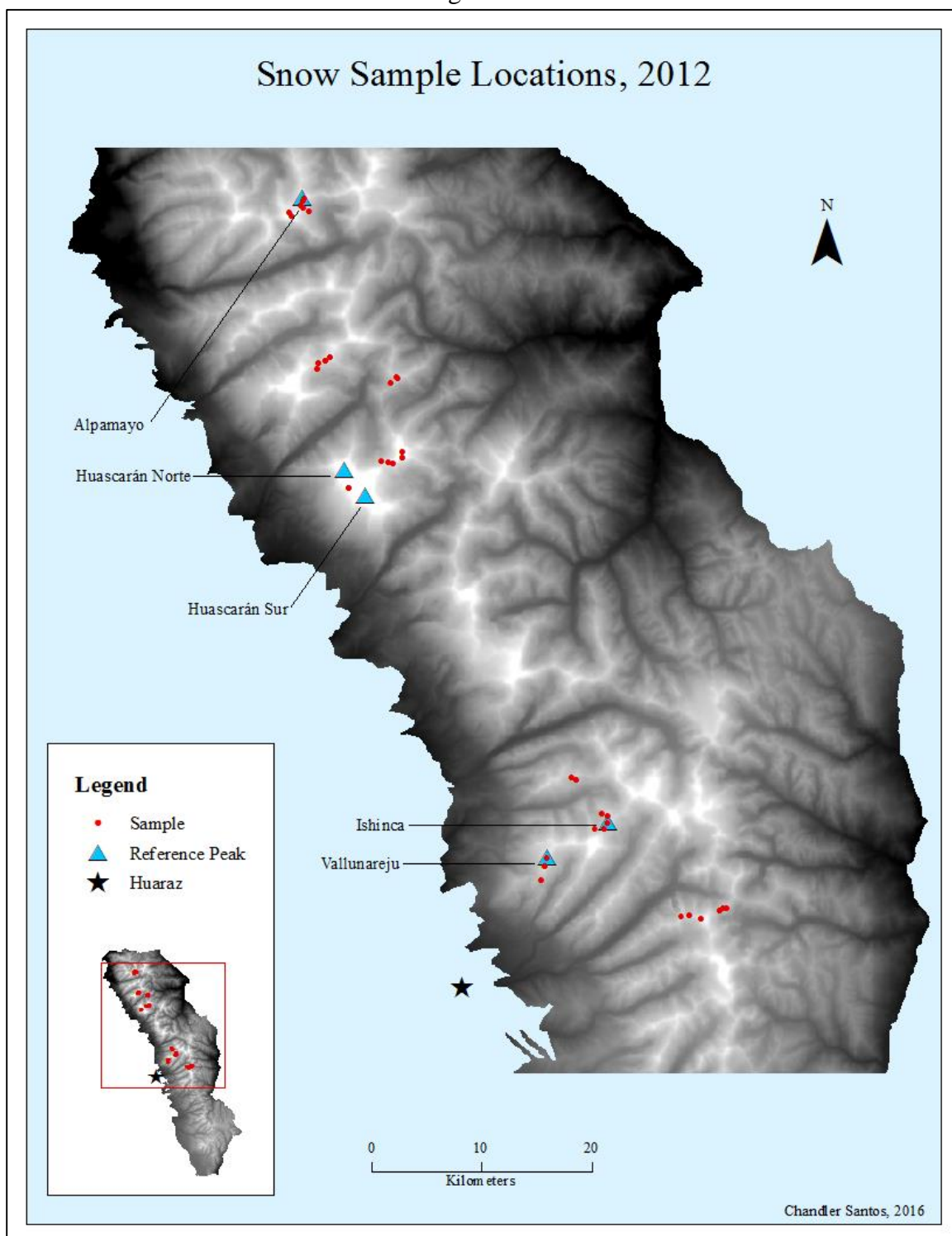


Figure A4

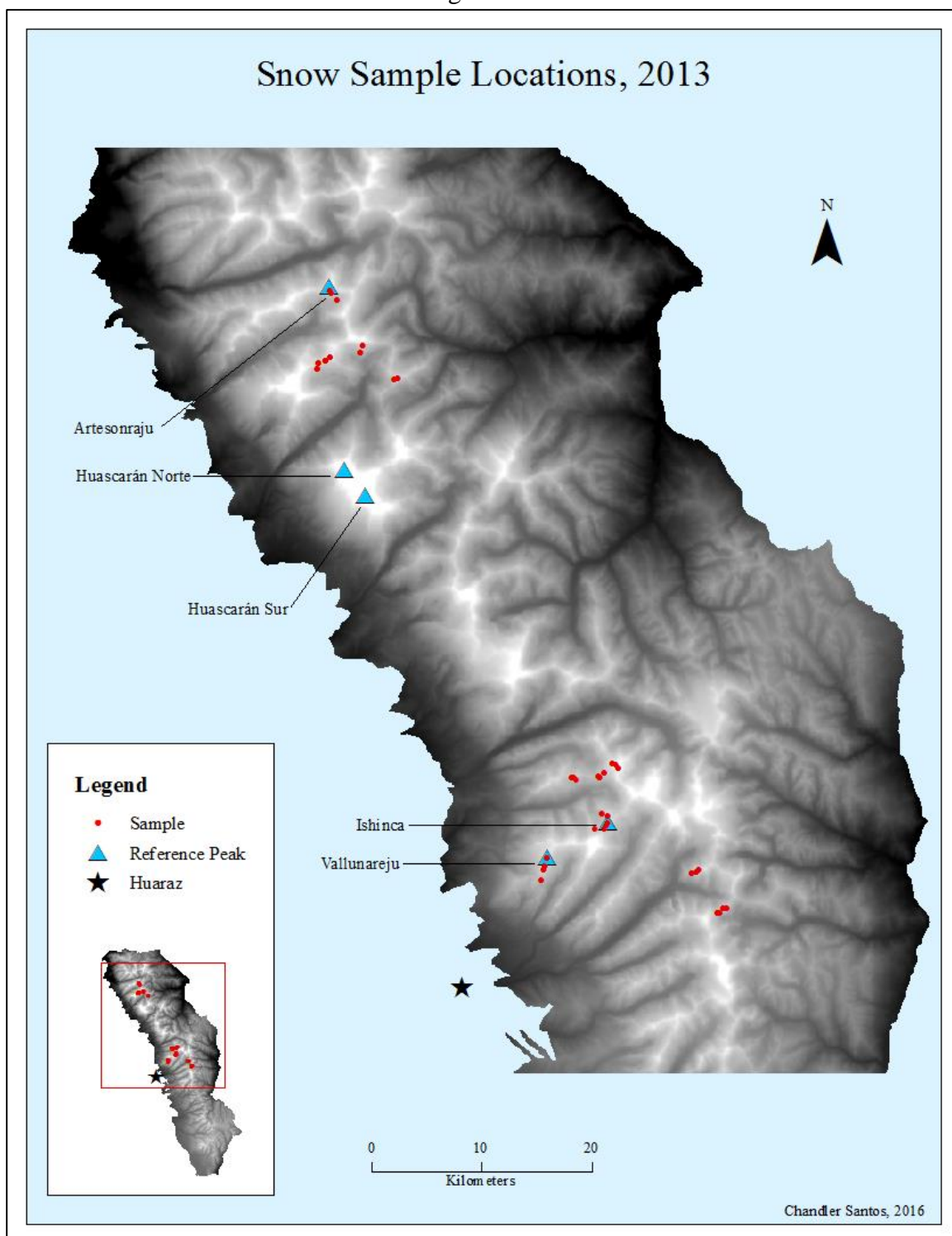


Figure A5

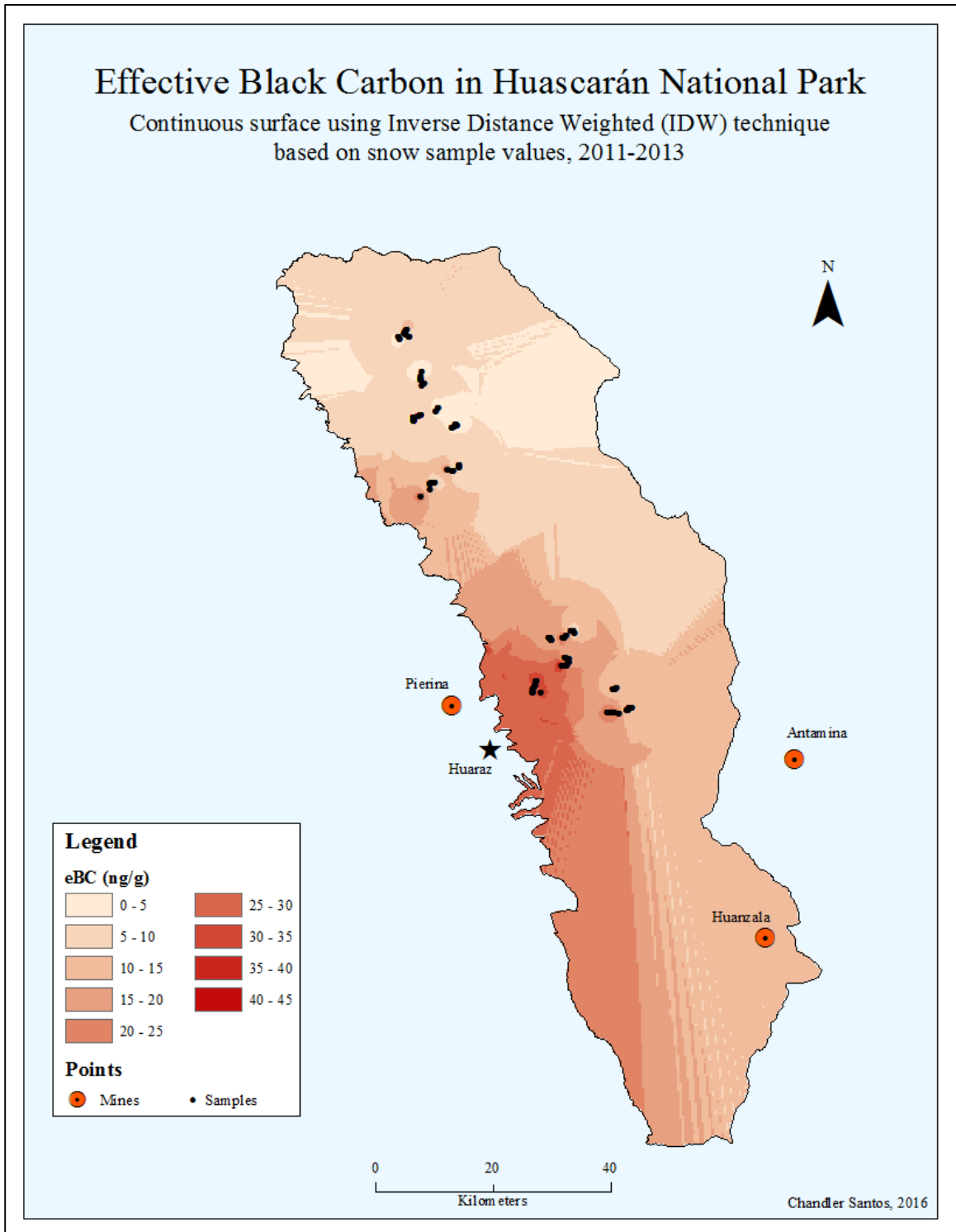


Figure A6

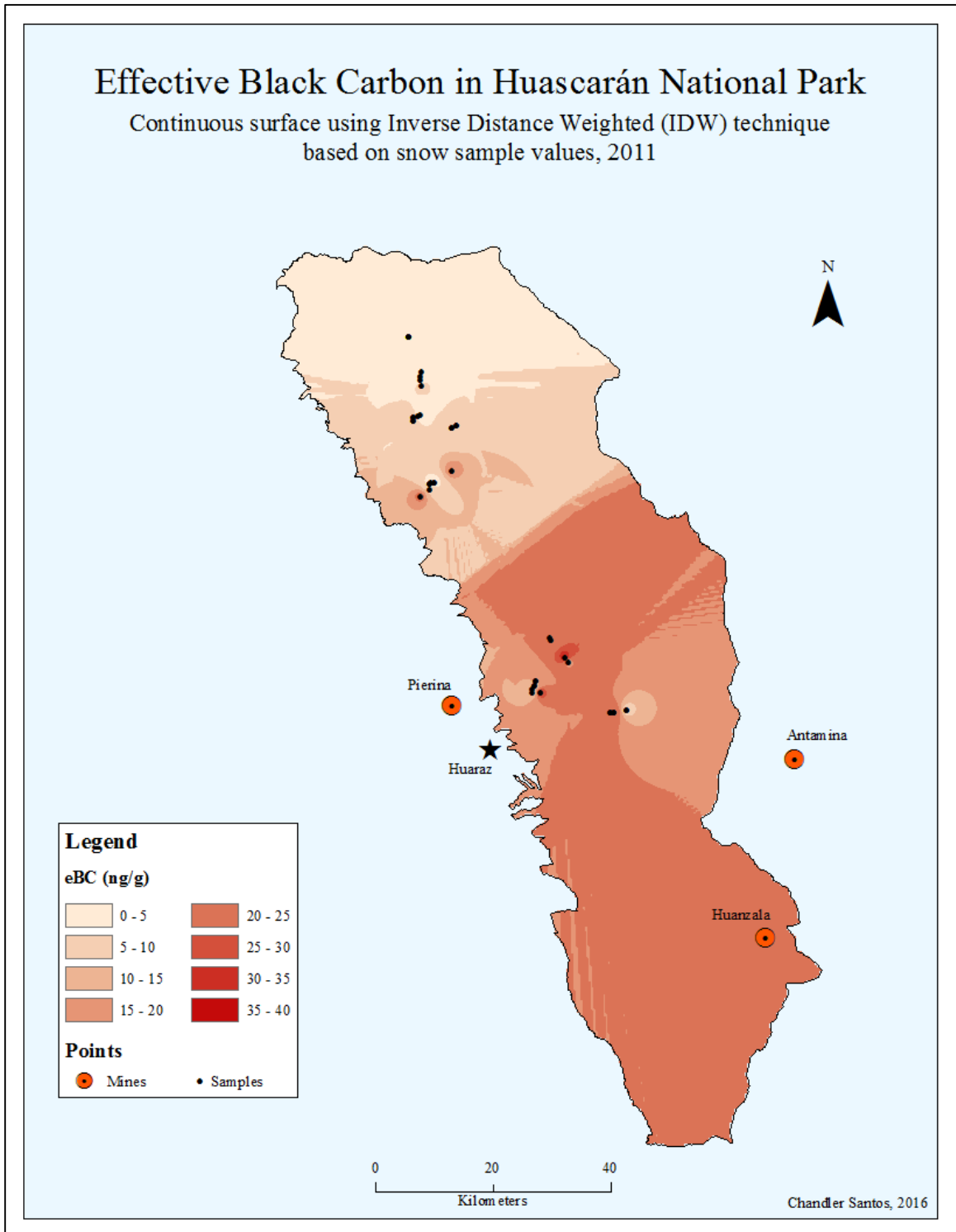


Figure A7

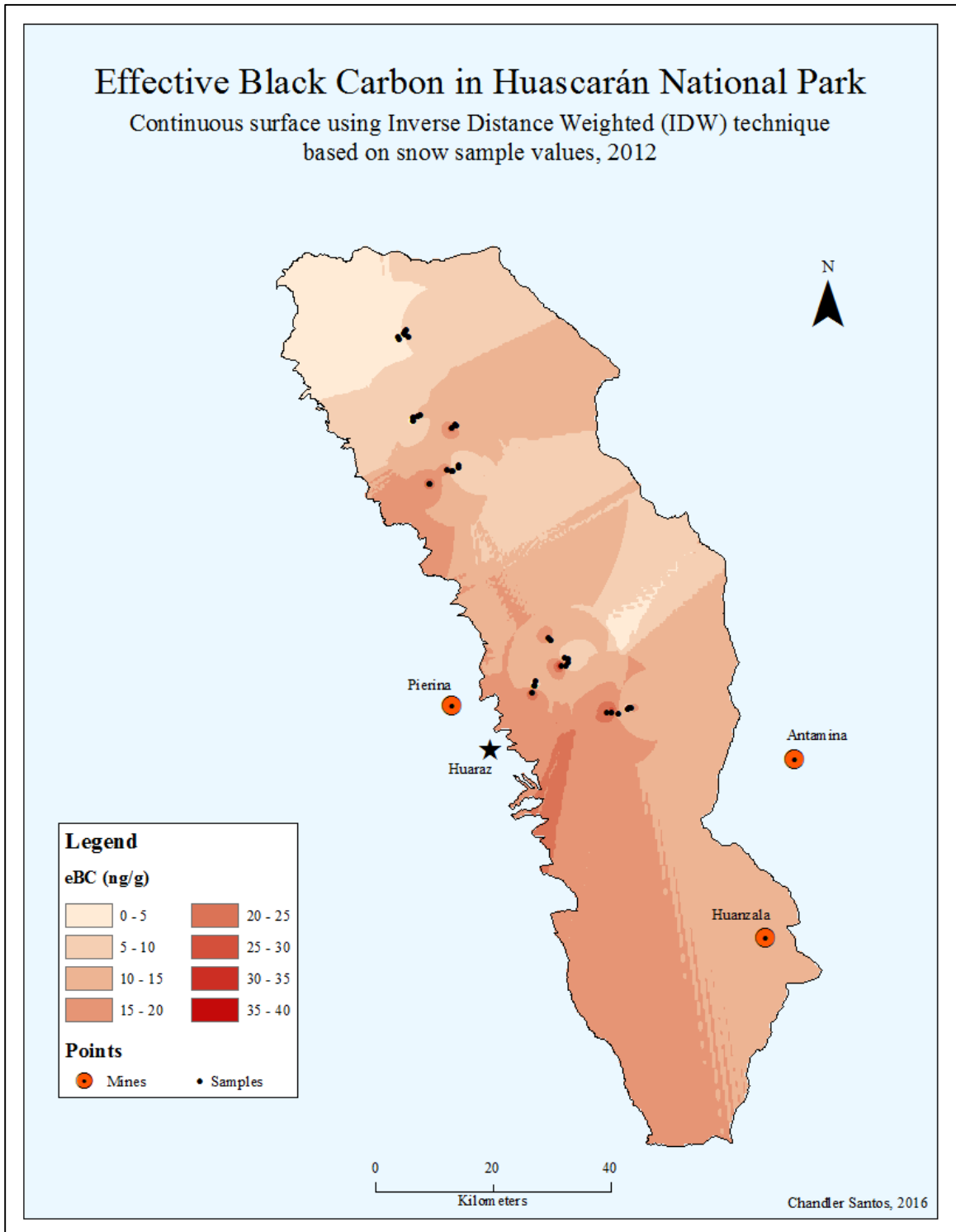


Figure A8

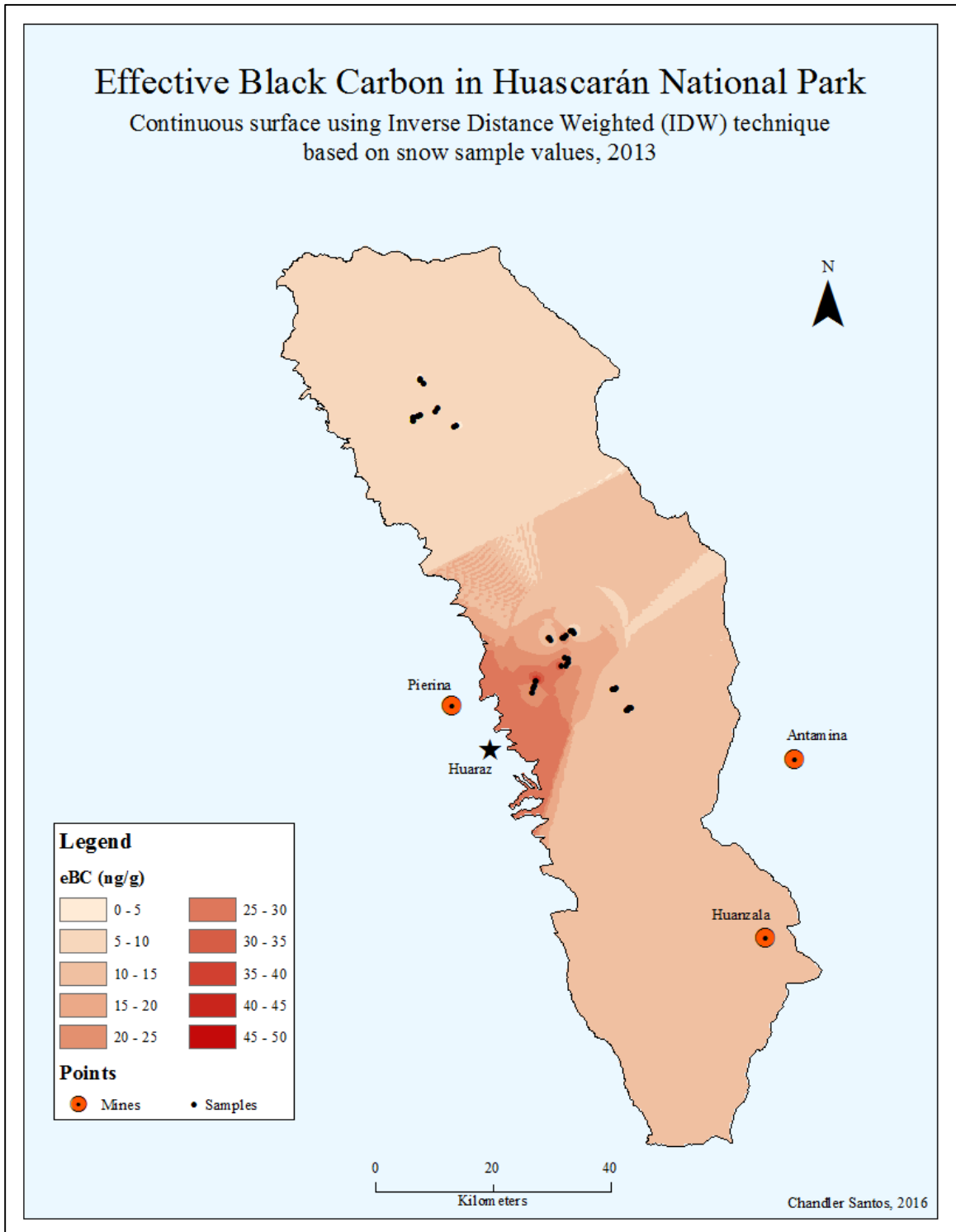


Figure A9

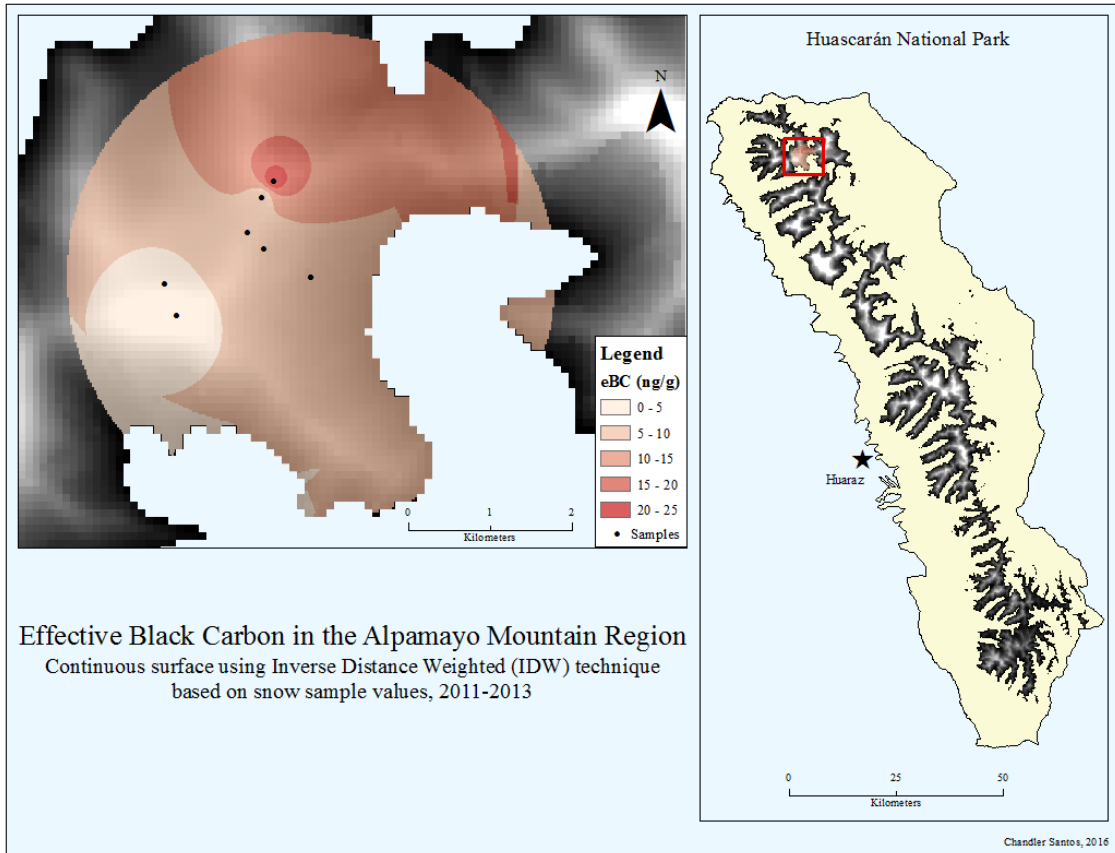


Figure A10

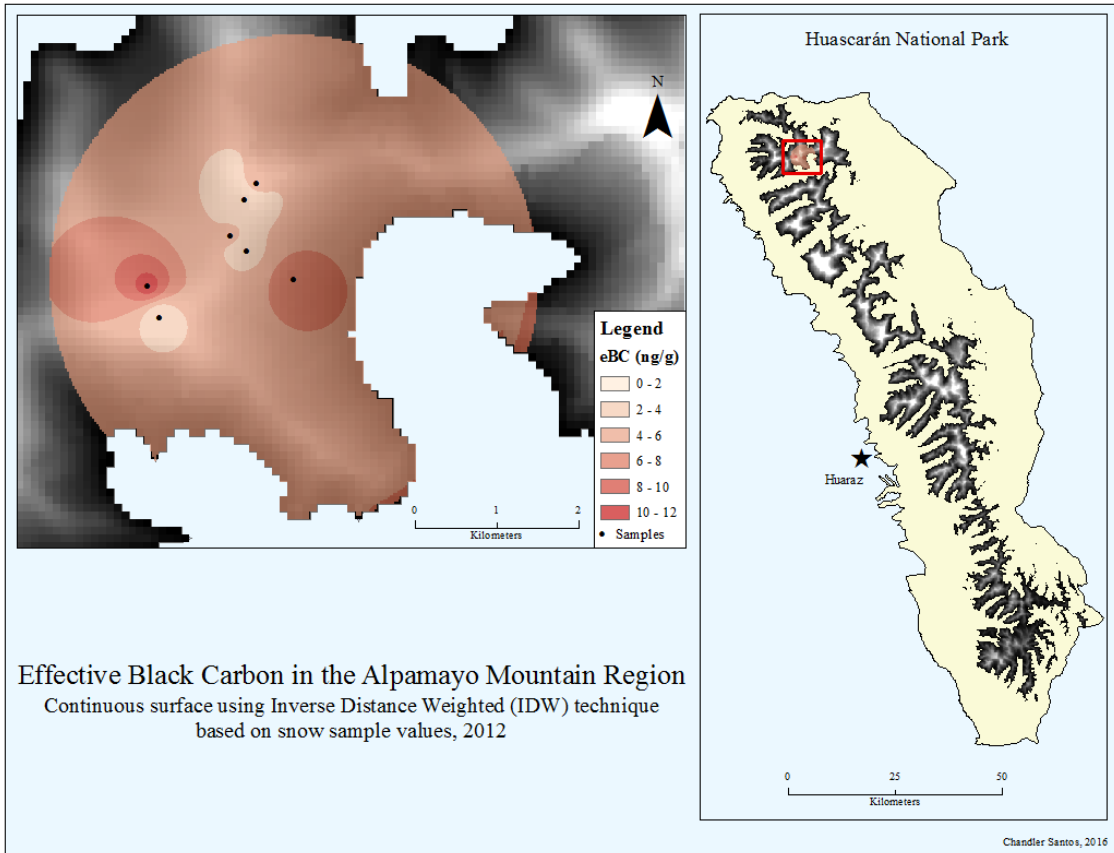


Figure A11

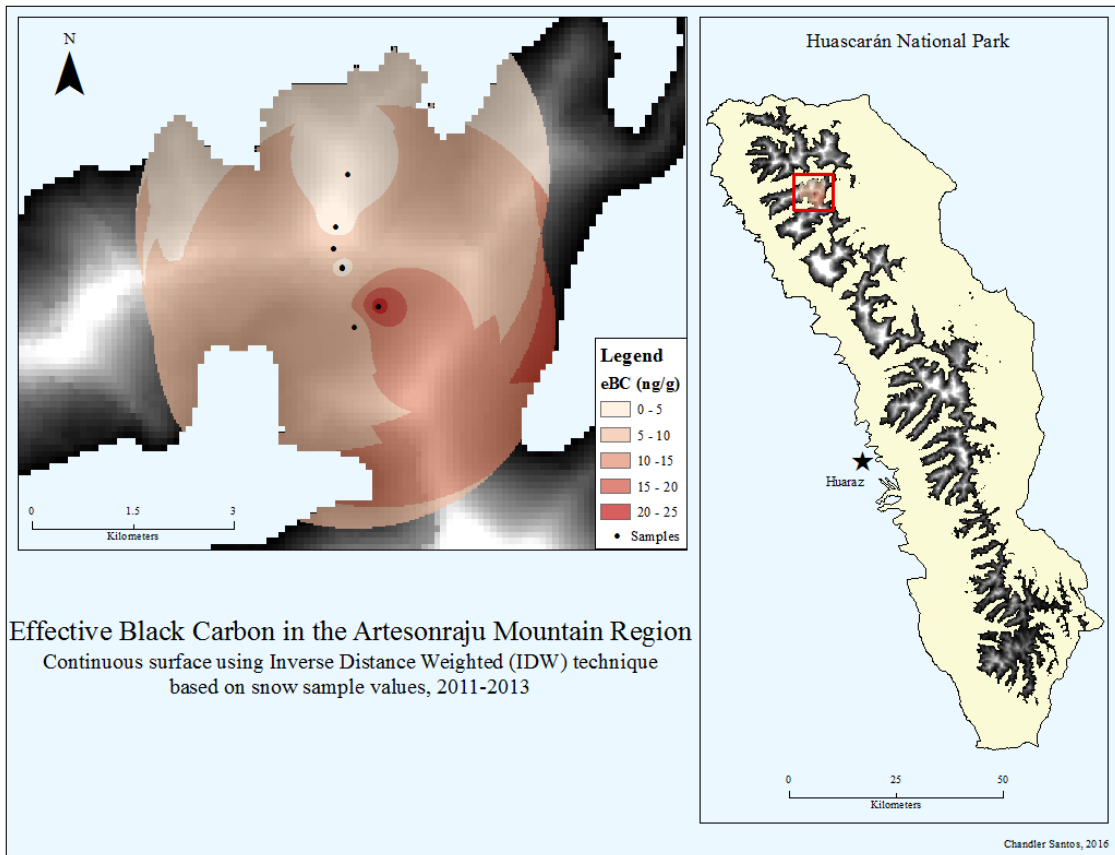


Figure A12

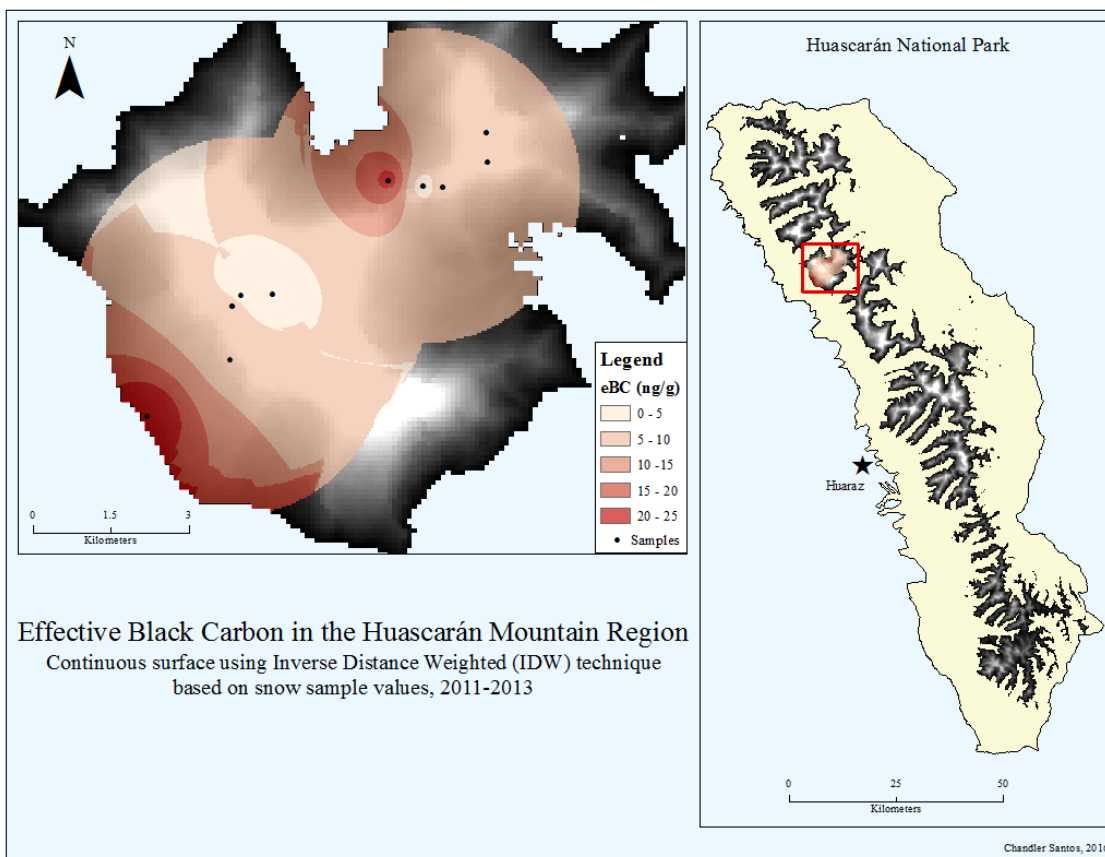


Figure A13

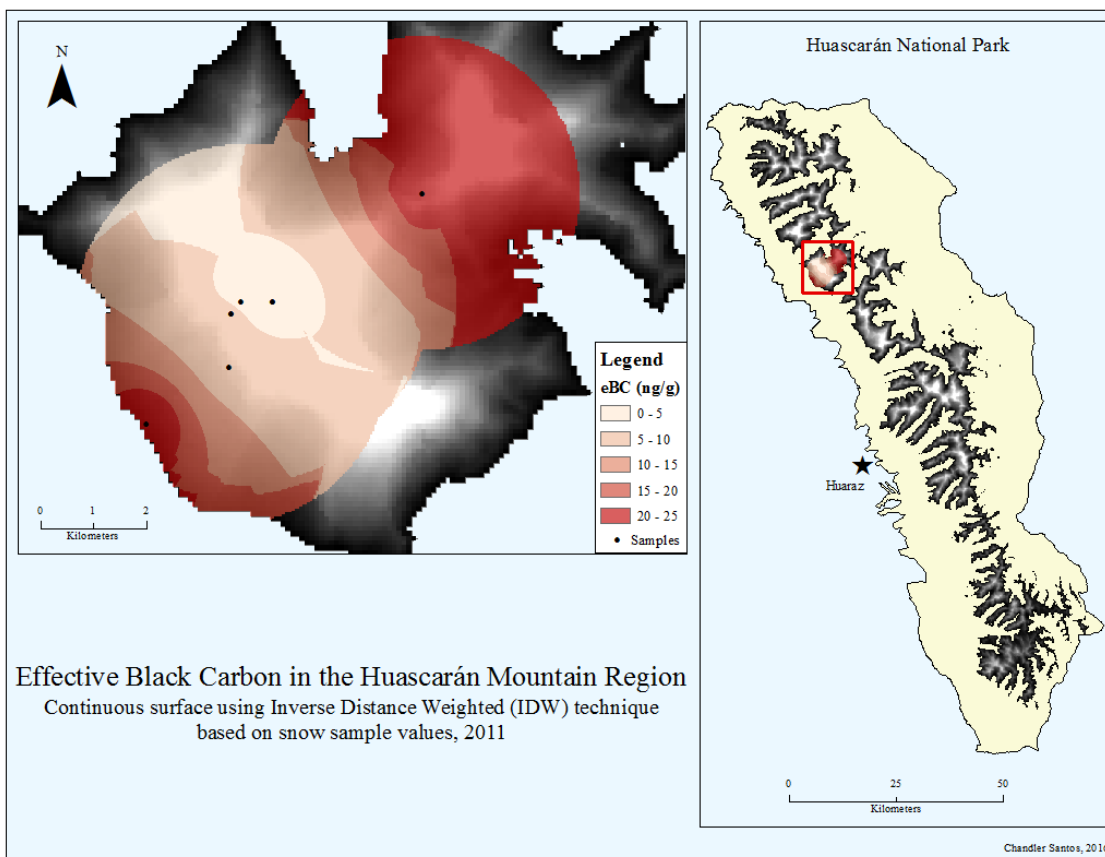


Figure A14

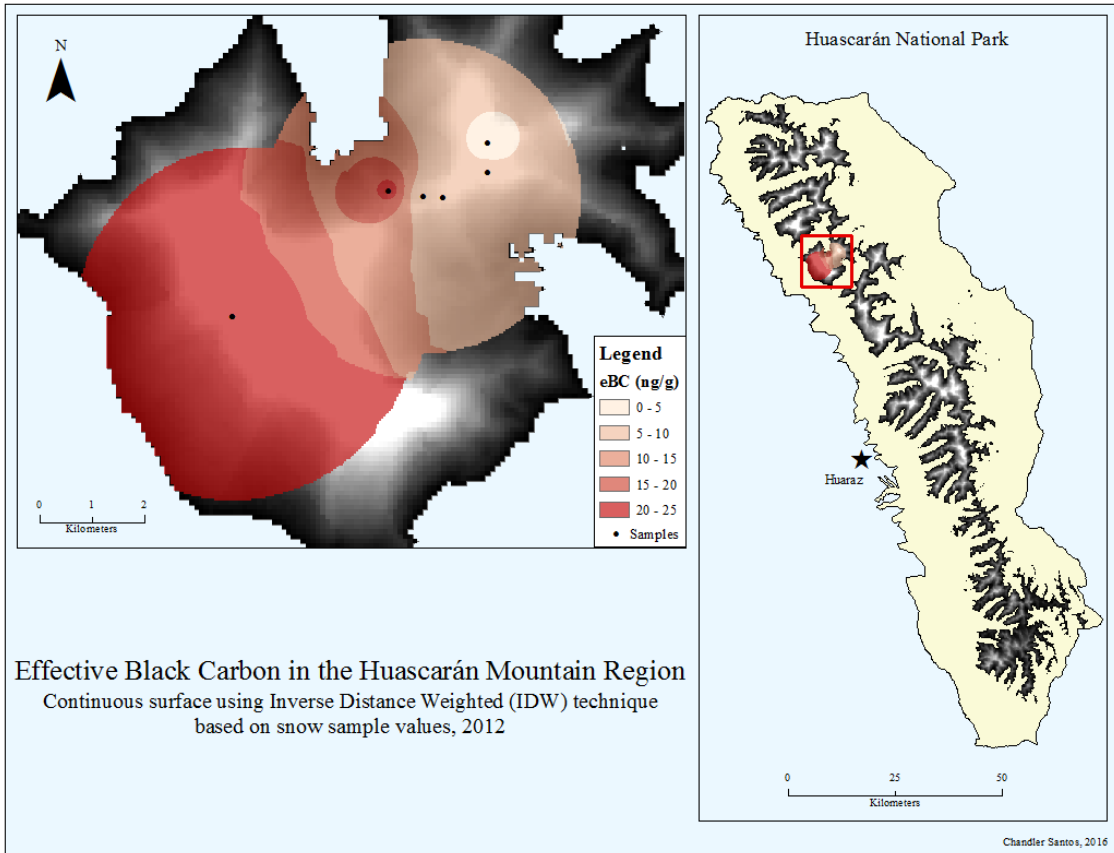


Figure A15

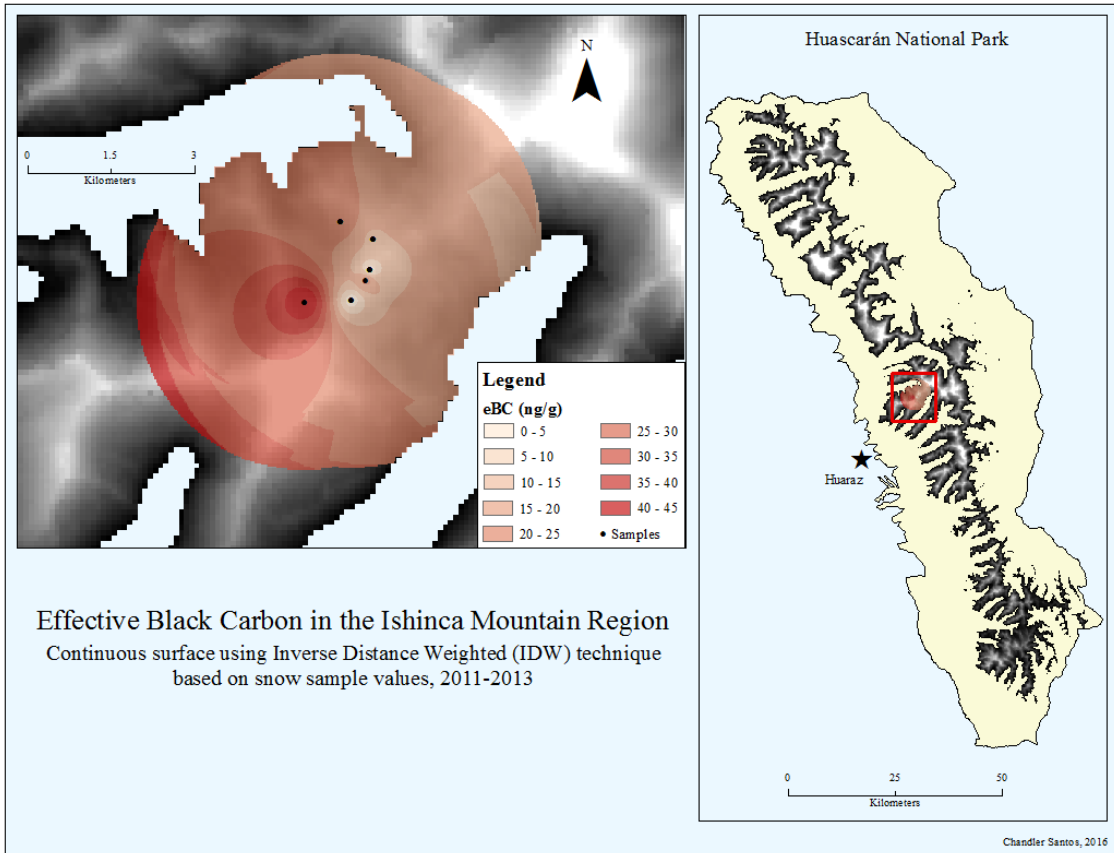


Figure A16

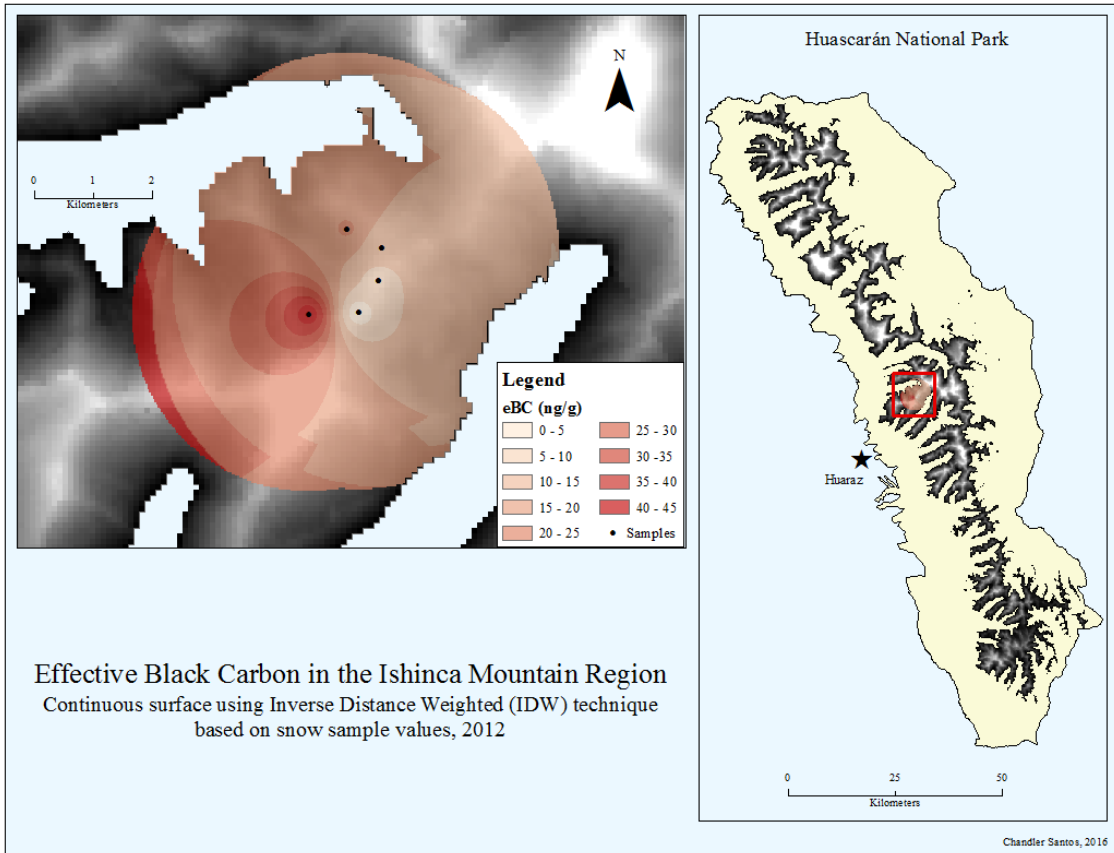


Figure A17

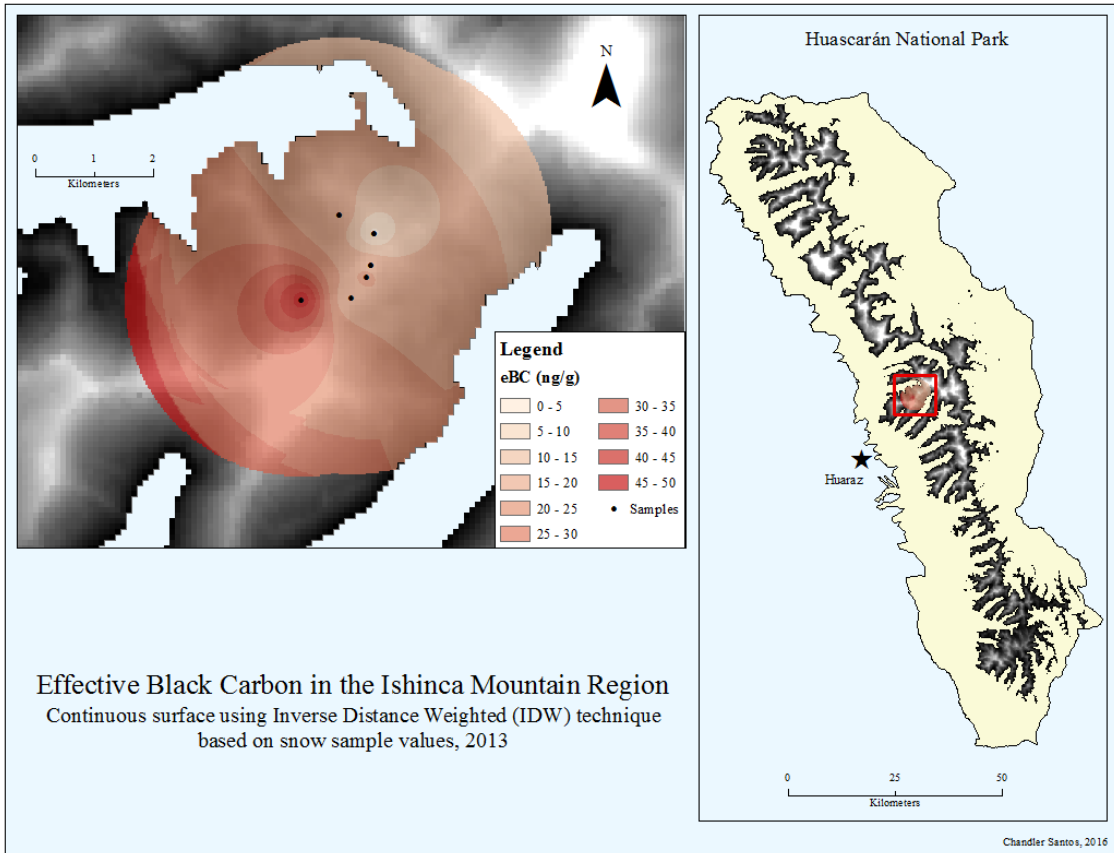


Figure A18

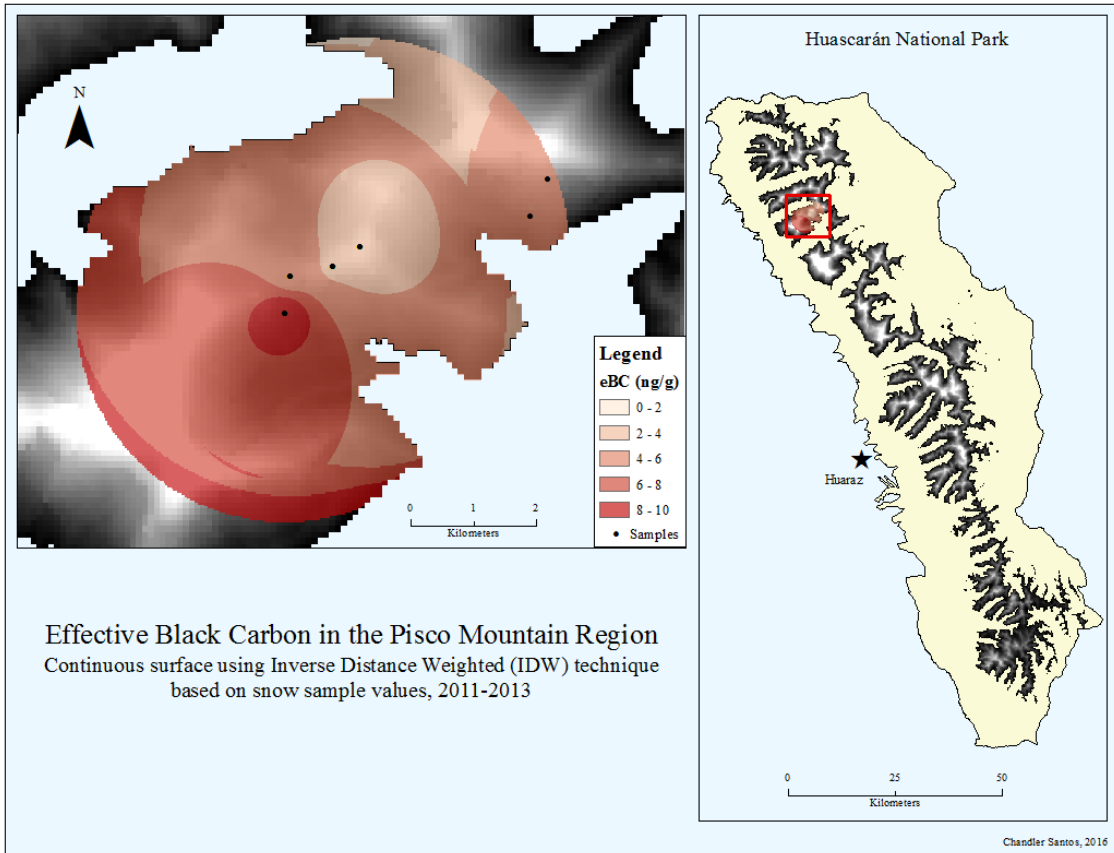


Figure A19

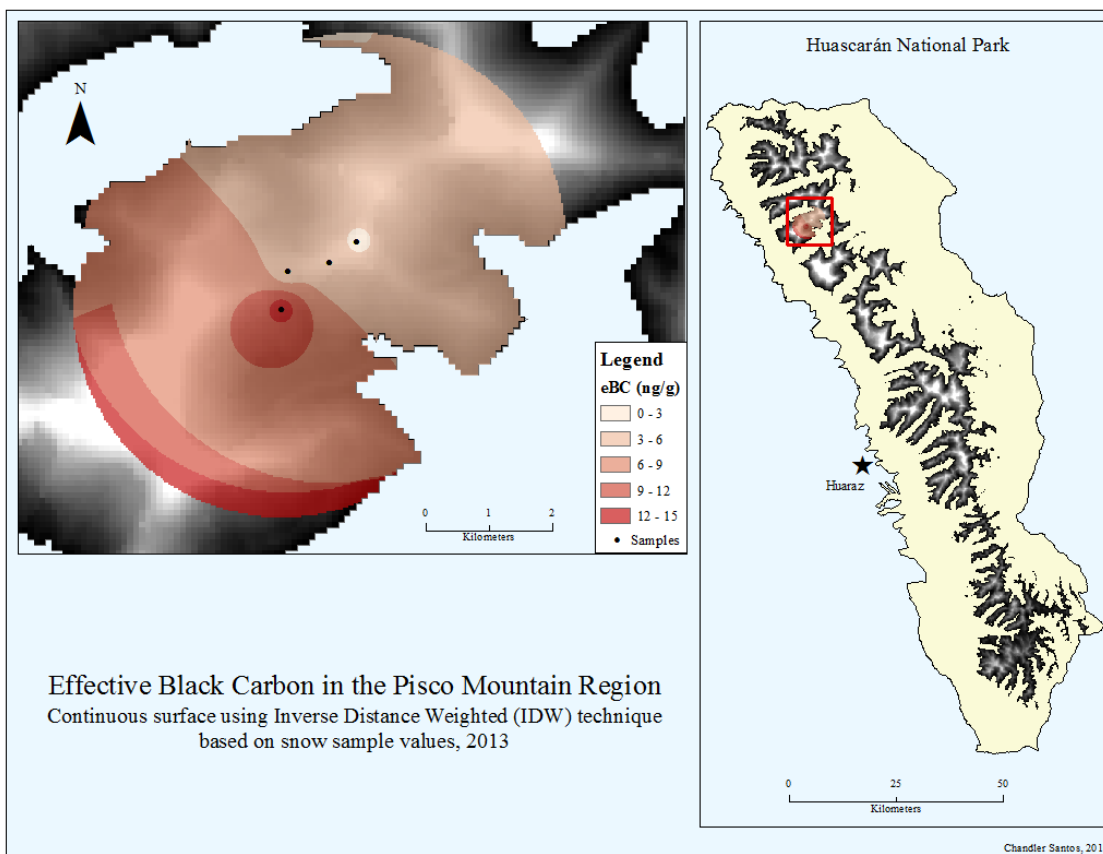


Figure A20

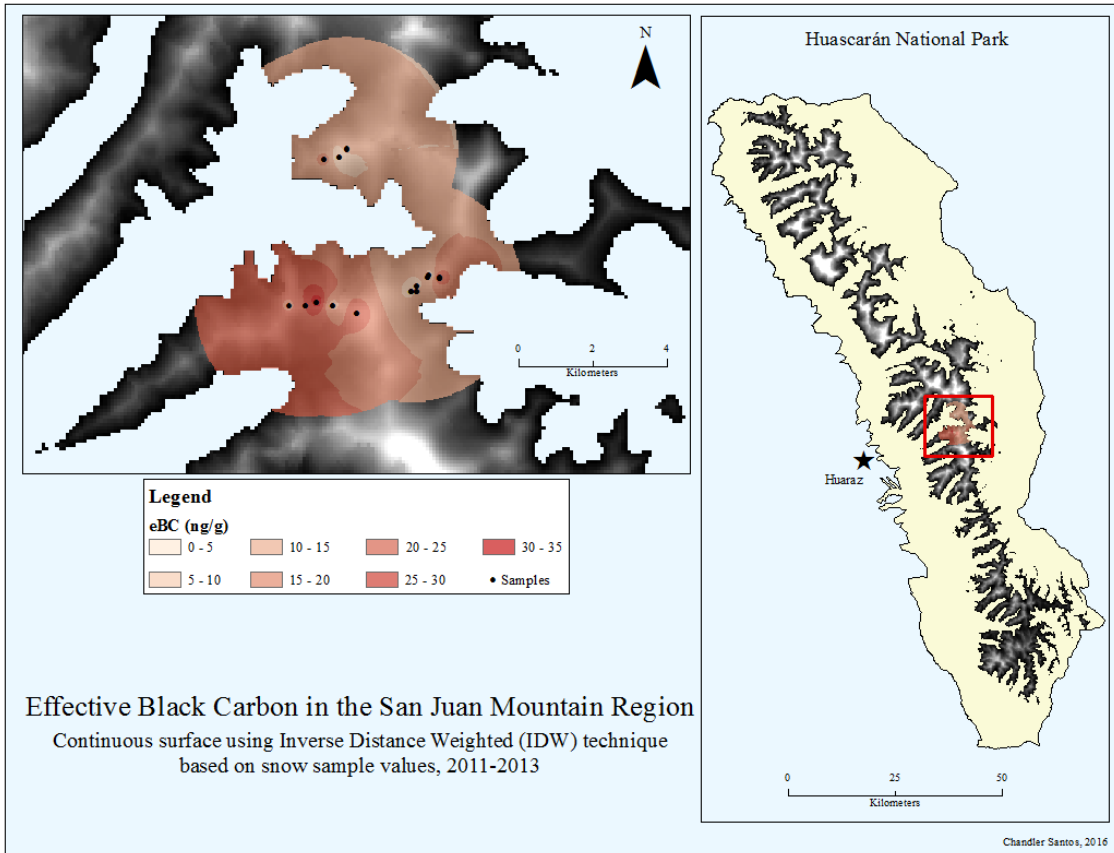


Figure A21

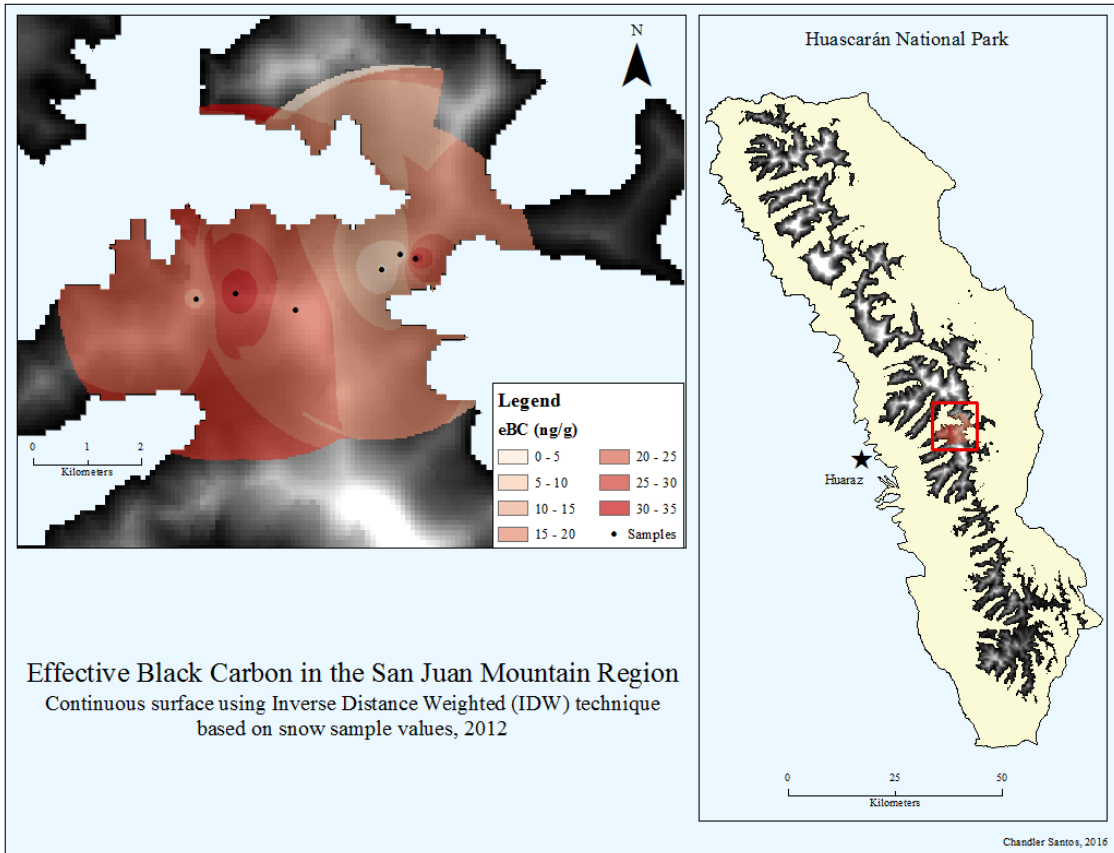


Figure A22

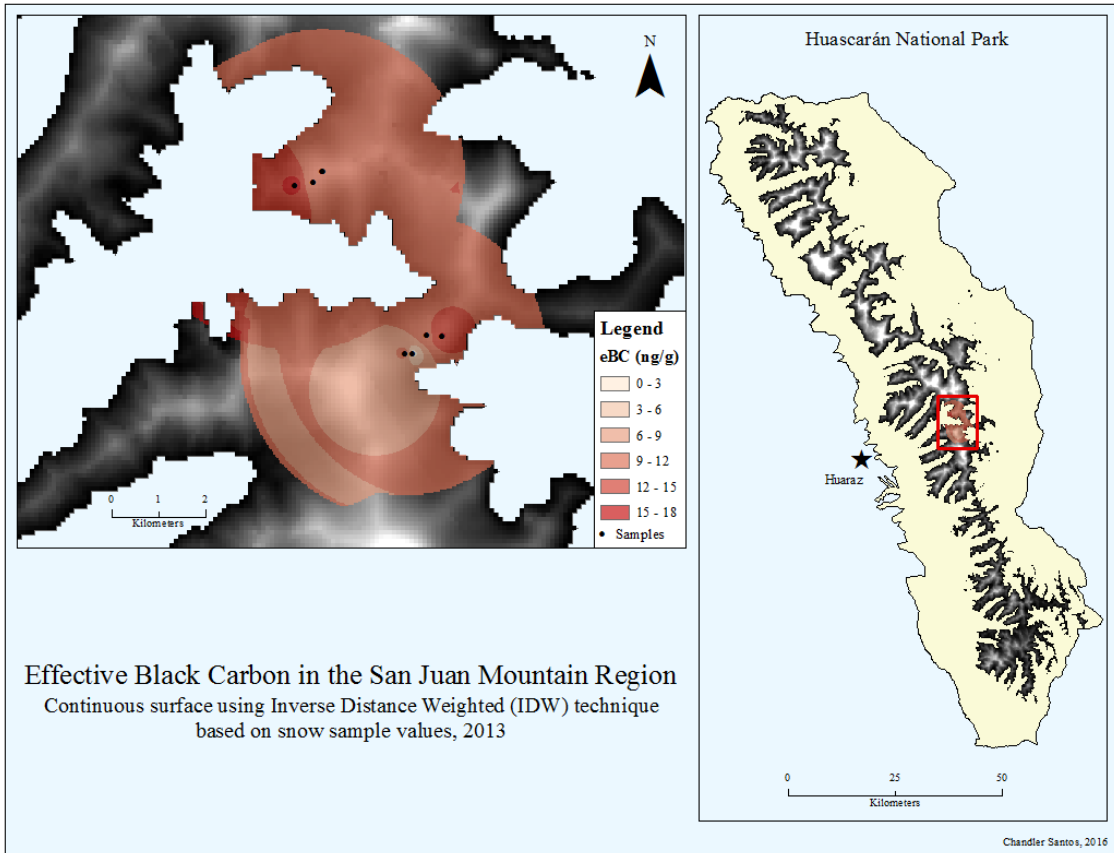


Figure A23

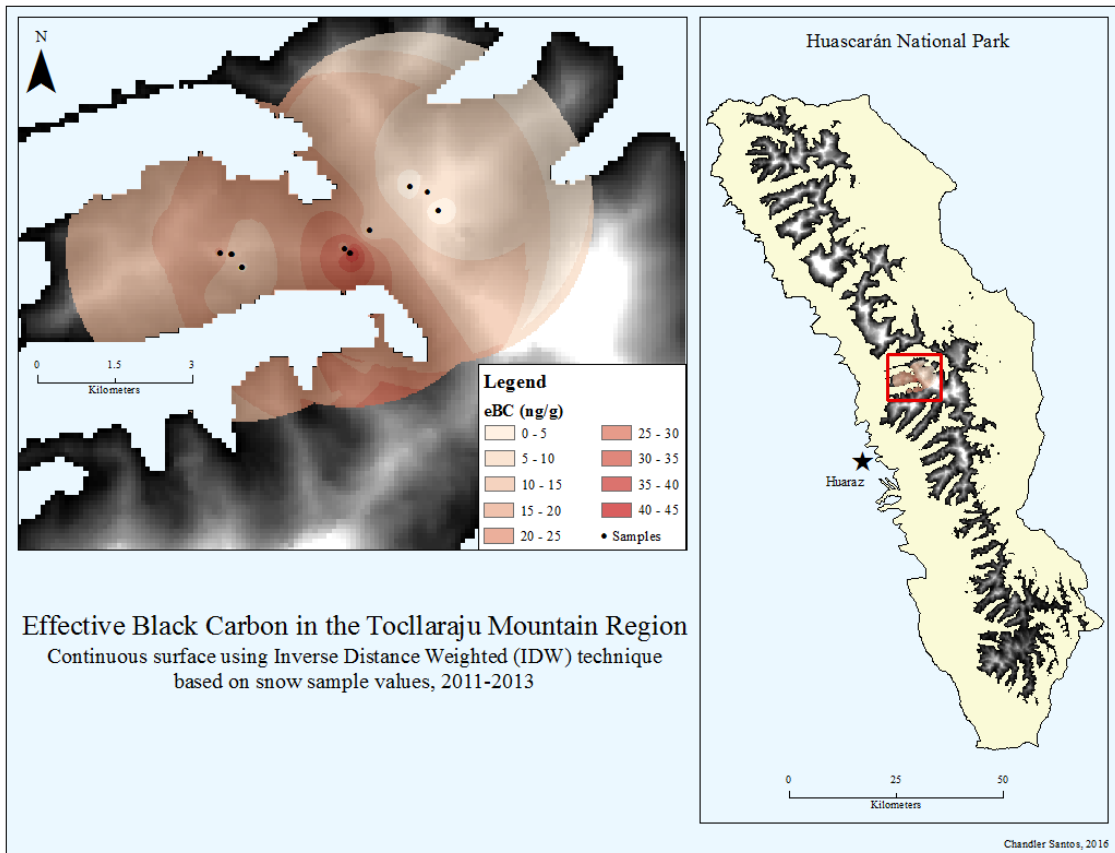


Figure A24

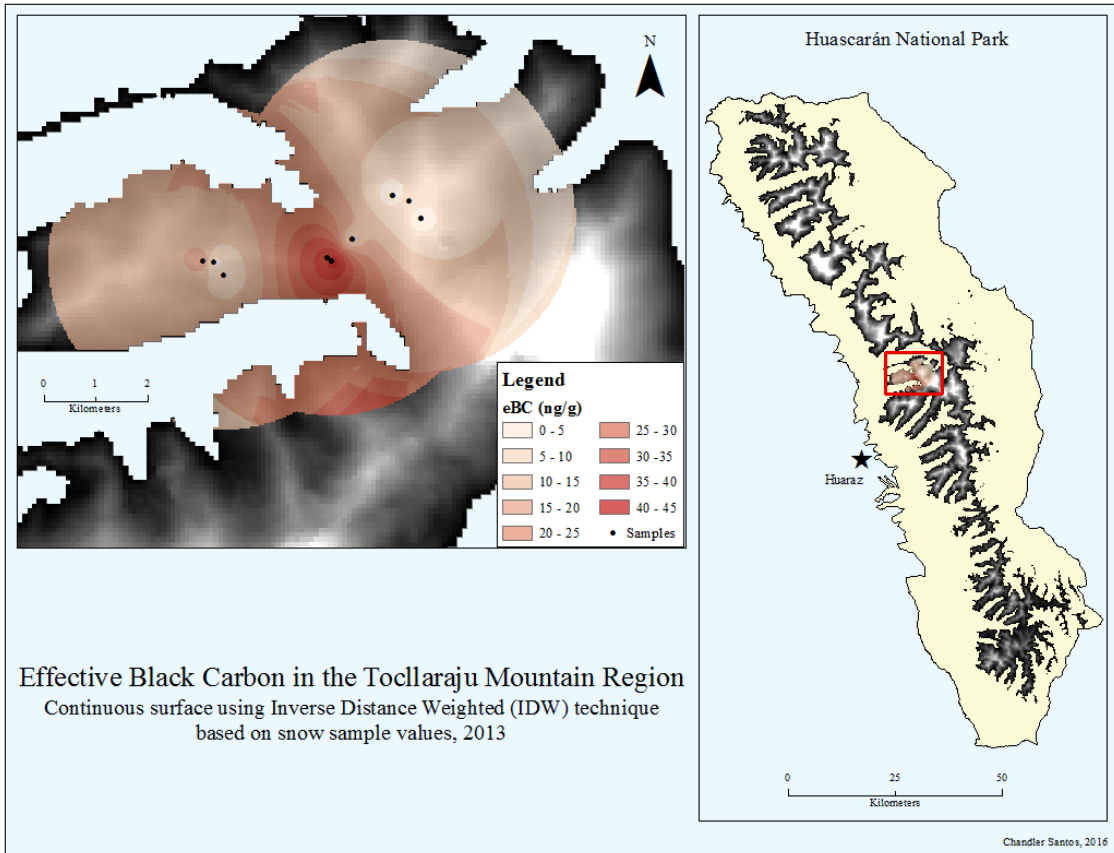


Figure A25

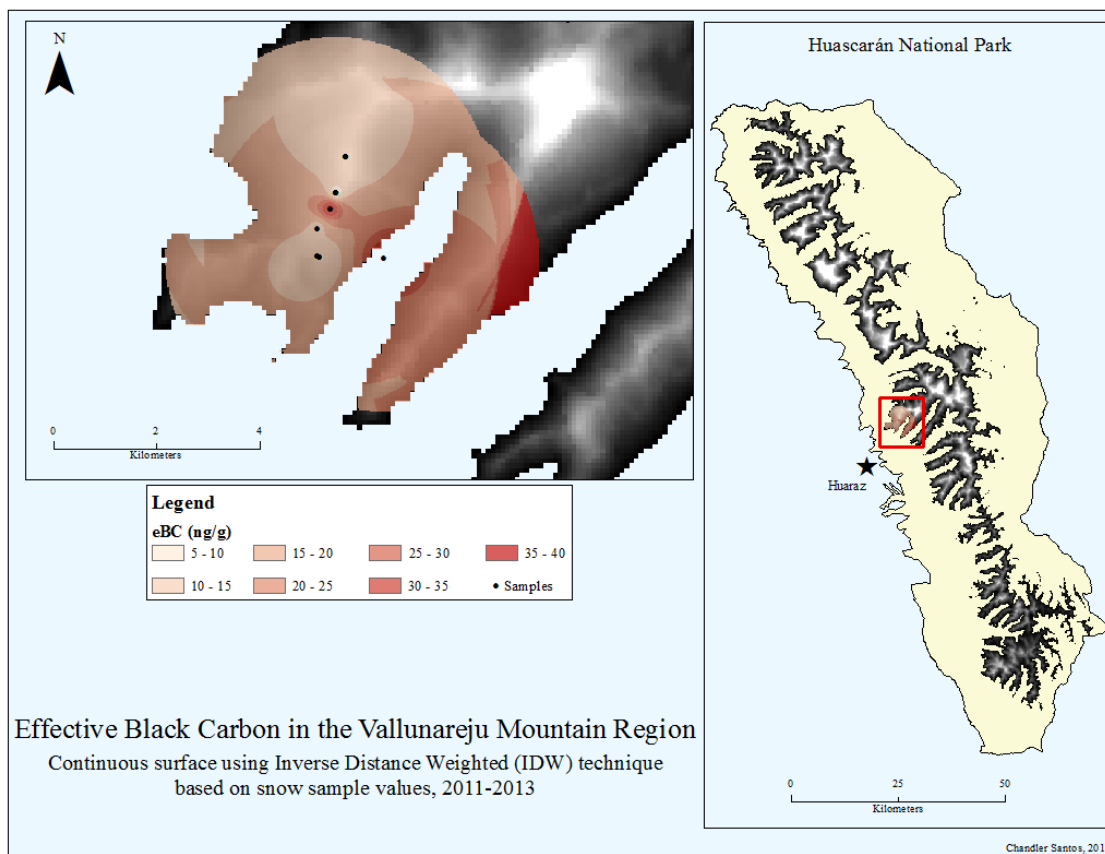


Figure A26

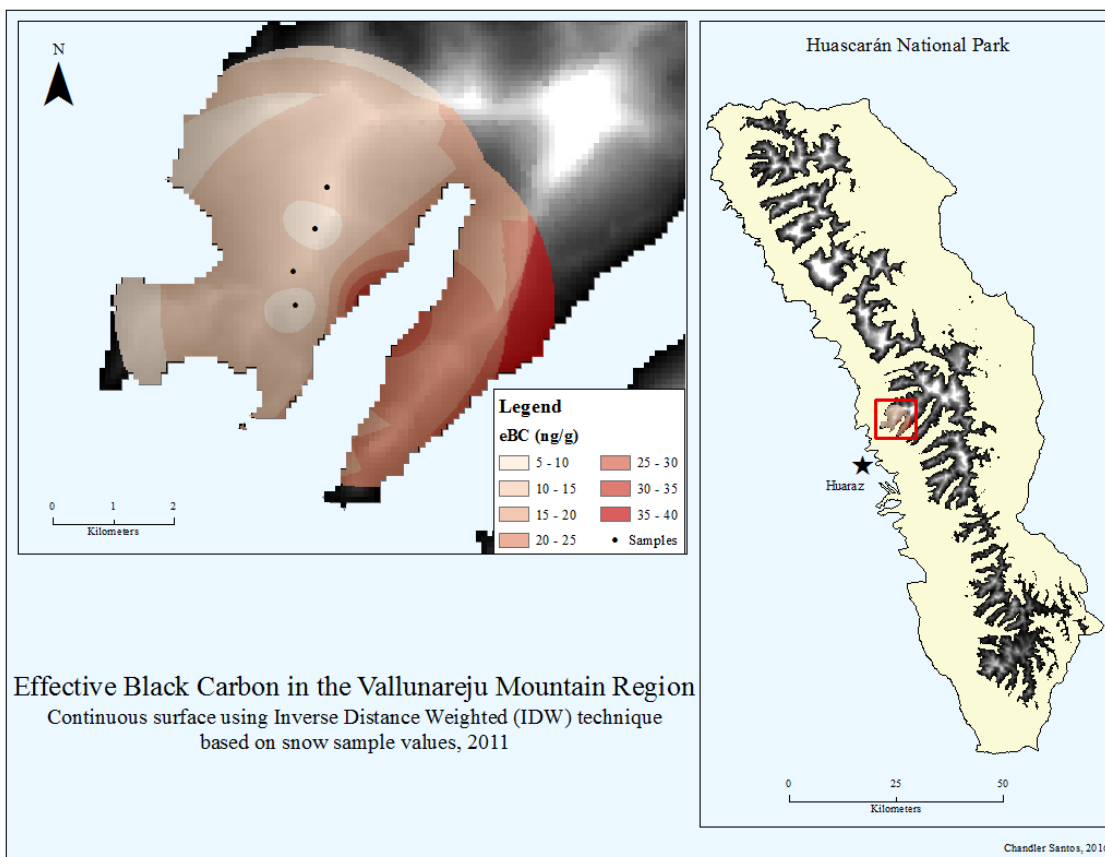


Figure A27

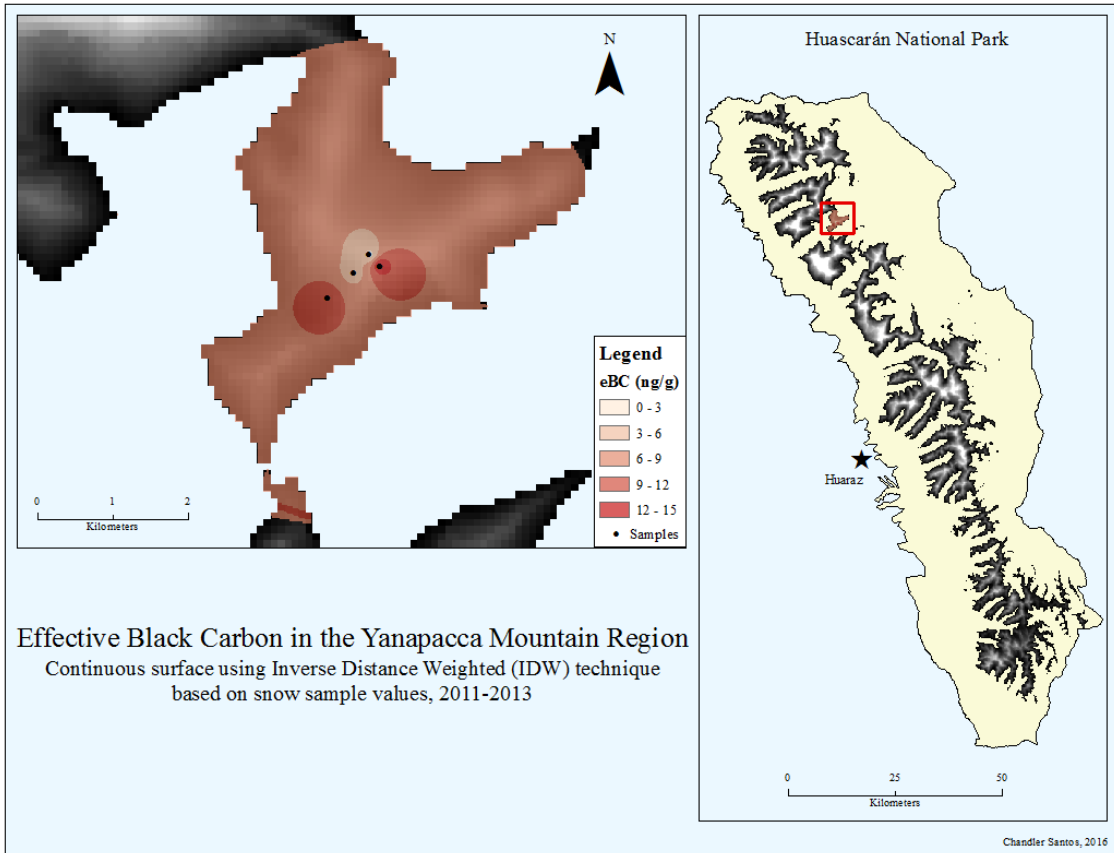


Figure A28

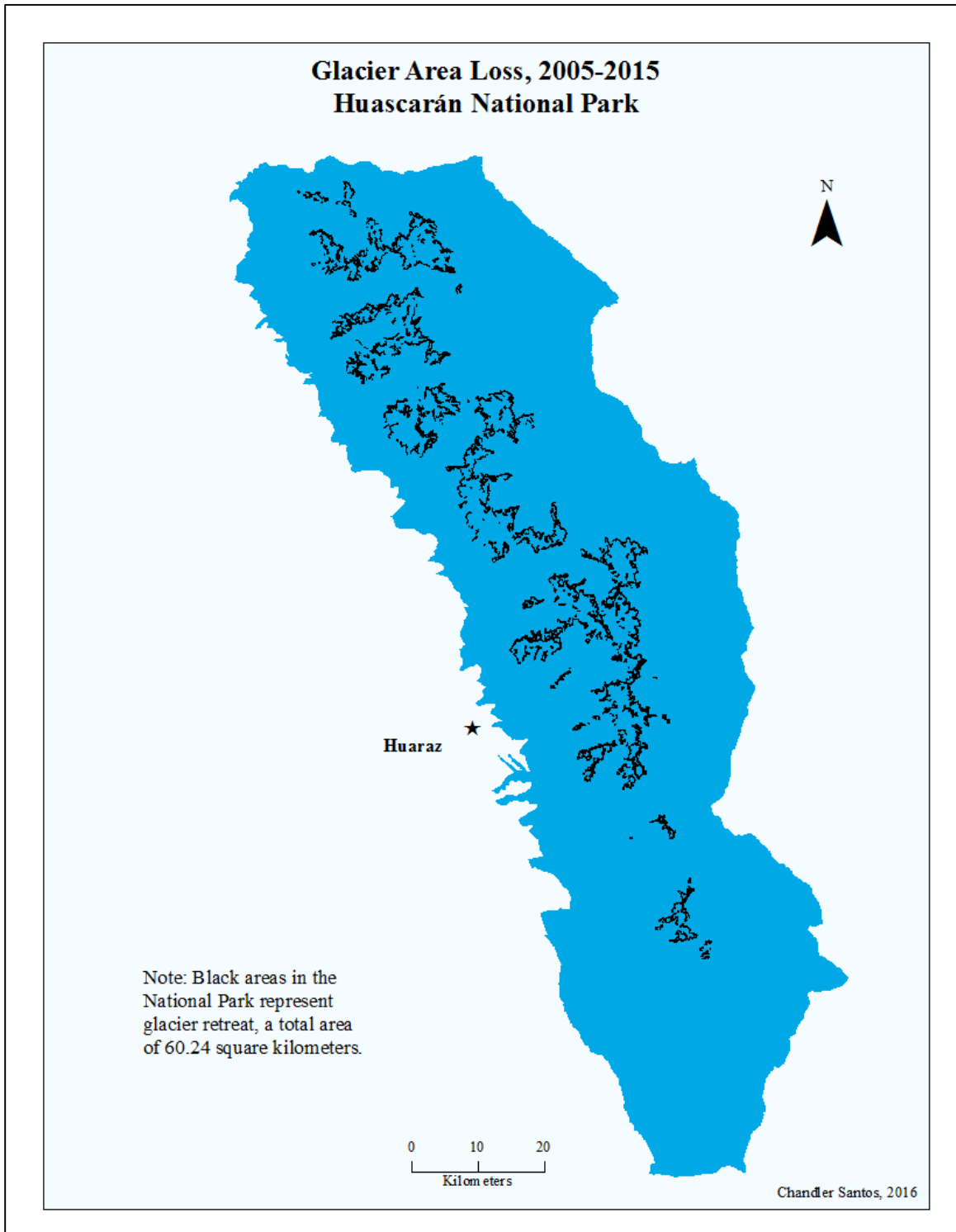


Figure A29

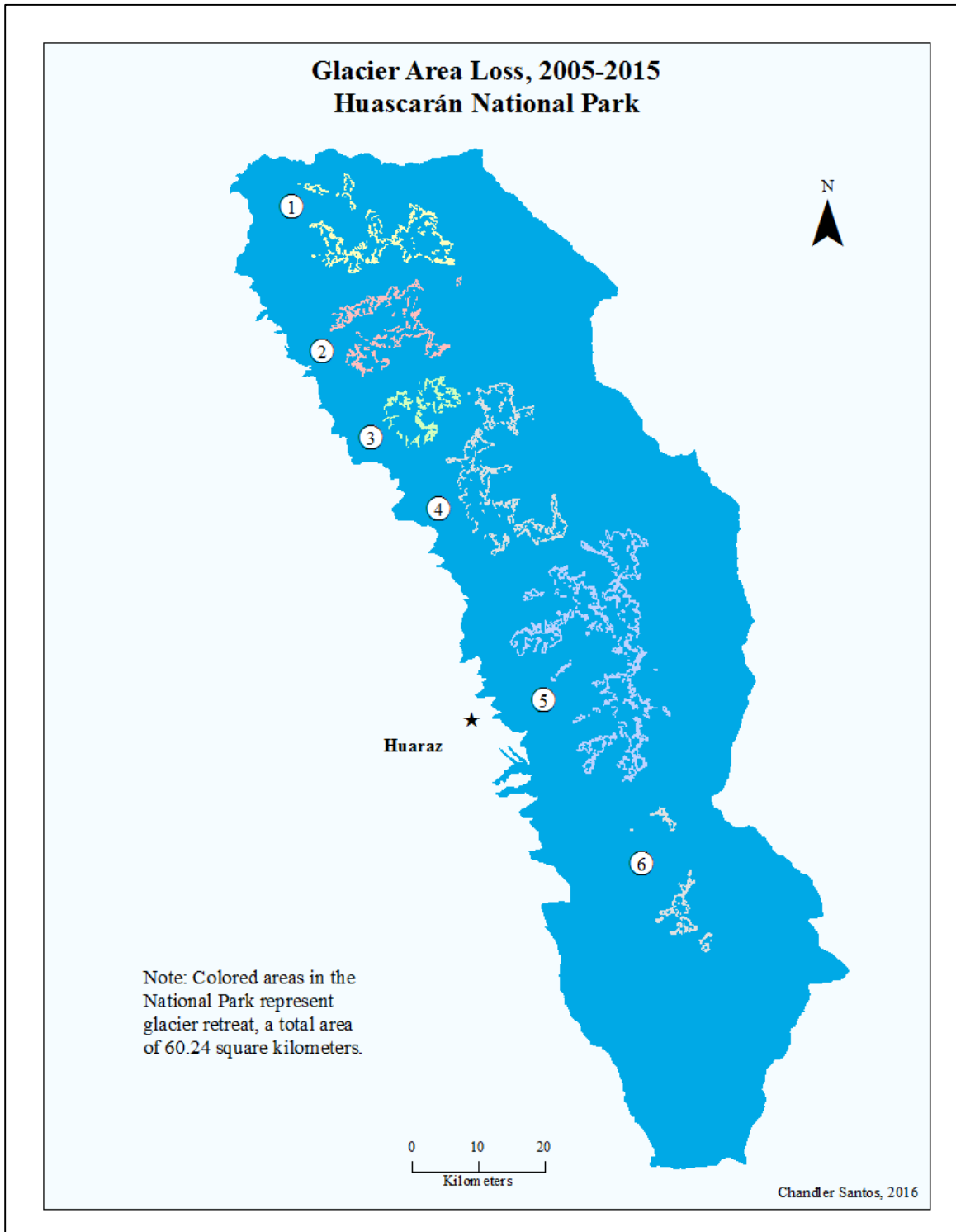
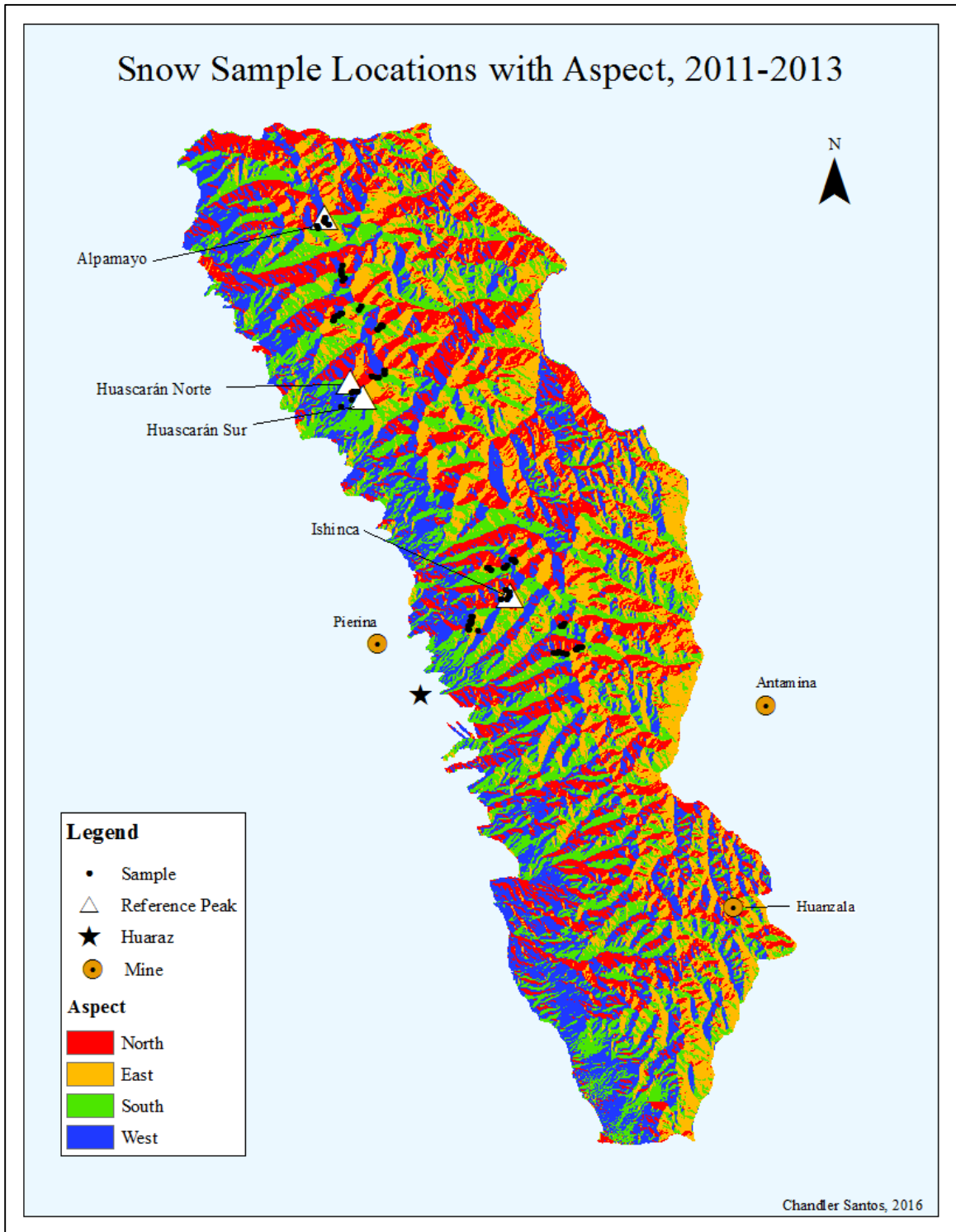


Figure A30



APPENDIX B: Tables and Graphs

Note for all tables: *Correlation is significant at the 0.05 level. **Correlation is significant at the 0.05 level.

Table B1: 2011 Snow Sample Data

Filter	Latitude	Longitude	Total	Quartz	Muscovite	Albite	Kaolinite	Annite
1	-9.384	-77.411	1.896	1.147	0.268	0.308	0.172	0.000
2	-9.096	-77.585	0.982	0.513	0.105	0.237	0.127	0.000
3	-9.392	-77.406	0.962	0.481	0.000	0.191	0.171	0.119
5	-9.117	-77.618	5.970	0.230	5.291	0.119	0.232	0.098
6	-9.117	-77.618	0.687	0.299	0.281	0.107	0.000	0.000
7	-8.890	-77.649	0.279	0.000	0.211	0.068	0.000	0.000
8	-8.890	-77.649	0.279	0.000	0.211	0.068	0.000	0.000
9	-8.890	-77.649	5.956	5.529	0.182	0.245	0.000	0.000
10	-8.890	-77.649	0.490	0.000	0.188	0.098	0.205	0.000
11	-8.890	-77.649	0.588	0.263	0.154	0.000	0.171	0.000
12	-9.010	-77.632	0.304	0.102	0.081	0.050	0.070	0.000
14	-9.439	-77.461	0.455	0.184	0.098	0.047	0.126	0.000
15	-9.419	-77.460	1.789	1.147	0.178	0.151	0.312	0.000
16	-9.012	-77.636	1.789	1.147	0.178	0.151	0.312	0.000
17	-9.014	-77.642	0.864	0.464	0.167	0.068	0.165	0.000
18	-9.014	-77.642	1.858	1.024	0.285	0.149	0.399	0.000
19	-9.019	-77.643	0.689	0.350	0.118	0.063	0.158	0.000
20	-9.019	-77.643	0.731	0.380	0.115	0.063	0.172	0.000
21	-9.470	-77.335	0.568	0.231	0.078	0.101	0.158	0.000
22	-9.470	-77.342	1.157	0.587	0.162	0.133	0.274	0.000
23	-9.470	-77.335	0.479	0.294	0.072	0.052	0.062	0.000
24	-9.470	-77.342	0.422	0.048	0.119	0.112	0.143	0.000
25	-9.466	-77.316	0.265	0.015	0.075	0.050	0.125	0.000
26	-9.466	-77.316	0.285	0.106	0.059	0.054	0.067	0.000
27	-9.427	-77.458	0.694	0.391	0.098	0.082	0.123	0.000
28	-9.427	-77.458	0.781	0.430	0.123	0.073	0.155	0.000
29	-9.434	-77.462	1.160	0.726	0.199	0.119	0.117	0.000
30	-9.421	-77.457	0.664	0.393	0.129	0.057	0.086	0.000
31	-9.439	-77.450	1.063	0.623	0.184	0.094	0.162	0.000
32	-9.421	-77.457	1.509	0.863	0.312	0.211	0.122	0.000
33	-9.357	-77.432	0.703	0.338	0.184	0.088	0.093	0.000
34	-9.355	-77.434	1.234	0.743	0.225	0.119	0.147	0.000
35	-8.944	-77.630	0.289	0.131	0.049	0.034	0.076	0.000

36	-8.952	-77.632	0.439	0.161	0.095	0.048	0.135	0.000
37	-8.957	-77.631	0.236	0.069	0.073	0.037	0.056	0.000
38	-8.965	-77.630	0.532	0.219	0.100	0.071	0.141	0.000
39	-9.027	-77.577	0.544	0.261	0.096	0.071	0.117	0.000
40	-9.027	-77.577	0.399	0.200	0.073	0.043	0.082	0.000
41	-9.031	-77.583	0.742	0.454	0.098	0.049	0.140	0.000
42	-9.031	-77.583	0.527	0.274	0.100	0.056	0.098	0.000
43	-9.136	-77.633	0.993	0.577	0.174	0.109	0.133	0.000
44	-9.126	-77.619	0.576	0.300	0.105	0.055	0.116	0.000
45	-9.115	-77.617	0.576	0.300	0.105	0.055	0.116	0.000
46	-9.115	-77.611	0.229	0.097	0.050	0.035	0.047	0.000
47	-9.115	-77.611	0.178	0.034	0.056	0.038	0.049	0.000

Table B2: 2012 Snow Sample Data

Filter		Latitude	Longitude	Total	Quartz	Muscovite	Albite	Kaolinite	Annite
1		-9.010	-77.632	0.917	0.430	0.283	0.098	0.000	0.105
2		-9.010	-77.632	0.712	0.061	0.000	0.246	0.405	0.000
3		-9.012	-77.636	8.972	1.042	0.160	0.488	7.282	0.000
4		-9.012	-77.636	12.346	0.219	2.675	0.167	9.284	0.000
5		-9.014	-77.642	0.484	0.000	0.000	0.290	0.000	0.194
6		-9.014	-77.642	1.881	0.322	0.112	0.473	0.974	0.000
7		-9.019	-77.643	1.000	0.455	0.131	0.222	0.192	0.000
8		-9.019	-77.643	0.508	0.000	0.114	0.231	0.164	0.000
9		-9.117	-77.618	0.773	0.000	0.231	0.385	0.157	0.000
10		-9.117	-77.618	0.980	0.299	0.198	0.270	0.213	0.000
11		-9.117	-77.618	0.489	0.129	0.103	0.171	0.086	0.000
12		-9.117	-77.618	0.493	0.000	0.110	0.250	0.106	0.027
13		-9.117	-77.618	1.197	0.466	0.204	0.276	0.149	0.101
14		-9.355	-77.436	0.396	0.026	0.099	0.181	0.090	0.000
15		-9.355	-77.436	0.436	0.000	0.061	0.103	0.181	0.090
16		-9.357	-77.432	0.361	0.000	0.068	0.101	0.118	0.073
17		-9.357	-77.432	0.452	0.000	0.095	0.098	0.187	0.071
18		-9.357	-77.432	0.643	0.168	0.106	0.135	0.172	0.061
19		-9.384	-77.411	0.822	0.064	0.176	0.231	0.249	0.102
20		-9.384	-77.411	0.531	0.057	0.141	0.158	0.130	0.045
21		-9.397	-77.409	0.720	0.000	0.120	0.300	0.150	0.151
22		-9.397	-77.409	0.517	0.119	0.089	0.092	0.167	0.050
23		-9.387	-77.406	0.694	0.067	0.152	0.233	0.155	0.086
24		-9.387	-77.406	0.584	0.140	0.105	0.156	0.125	0.059
25		-9.392	-77.406	0.322	0.000	0.103	0.064	0.074	0.081
26		-9.392	-77.406	0.449	0.161	0.071	0.097	0.095	0.026

27		-9.397	-77.417	0.476	0.000	0.073	0.227	0.061	0.114
28		-9.439	-77.461	0.796	0.000	0.130	0.265	0.212	0.189
29		-9.439	-77.461	0.657	0.000	0.144	0.165	0.238	0.111
30		-9.427	-77.458	0.531	0.048	0.092	0.208	0.160	0.023
31		-9.427	-77.458	0.374	0.000	0.111	0.119	0.102	0.041
32		-9.427	-77.458	0.515	0.096	0.119	0.132	0.113	0.055
33		-9.427	-77.458	0.579	0.086	0.129	0.146	0.141	0.078
34		-9.427	-77.458	0.608	0.173	0.115	0.142	0.129	0.048
35		-9.427	-77.458	0.616	0.133	0.120	0.203	0.127	0.033
36		-9.427	-77.458	0.548	0.117	0.112	0.132	0.140	0.046
37		-9.427	-77.458	0.538	0.150	0.111	0.126	0.095	0.056
38		-9.427	-77.458	0.474	0.116	0.122	0.119	0.073	0.043
39		-9.427	-77.458	0.412	0.000	0.120	0.139	0.073	0.081
40		-9.427	-77.458	0.780	0.087	0.143	0.228	0.050	0.272
41		-9.427	-77.458	0.637	0.148	0.130	0.156	0.130	0.073
42		-9.427	-77.458	0.615	0.196	0.116	0.124	0.119	0.060
43		-9.427	-77.458	0.508	0.125	0.109	0.103	0.118	0.053
44		-9.427	-77.458	0.785	0.000	0.162	0.251	0.167	0.205
45		-9.421	-77.456	0.903	0.107	0.178	0.248	0.175	0.195
46		-9.421	-77.456	0.808	0.000	0.136	0.278	0.121	0.273
47		-9.427	-77.458	0.949	0.000	0.141	0.307	0.255	0.247
48		-9.427	-77.458	0.774	0.000	0.136	0.219	0.226	0.193
49		-9.031	-77.583	0.795	0.161	0.084	0.235	0.100	0.214
50		-9.031	-77.583	0.447	0.000	0.096	0.121	0.142	0.088
51		-9.026	-77.578	0.573	0.000	0.172	0.168	0.167	0.066
52		-9.026	-77.578	0.452	0.000	0.134	0.116	0.136	0.066
53		-9.027	-77.577	0.823	0.151	0.183	0.180	0.194	0.115
54		-9.027	-77.577	0.823	0.199	0.178	0.154	0.196	0.095
55		-9.095	-77.591	0.306	0.000	0.054	0.128	0.087	0.036
56		-9.095	-77.591	0.471	0.102	0.123	0.109	0.098	0.040
57		-9.096	-77.585	0.495	0.126	0.110	0.095	0.104	0.059
58		-9.096	-77.585	0.590	0.083	0.104	0.151	0.125	0.127
59		-9.096	-77.582	0.753	0.240	0.144	0.160	0.128	0.082
60		-9.096	-77.582	0.930	0.335	0.144	0.198	0.171	0.081
61		-9.092	-77.574	0.627	0.130	0.132	0.127	0.120	0.118
62		-9.092	-77.574	0.570	0.184	0.099	0.095	0.118	0.074
63		-9.087	-77.574	0.437	0.000	0.122	0.091	0.111	0.114
64		-9.087	-77.574	0.421	0.000	0.103	0.108	0.134	0.076
65		-8.881	-77.654	0.899	0.378	0.101	0.166	0.106	0.149
66		-8.881	-77.654	0.689	0.204	0.147	0.156	0.120	0.060
67		-8.879	-77.653	2.281	1.137	0.290	0.407	0.421	0.026
68		-8.879	-77.653	1.098	0.449	0.145	0.188	0.257	0.059
69		-8.890	-77.649	1.435	0.766	0.135	0.197	0.122	0.215
70		-8.890	-77.649	1.438	0.618	0.143	0.098	0.398	0.181
71		-8.887	-77.654	0.619	0.138	0.162	0.155	0.092	0.072
72		-8.887	-77.654	1.516	0.717	0.169	0.155	0.295	0.178
73		-8.890	-77.665	0.487	0.132	0.094	0.096	0.115	0.049
74		-8.890	-77.665	1.559	0.597	0.126	0.248	0.340	0.248

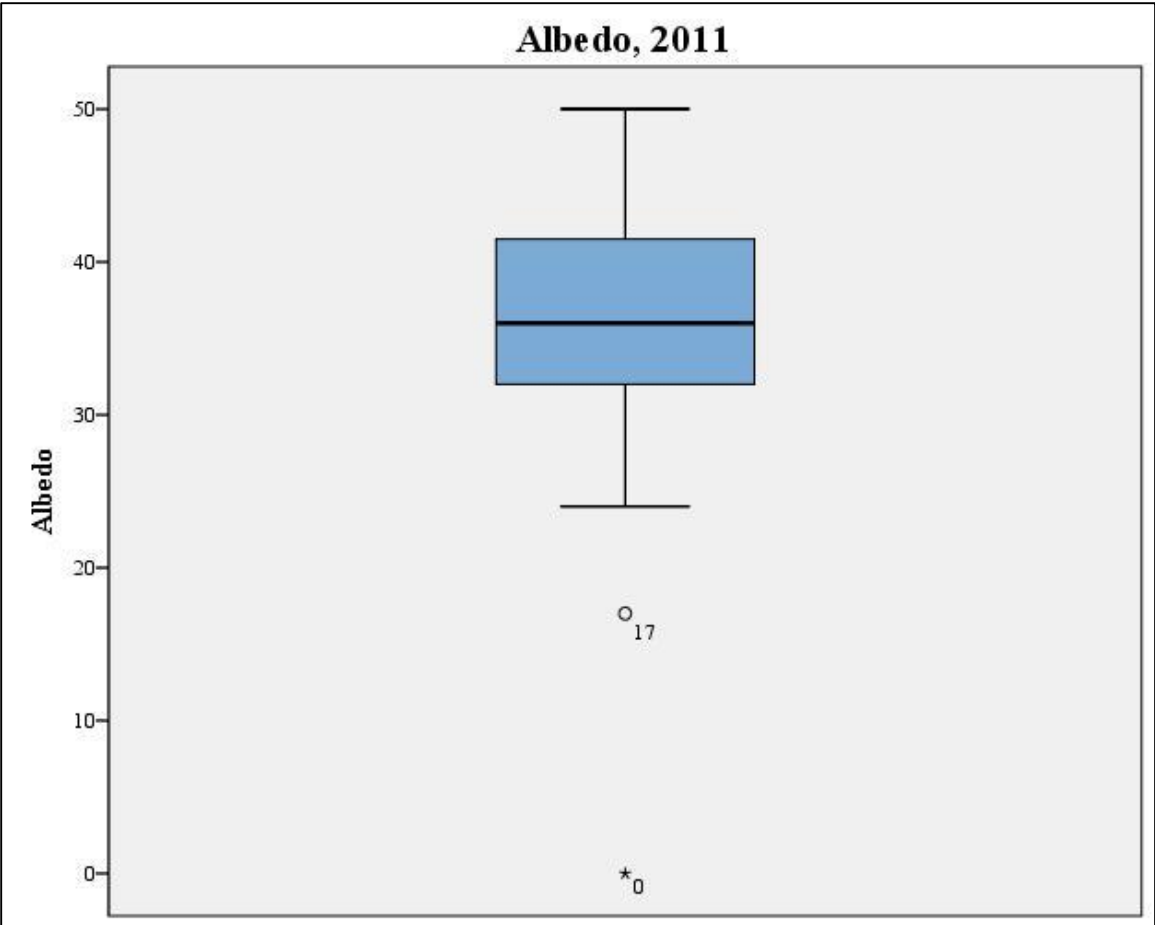
75		-8.894	-77.664	0.757	0.351	0.149	0.124	0.132	0.000
76		-8.894	-77.664	0.271	0.000	0.088	0.110	0.073	0.000
77		-8.885	-77.656	0.568	0.185	0.105	0.167	0.111	0.000
78		-8.885	-77.656	1.923	1.080	0.220	0.258	0.155	0.210
79		-9.465	-77.314	0.690	0.263	0.086	0.138	0.068	0.135
80		-9.465	-77.314	0.847	0.356	0.136	0.127	0.109	0.120
81		-9.392	-77.406	0.688	0.329	0.106	0.105	0.095	0.053
82		-9.392	-77.406	1.719	0.824	0.168	0.248	0.165	0.314
83		-9.463	-77.311	1.071	0.336	0.117	0.191	0.313	0.114
84		-9.463	-77.311	1.124	0.417	0.133	0.173	0.244	0.157
85		-9.463	-77.309	1.515	0.524	0.119	0.103	0.287	0.482
86		-9.463	-77.309	3.476	2.067	0.311	0.312	0.278	0.507
87		-9.472	-77.329	1.627	0.959	0.146	0.133	0.200	0.188
88		-9.472	-77.329	1.101	0.573	0.120	0.220	0.000	0.189
89		-9.470	-77.346	1.534	0.975	0.084	0.138	0.126	0.209
90		-9.470	-77.346	0.267	0.000	0.000	0.000	0.122	0.146
91		-9.469	-77.339	1.496	0.873	0.127	0.000	0.304	0.191
92		-9.469	-77.339	3.367	2.117	0.123	0.118	0.775	0.234
93		-9.010	-77.632	2.269	1.051	0.180	0.262	0.705	0.071
94		-9.010	-77.632	0.266	0.000	0.090	0.000	0.082	0.094
95		-9.012	-77.636	0.643	0.436	0.074	0.060	0.000	0.073
96		-9.012	-77.636	0.775	0.000	0.196	0.153	0.181	0.245
97		-9.014	-77.642	1.304	0.790	0.152	0.118	0.113	0.132
98		-9.014	-77.642	1.943	1.346	0.163	0.141	0.182	0.110
99		-9.019	-77.643	1.303	0.741	0.147	0.154	0.109	0.151
100		-9.019	-77.643	0.000	0.000	0.000	0.000	0.000	0.000

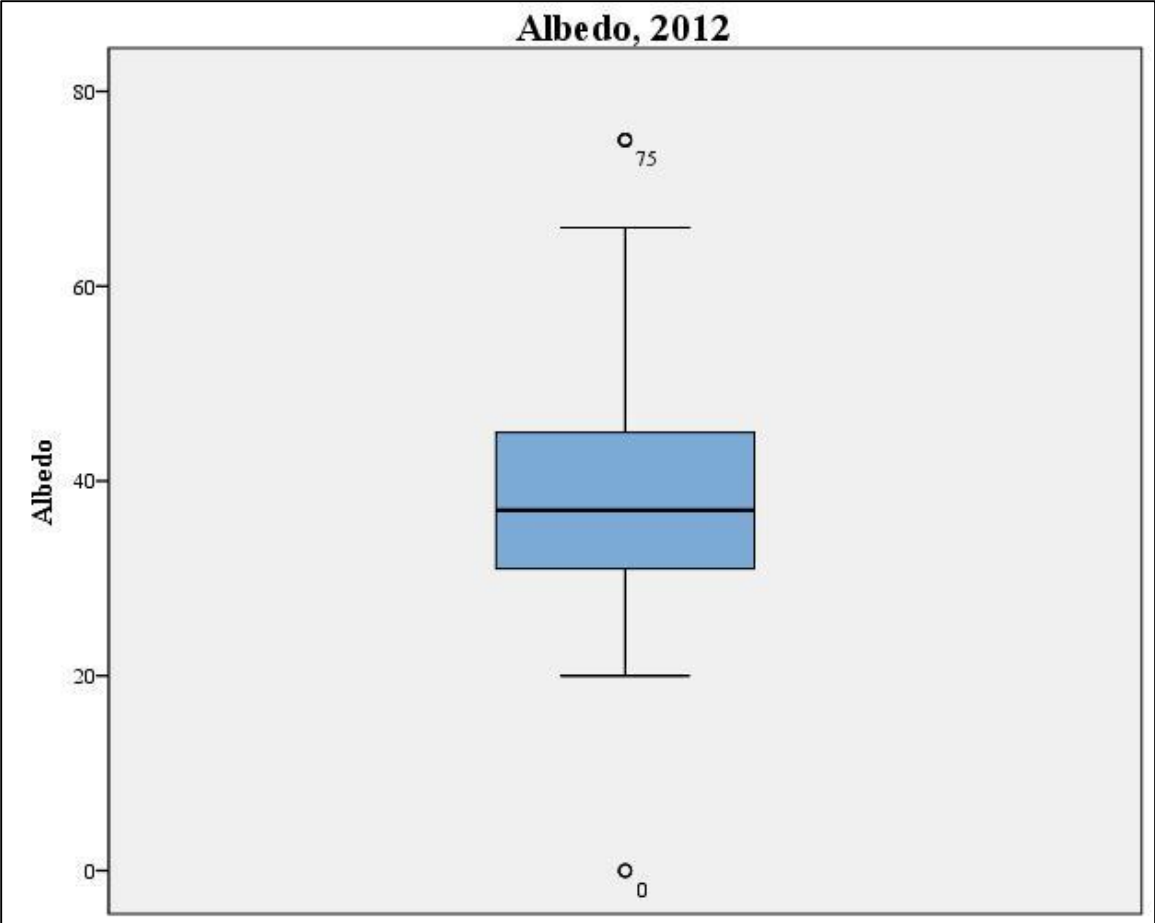
Table B3: 2013 Snow Sample Data

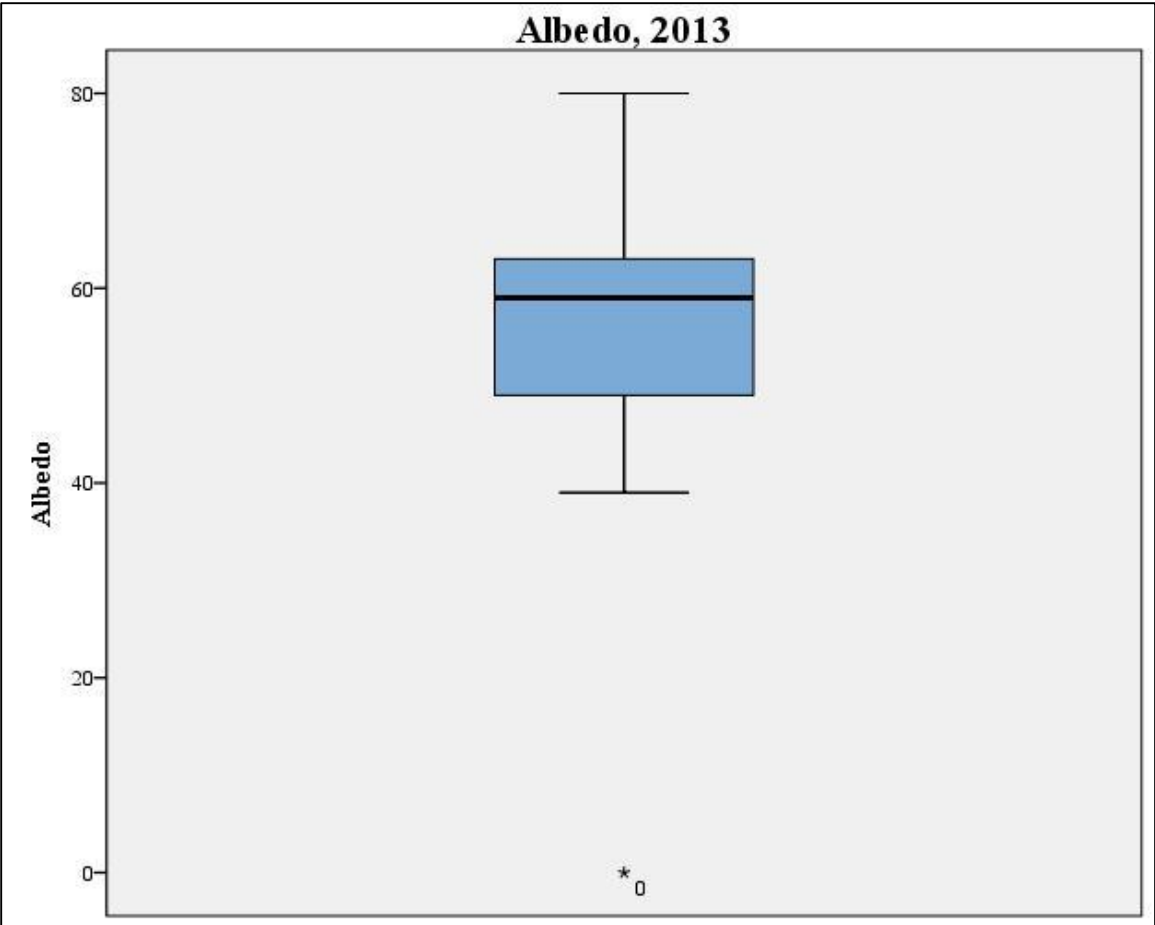
Filter	Latitude	Longitude	Total	Quartz	Muscovite	Albite	Kaolinite	Annite	Illite
1	-9.354	-77.414	0.845	0.133	0.082	0.127	0.219	0.094	0.190
2	-9.354	-77.414	0.237	0.000	0.042	0.056	0.091	0.048	0.000
3	-9.351	-77.409	0.355	0.081	0.036	0.056	0.079	0.050	0.054
4	-9.351	-77.409	0.588	0.176	0.028	0.058	0.155	0.082	0.089
5	-9.355	-77.413	0.656	0.239	0.036	0.069	0.119	0.089	0.105
6	-9.355	-77.413	0.703	0.239	0.055	0.111	0.180	0.118	0.000
7	-9.355	-77.413	0.340	0.071	0.055	0.061	0.078	0.076	0.000
8	-9.355	-77.413	0.751	0.184	0.138	0.141	0.191	0.098	0.000
9	-9.355	-77.413	1.065	0.281	0.154	0.152	0.353	0.124	0.000
10	-9.343	-77.402	0.405	0.086	0.070	0.067	0.092	0.089	0.000
11	-9.343	-77.402	0.389	0.088	0.078	0.062	0.069	0.092	0.000
12	-9.344	-77.399	0.559	0.205	0.079	0.078	0.103	0.093	0.000
13	-9.344	-77.399	0.455	0.144	0.073	0.066	0.076	0.095	0.000
14	-9.348	-77.397	0.443	0.094	0.062	0.069	0.076	0.081	0.061

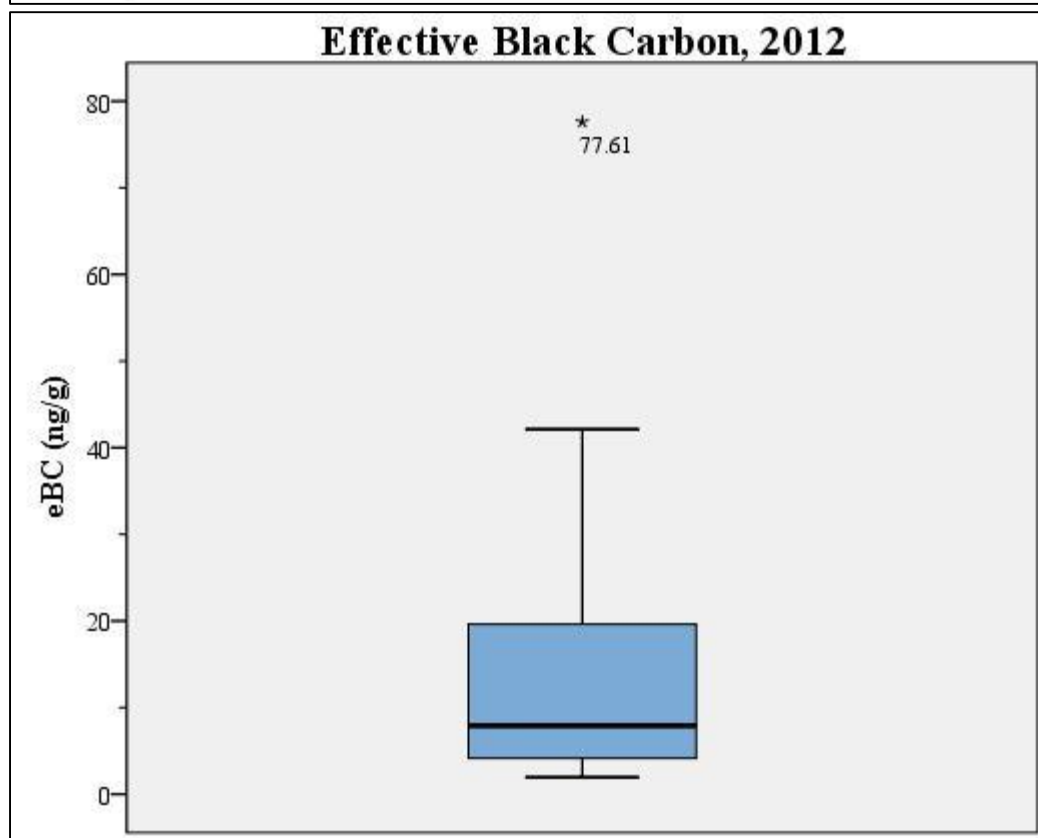
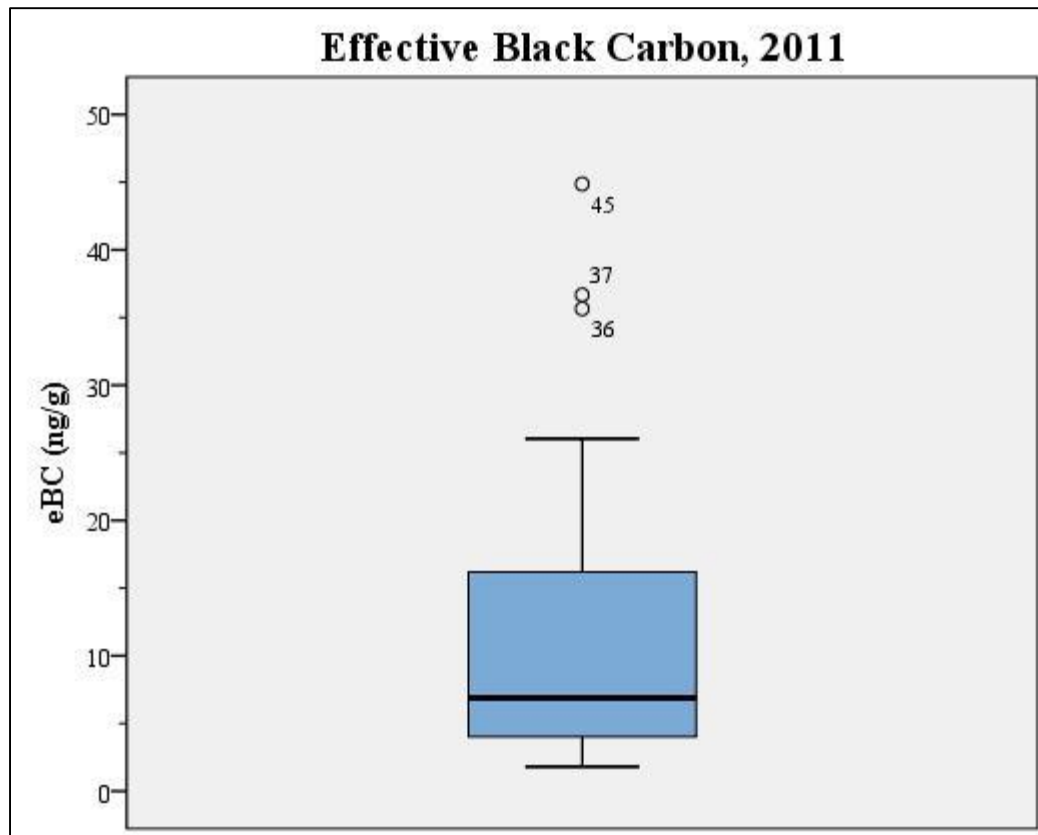
15	-9.348	-77.397	0.455	0.087	0.068	0.061	0.093	0.079	0.068
16	-9.439	-77.462	0.779	0.079	0.079	0.121	0.195	0.059	0.246
17	-9.439	-77.462	0.660	0.189	0.092	0.104	0.181	0.094	0.000
18	-9.430	-77.459	0.826	0.195	0.080	0.124	0.278	0.019	0.130
19	-9.430	-77.459	0.477	0.000	0.096	0.076	0.111	0.087	0.107
20	-9.421	-77.456	1.244	0.231	0.101	0.121	0.265	0.268	0.258
21	-9.421	-77.456	0.430	0.166	0.064	0.105	0.055	0.040	0.000
22	-9.427	-77.458	0.528	0.182	0.075	0.070	0.093	0.079	0.029
23	-9.427	-77.458	0.341	0.085	0.077	0.035	0.036	0.035	0.071
24	-9.421	-77.456	0.855	0.275	0.083	0.050	0.269	0.093	0.084
25	-9.421	-77.456	0.472	0.114	0.080	0.052	0.107	0.047	0.072
26	-9.005	-77.608	0.607	0.143	0.153	0.081	0.072	0.057	0.100
27	-9.005	-77.608	0.667	0.095	0.084	0.086	0.141	0.058	0.204
28	-9.000	-77.605	0.518	0.139	0.097	0.082	0.091	0.000	0.108
29	-9.000	-77.605	0.552	0.154	0.093	0.081	0.082	0.067	0.076
30	-9.012	-77.636	0.774	0.179	0.132	0.116	0.155	0.079	0.112
31	-9.012	-77.636	0.950	0.124	0.055	0.116	0.282	0.206	0.167
32	-9.384	-77.411	0.746	0.103	0.075	0.145	0.195	0.071	0.157
33	-9.384	-77.411	1.344	0.296	0.259	0.212	0.204	0.149	0.224
34	-9.392	-77.406	0.782	0.198	0.111	0.090	0.088	0.083	0.212
35	-9.397	-77.409	0.612	0.137	0.078	0.058	0.141	0.097	0.100
36	-9.392	-77.406	0.476	0.237	0.077	0.093	0.070	0.000	0.000
37	-9.434	-77.337	0.472	0.220	0.074	0.057	0.044	0.077	0.000
38	-9.432	-77.331	0.495	0.217	0.053	0.072	0.070	0.083	0.000
39	-9.434	-77.337	0.751	0.372	0.086	0.089	0.123	0.081	0.000
40	-9.434	-77.333	0.503	0.230	0.074	0.063	0.136	0.000	0.000
41	-9.432	-77.331	0.522	0.224	0.048	0.053	0.130	0.067	0.000
42	-9.434	-77.333	0.398	0.082	0.071	0.066	0.077	0.051	0.052
43	-9.027	-77.577	0.233	0.000	0.055	0.050	0.041	0.031	0.056
44	-9.027	-77.577	0.427	0.080	0.072	0.060	0.076	0.048	0.091
45	-9.028	-77.580	0.368	0.098	0.069	0.039	0.054	0.039	0.068
46	-9.028	-77.580	0.429	0.069	0.071	0.076	0.077	0.072	0.064
47	-9.387	-77.406	0.310	0.090	0.067	0.040	0.060	0.052	0.000
48	-9.387	-77.406	0.270	0.060	0.038	0.058	0.064	0.000	0.050
49	-9.397	-77.417	0.746	0.162	0.049	0.125	0.169	0.091	0.150
50	-9.394	-77.407	0.298	0.051	0.028	0.082	0.043	0.032	0.061
51	-9.357	-77.432	0.275	0.055	0.027	0.051	0.056	0.039	0.048
52	-9.355	-77.434	0.394	0.119	0.058	0.052	0.095	0.041	0.030
53	-9.355	-77.436	0.776	0.161	0.105	0.135	0.084	0.150	0.142
54	-9.466	-77.316	0.665	0.245	0.050	0.066	0.136	0.074	0.095
55	-9.467	-77.314	0.517	0.159	0.053	0.061	0.093	0.092	0.058

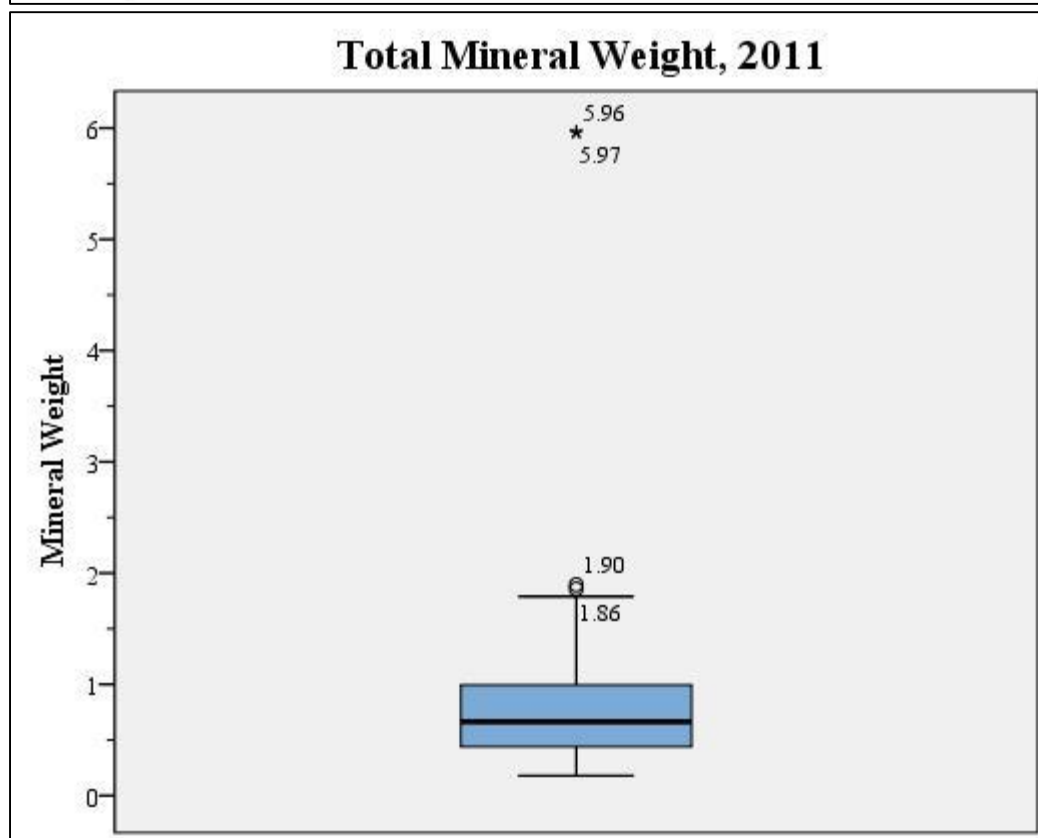
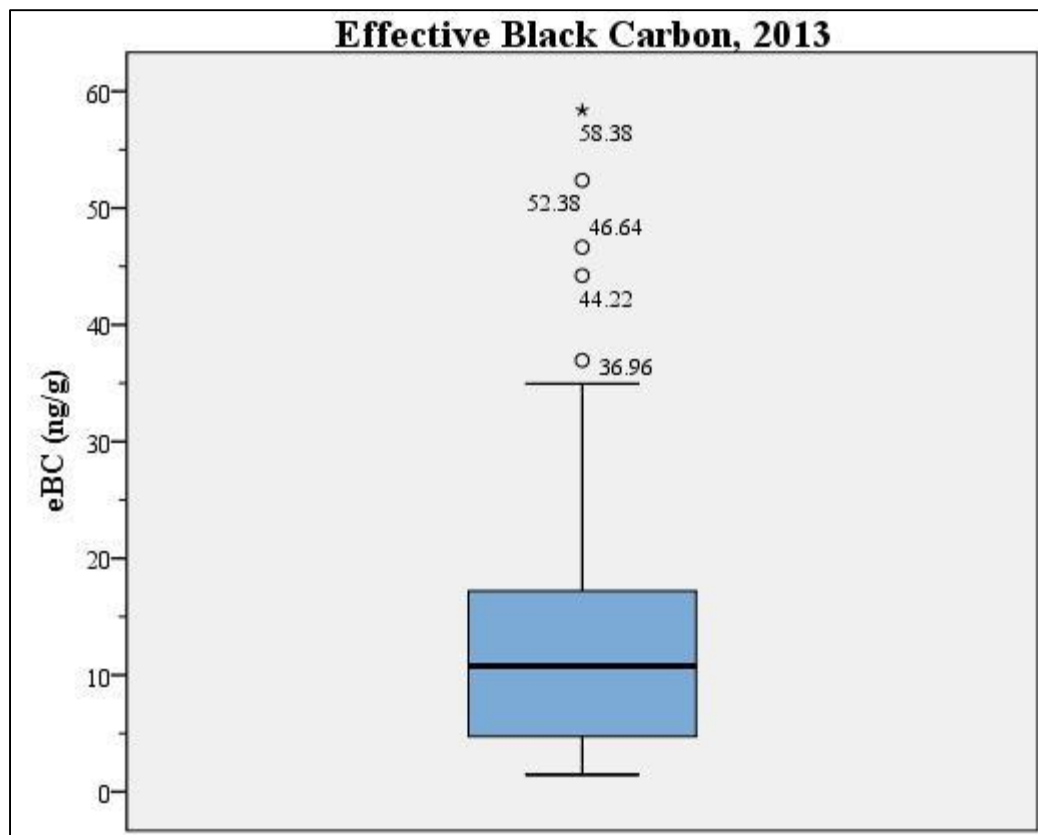
56	-9.463	-77.309	0.677	0.266	0.063	0.078	0.085	0.082	0.104
57	-9.467	-77.314	0.492	0.215	0.049	0.080	0.092	0.056	0.000
58	-9.463	-77.312	0.672	0.213	0.080	0.093	0.086	0.111	0.090
59	-9.463	-77.309	0.961	0.433	0.095	0.115	0.109	0.079	0.131
60	-9.463	-77.312	0.821	0.289	0.102	0.087	0.161	0.094	0.089
61	-9.466	-77.316	1.140	0.526	0.086	0.121	0.144	0.112	0.151
62	-9.010	-77.632	0.577	0.233	0.048	0.063	0.081	0.060	0.093
63	-9.010	-77.632	0.550	0.166	0.055	0.076	0.089	0.063	0.100
64	-9.010	-77.632	0.512	0.223	0.056	0.081	0.090	0.063	0.000
65	-9.010	-77.632	0.695	0.257	0.065	0.078	0.135	0.063	0.097
66	-9.012	-77.636	0.644	0.230	0.056	0.079	0.104	0.057	0.118
67	-9.012	-77.636	1.592	0.745	0.186	0.198	0.147	0.137	0.178
68	-9.012	-77.636	0.767	0.281	0.079	0.081	0.113	0.088	0.124
69	-9.012	-77.636	0.635	0.214	0.071	0.059	0.112	0.060	0.119
70	-9.014	-77.642	0.542	0.224	0.056	0.061	0.078	0.049	0.074
71	-9.014	-77.642	0.939	0.430	0.117	0.097	0.117	0.084	0.094
72	-9.014	-77.642	0.653	0.307	0.078	0.087	0.091	0.040	0.050
73	-9.014	-77.642	0.635	0.259	0.073	0.081	0.063	0.073	0.087
74	-9.019	-77.643	0.989	0.357	0.131	0.196	0.114	0.022	0.169
75	-9.019	-77.643	0.726	0.331	0.078	0.092	0.073	0.054	0.097
76	-9.019	-77.643	0.635	0.297	0.064	0.083	0.079	0.058	0.055
77	-9.019	-77.643	0.878	0.360	0.133	0.103	0.098	0.045	0.140
78	-9.010	-77.632	0.546	0.154	0.078	0.081	0.137	0.096	0.000
79	-9.012	-77.636	0.733	0.351	0.073	0.091	0.105	0.113	0.000
80	-9.014	-77.642	1.016	0.510	0.171	0.132	0.095	0.107	0.000
81	-9.019	-77.643	1.365	0.827	0.026	0.155	0.118	0.103	0.135
82	-8.954	-77.632	0.911	0.528	0.018	0.083	0.083	0.082	0.117
83	-8.957	-77.631	0.662	0.369	0.044	0.119	0.000	0.000	0.129
84	-8.962	-77.626	0.924	0.450	0.035	0.121	0.051	0.000	0.268
85	-8.957	-77.631	0.465	0.120	0.069	0.091	0.084	0.100	0.000
86	-8.962	-77.626	0.652	0.305	0.090	0.074	0.096	0.087	0.000
87	-8.954	-77.632	0.470	0.198	0.073	0.088	0.111	0.000	0.000











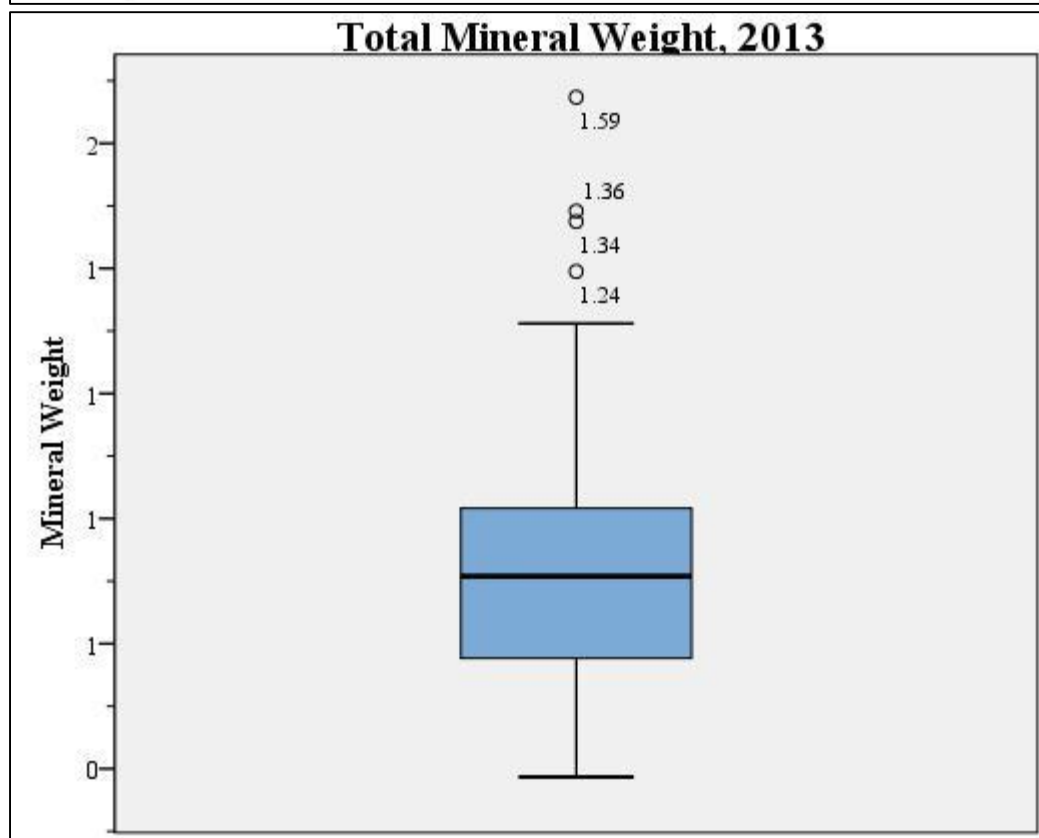
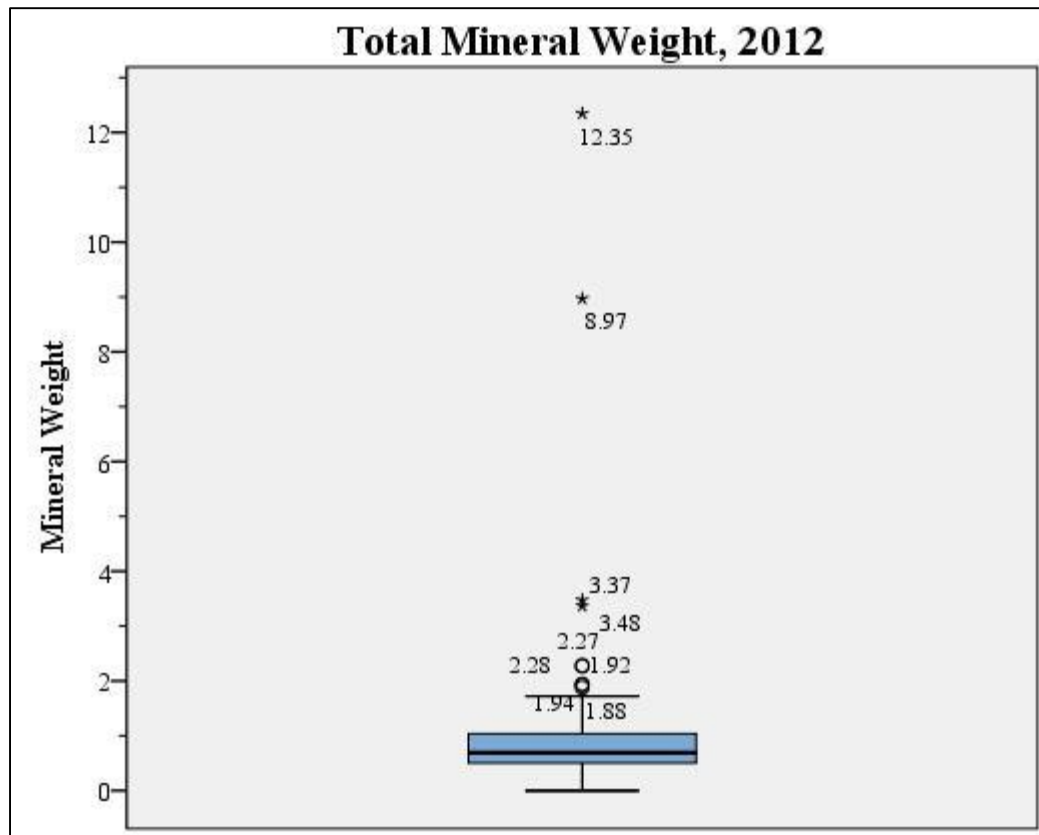


Table B4: Pearson correlation coefficients - sample attributes and mineral weight, 2011

2011	Altitude	Albedo	eBC	Total Mineral Weight
Quartz	-0.038	0.033	0.093	0.721**
Muscovite	-0.142	-0.065	-0.091	0.671**
Albite	-0.201	0.107	0.518**	0.558**
Kaolinite	-0.221	-0.086	0.317*	0.234
Annite	-0.032	0.063	-0.020	0.415**

Table B5: Pearson correlation coefficients - sample attributes and mineral weight, 2012

2012	Altitude	Albedo	eBC	Total Mineral Weight
Quartz	-0.066	-0.071	0.187	0.437**
Muscovite	0.042	0.088	-0.041	0.786**
Albite	-0.090	0.274	0.199*	0.332**
Kaolinite	0.039	0.071	-0.078	0.947**
Annite	-0.100	-0.304	0.389**	0.060

Table B6: Pearson correlation coefficients - sample attributes and mineral weight, 2013

2013	Altitude	Albedo	eBC	Total Mineral Weight
Quartz	-0.141	0.003	0.024	0.784**
Muscovite	-0.122	-0.035	0.109	0.548**
Albite	-0.253*	-0.043	0.406**	0.810**
Kaolinite	-0.084	0.015	0.595**	0.561**
Annite	0.057	0.045	0.372**	0.535**
Illite	-0.164	-0.140	0.228*	0.589**

Table B7: Pearson correlation coefficients - snow sample attributes, 2011

2011	Altitude	Albedo	eBC	Total Mineral Weight
Altitude	1	0.111	-0.369*	-0.146
Albedo	0.111	1	-0.339*	-0.020
eBC	-0.369*	-0.339*	1	0.055
Total Mineral Weight	-0.146	-0.020	0.055	1

Table B8: Pearson correlation coefficients - snow sample attributes, 2012

2012	Altitude	Albedo	eBC	Total Mineral Weight
Altitude	1	-0.062	-0.141	0.008
Albedo	-0.062	1	-0.062	0.047
eBC	-0.141	-0.062	1	0.020
Total Mineral Weight	0.008	0.047	0.020	1

Table B9: Pearson correlation coefficients - snow sample attributes, 2013

2013	Altitude	Albedo	eBC	Total Mineral Weight
Altitude	1	0.254*	-0.250*	-0.184
Albedo	0.254*	1	-0.172	-0.033
eBC	-0.250*	-0.172	1	0.343**
Total Mineral Weight	-0.184	-0.033	0.343**	1

Table B10: Pearson correlation coefficients – mineral weight, 2011

2011	Quartz	Muscovite	Albite	Kaolinite	Annite
Quartz	1	-0.021	0.585	0.016	-0.033
Muscovite	-0.021	1	0.106	0.205	0.603
Albite	0.585	0.106	1	0.288	0.221
Kaolinite	0.016	0.205	0.288	1	0.176
Annite	-0.033	0.603	0.221	0.176	1

Table B11: Pearson correlation coefficients – mineral weight, 2012

2012	Quartz	Muscovite	Albite	Kaolinite	Annite
Quartz	1	0.071	0.191	0.154	0.428
Muscovite	0.071	1	0.077	0.777	-0.061
Albite	0.191	0.077	1	0.266	0.091
Kaolinite	0.154	0.777	0.266	1	-0.146
Annite	0.428	-0.061	0.091	-0.146	1

Table B12: Pearson correlation coefficients – mineral weight, 2013

2013	Quartz	Muscovite	Albite	Kaolinite	Annite	Illite
Quartz	1	0.243	0.536	0.103	0.185	0.233
Muscovite	0.243	1	0.604	0.344	0.320	0.211
Albite	0.536	0.604	1	0.462	0.343	0.474
Kaolinite	0.103	0.344	0.462	1	0.526	0.280
Annite	0.185	0.320	0.343	0.526	1	0.207
Illite	0.233	0.211	0.474	0.280	0.207	1

Table B13: Pearson correlation coefficients – mineral weight and mine proximity

Mines	Quartz	Muscovite	Albite	Kaolinite	Annite	Illite
2011	0.115	-0.176	-0.035	-0.064	-0.159	-
2012	0.513	0.016	-0.105	0.036	0.275	-
2013	0.459	-0.038	0.107	-0.090	-0.054	0.112

Table B14: Pearson correlation coefficients – mineral weight and Huaraz proximity

Huaraz	Quartz	Muscovite	Albite	Kaolinite	Annite	Illite
2011	0.054	0.031	-0.254	-0.187	-0.096	-
2012	0.186	0.118	0.082	0.139	-0.177	-
2013	0.355	0.041	0.099	-0.250	-0.153	0.118

Table B15: Pearson correlation coefficients – snow sample attributes and mine proximity

Mines	Altitude	Albedo	eBC	Total Mineral Weight
2011	-0.062	-0.009	-0.008	0.030
2012	0.109	-0.194	-0.128	0.180
2013	-0.184	-0.115	-0.210	0.267

Table B16: Pearson correlation coefficients – snow sample attributes and Huaraz proximity

Huaraz	Altitude	Albedo	eBC	Total Mineral Weight
2011	0.188	0.519**	-0.617	0.030
2012	0.187	0.487**	-0.358	0.171
2013	0.044	0.139	-0.469	0.167

Table B17: Pearson correlation coefficients – mine proximity, eBC, and mineral weights based on sample vs. mine aspect

Mines	eBC	Quartz	Muscovite	Albite	Kaolinite	Annite	Illite
Opposite	0.030	0.545	0.330	0.410	0.256	0.130	-0.098
Ninety Degree	-0.465	0.268	-0.103	-0.105	0.038	0.113	-0.087
Matching	0.066	0.416	-0.056	-0.109	0.303	0.143	0.048

Table B18: Pearson correlation coefficients – Huaraz proximity, eBC, and mineral weights based on sample vs. Huaraz aspect

Huaraz	eBC	Quartz	Muscovite	Albite	Kaolinite	Annite	Illite
Opposite	-0.451	0.105	0.318	0.392	0.164	-0.035	-0.400
Ninety Degree	-0.386	0.140	0.069	-0.089	-0.085	-0.198	-0.090
Matching	-0.504	0.268	0.080	0.072	0.101	-0.176	0.071